

الجمهورية الجزائرية الديمقراطية الشعبية

People's Democratic Republic of Algeria

وزارة التعليم العالي والبحث العلمي

Ministry of Higher Education and Scientific Research

جامعة أبي بكر بلقايد - تلمسان

Aboubakr Belkaïd University – Tlemcen –
Faculty of Technology



Thesis

Presented for obtaining the **MASTER's degree**

In: Biomedical Engineering

Specialty: Medical imaging

By: Benbettit Wassila & Hafallah Chaima

Topic

**Multifractal Analysis Of Histological Images:
Application For Thyroid
(Python Programming Environment)**

Publicly defended, on **26 /06 / 2022**, before the jury composed of:

Mr. Bechar Hassane

Mrs. Khemis Kamila

Mrs. Benseghir Sihem Amel

Prof.

Prof.

Prof.

Tlemcen University

Tlemcen University

Tlemcen University

President

Supervisor

Examiner

Academic Year: 2021/ 2022

الجمهورية الجزائرية الديمقراطية الشعبية

République algérienne démocratique et populaire

وزارة التعلّم والعالي والبحث العلمي

Ministère de l'Enseignement Supérieur et de la Recherche Scientifique

جامعة أبي بكر بلقايد - تلمسان

Université Abou bekr Belkaïd – Tlemcen –

Faculté de technologie



Mémoire

Présenté pour l'obtention du diplôme de MASTER

En : Génie biomédical

Spécialité : Imagerie médicale

Par: Benbettit Wassila & Hafallah Chaima

Thème

**Analyse Multifractale des images Histologiques :
Application pour la thyroïde
(Environnement de programmation Python)**

Soutenue publiquement, le **26 /06/ 2022**, devant le jury composé de :

Mr. Bechar Hassane

MCA

Université de Tlemcen

Président

Mme. Khemis Kamila

MCA

Université de Tlemcen

Encadreuse

Mme. Benseghir Sihem Amel

MCB

Université de Tlemcen

Examinatrice

Année Universitaire : 2021/ 2022

Abstract

Due to the highly irregular image shapes and complex spatial arrangements, thyroid histological image classification is a difficult problem. Since it can accurately resolve local densities and represent different structures in the image, the multifractal analysis (fractal geometry extension) has been found useful in characterizing the intensity distribution present in such images. In this work, we propose a multifractal method based on the local characterization (Holder exponent) and global characterization (multifractal spectrum) of histological thyroid images.

The algorithm is implemented in three major stages in the Python programming environment: preprocessing; Estimating the Hölder exponents, which consist of extracting the Hölder image (image of local singularity) based on the local maximum value (linear regression "Log (maximum values)" against the "Log (window dimension)"). Multifractal spectrum based on the box-counting method that counts the number of redundancies of each α value in the Holder image. The results obtained are saved in Excel in order to extract pertinent parameters for classifier layer (perspective work).

We settle for visually interpreting the multifractal spectra. We noticed that these spectra show differences from one class of tissue to another: healthy tissue/adenoma/carcinoma; and allow differentiation between different types of carcinoma. Therefore, the results obtained show the importance and adaptability of multi-fractal analysis in the diagnosis aid of thyroid pathologies.

Keywords:

Medical images, Histology, Thyroid, Fractal geometry, Fractal dimension, Multifractal analysis, Hölder exponent, Multifractal spectrum, Box counting, Diagnosis aid.

التحليل متعدد الكسيريات للصور النسيجية: تطبيق على الغدة الدرقية (بيئة البرمجة بايثون)

ملخص

يعتبر تصنيف صور الغدة الدرقية النسيجية مشكلة صعبة بسبب أشكال الصور غير المنتظمة للغاية والترتيبات المكانية المعقدة. أثبت التحليل متعدد الكسيريات (امتداد الهندسة الكسيرية) فائدته في توصيف توزيع الشدة الموجود في مثل هذه الصور: يمكنه حل الكثافات المحلية بدقة وتمثيل الهياكل المختلفة في الصورة. في هذا العمل، نقترح طريقة متعددة الكسيريات تستند بشكل أساسي إلى التوصيف المحلي (أس هولدر) والتوصيف الشامل (الطيف متعدد الكسيريات) للصور الطبية.

يتم تنفيذ الخوارزمية على ثلاث مراحل رئيسية على بيئة البرمجة بايثون: المعالجة المسبقة؛ تقدير أس هولدر الذي يهدف إلى استخراج صورة هولدر (صورة التفرد المحلي) بناءً على القيمة القصوى المحلية (الانحدار الخطي «لوغاريتم (القيم القصوى)» بدلالة «لوغاريتم (بعد النافذة)»؛ الطيف متعدد الكسيريات يعتمد على طريقة عد الصناديق التي تحسب عدد التكرارات لكل قيمة ألفا في الصورة هولدر. يتم حفظ النتائج التي تم الحصول عليها في الإكسال من أجل استخراج المعلومات ذات الصلة لطبقة المصنف (العمل المنظوري).

ببساطة فسرنا بصرياً الأطياف متعددة الكسيريات. لاحظنا أن هذه الأطياف تختلف من فئة إلى أخرى: الأنسجة السليمة/الورم الغدي/السرطان؛ والسماح بالتمييز بين مختلف أنواع السرطان. وبالتالي، تظهر النتائج التي تم الحصول عليها أهمية وقابلية التكيف للتحليل متعدد الكسيريات للمساعدة في تشخيص أمراض الغدة الدرقية.

الكلمات المفتاحية:

الصور الطبية، علم الأنسجة، الغدة الدرقية، الهندسة الكسيرية، البعد الكسيري، التحليل متعدد الكسيريات، أس هولدر، الطيف متعدد الكسيريات، العد الصندوقي، المساعدة في التشخيص.

Résumé

La classification des images histologiques de la thyroïde est un problème difficile en raison des formes d'image très irrégulières et des arrangements spatiaux complexes. L'analyse multifractale (extension de la géométrie fractale) s'est avérée utile pour caractériser la distribution d'intensité présente dans de telles images : Elle peut résoudre avec précision les densités locales et représenter différentes structures dans l'image. Dans ce travail, nous proposons une méthode multi fractale qui repose principalement sur la caractérisation locale (exposant de Hölder) et la caractérisation globale (spectre multifractal) d'images médicales.

L'algorithme est implémenté en trois étapes dans l'environnement de programmation Python : Prétraitement ; Estimation des exposants de Hölder qui consiste à extraire l'image de Hölder (image de la singularité locale) à partir de la valeur maximale locale (droite de régression linéaire "Log (valeurs maximales)" en fonction du "Log (dimension de la fenêtre)"); Spectre multifractal basée sur la méthode de comptage de boîtes qui compte le nombre de redondances de chaque valeur α dans d'image de Hölder. Les résultats obtenus sont enregistrés dans Excel afin d'en extraire les paramètres pertinents pour la couche classifieur (travail en perspective).

Nous nous contentons d'interpréter visuellement les spectres multi fractals. Nous avons remarqué que ces spectres présentent des différences d'une classe de tissus à l'autre : tissu sain/adénome/carcinome ; et permettent une différenciation entre les différents types de carcinome. Par conséquent, les résultats obtenus montrent l'importance et l'adaptabilité de l'analyse multi fractale pour l'aide au diagnostic des pathologies thyroïdiennes.

Mots-clés :

Images médical, Histologie, thyroïde, géométrie fractal, Dimension fractal, analyse multifractal, Exposant de Hölder, spectre multifractal, comptage de boîtes, Aide au diagnostic.

ACKNOWLEDGMENTS

In the Name of Allah, the Merciful, the Beneficent.

Praise be to the Lord of all worlds. Prayers and peace be upon our Prophet, Muhammad, his family, all of his companions, and all those who follow his way.

We would like to express our thanks and appreciations to the following people who helped us achieve our goal.

We would like to express our deepest gratitude to our supervisor, Mrs. Khemis Kamila, for her patience, guidance, and support. We have benefited greatly from her wealth of knowledge, for her continued guidance. She is the true definition of a leader and the ultimate role model.

Our sincere acknowledgements go to Mr. Bechar Hassen, and Mrs. Benseghir Sihem Amel, who have been so kind to accept to be members of the jury and to read our work. We thank all of them for their corrections, comments and criticism.

A special thank for Dr. Pathologist BELARBI Omar for his help and support.

A special thank for Dr. Pathologist Baghli Mohammed El Amine for his help and support.

A special thank for Mr. Riadh Azzoun for his help and support.

A special thank for PhD students; Bellal Linda, Amina and Aisha for their help and support

We take this opportunity to thank all the professors of the biomedical engineering department who have taught us during these five years of study.

Peace be upon you with the mercy and blessings of Allah.

Benbettit Wassila & Hafallah Chaima

DEDICATION

*In the Name of **Allah**, Most Gracious, Most Merciful.*

All the Pries is due to Allah alone, the Sustainers of all the worlds.

This work is dedicated to the following people who assisted me in achieving my goal.

*My great **parents**, who never stop giving of themselves in countless ways,*

*To my great **uncle** and **his wife**.*

*Who stand by me through thick and thin, my beloved **brothers** and **sisters**.*

*My beloved peony flowers: **Diaa Eddine**, and **Charaf-Eddine**, whom I cannot force myself to stop loving.*

*To **all my family**, the symbol of love and giving,*

*To **Sheikh Dr. Ali al-Rubaie***

***Mrs.Arwa** and to all **Mental Drills academy members** (Batch 130), my second magnificent family.*

*To Mrs. **Soomaya** and **Melek zardoub** from Tunisia.*

*To my friend **Alaa Kacem** and **Aya Khadija shanta**.*

My friends who encourage and support me,

This project is especially dedicated to the teachers who helped and guided us to successfully complete this project work

All the people in my life who touch my heart, I dedicate this research.

Benbettit Wassila

DEDICATION

Praise to ALLAH for giving me and allowing me this research work, which I dedicate to:

My Mother "LOUZANA" a strong and gentle soul, who taught me to trust Allah, believe in hard work and that so much could be with little.

My father "MOUHAMED ELSALEH" for earning an honest living for us supporting and encouraging me to believe in myself.

To My beloved brothers and sisters; "ABD ALLAH", "CHAHRA ZAD" and "NOUR ELHOUDA" particularly my dearests brothers, "ABD ALMALEK", "HOUCINE" who stands by me when things look bleak.

I am also hugely appreciative to Prof Sir "SALIM KERAI" who was credited with accepting and completing this major that I loved.

To my friend "WASSILA" who enlightened me on many points in this project.

To all my friends who I shared Moments of Joy and Happiness A special thanks to my best friend "RAWNAK" who was my best cheerleaders.

To all my great families from near and far who participated in the emancipation of my person especially dear uncle "ABDELHAFID".

To my teachers who instilled in me the knowledge to do it

To all my classmates I wish a bright future.

In the end, I dedicate this humble work to anyone who has helped me from near or far without exception.

Hafallah Chaima

TABLE OF CONTENTS

Abstract	iii
ملخص	iv
Résumé	v
ACKNOWLEDGMENTS	vi
DEDICATION.....	vii
DEDICATION.....	viii
List of figure.....	xii
List of tables.....	xv
General Introduction	xvi
Chapter I Medical context.....	2
Content	3
I.1 Introduction.....	4
I.2 Histological techniques and Histology imaging technologies.....	4
I.2.1 History.....	4
I.2.2 Histology Definition.....	4
I.2.3 Histological techniques	4
I.2.4 The microscope	7
I.3 The Thyroid gland	8
I.3.1 Anatomy.....	9
I.3.2 Histology.....	9
I.3.3 Thyroid Gland Function.....	10
I.3.4 Thyroid nodules	11
I.3.5 Types of thyroid nodules.....	11
I.3.6 Thyroid nodule diagnostic tools and evaluation methods.....	12
I.3.7 Bethesda Classification of Thyroid cytopathology	14
I.3.8 Follicular adenoma and papillary carcinoma	16
I.4 Conclusion	17
Chapter 2 Fractal Geometry and Multifractal Analyses of images	18
Content	19
II.1 Introduction	20
II.2 Fractal geometry and dimensions.....	20
II.2.1 History of Fractal geometry.....	20

II.2.2 Fractal geometry and Fractal objects	22
II.2.3 Properties of fractal objects	22
II.2.4 Examples of some famous fractal structures	23
II.2.5 Fractal and dimensions	24
II.2.6 Fractal dimension computing methods	26
II.3 Multifractal Analysis.....	30
II.3.1 Multifractal History	30
II.3.2 Methods of multifractal analysis.....	31
II.3.3 Concept of measure	31
II.3.4 Hurst exponent and fractal dimension	31
II.3.5 Local behavior: Hölder exponent (α -value)	32
II.3.6 Multifractal measures	32
II.3.7 Holder image (α -image).....	33
II.3.8 Global behavior: Multifractal Spectrum (Singularity spectrum).....	34
II.3.9 Methods for Multifractal Spectrum calculation.....	35
II.4 Conclusion.....	37
Chapter 3 Application of the multifractal analysis method And	
Results	38
Contents.....	39
III.1 Introduction.....	40
III.2 Image processing and analyzing generalities	40
III.3 Proposed approach	42
III.4 Data Acquisition.....	43
III.5 Programming Environment.....	44
III.6 Method description	47
III.6.1 First part: Prepossessing	47
III.6.2 Second part: Holder exponent estimation.....	48
III.6.3 Third part: Multifractal spectrum estimation.....	49
III.7 Application and results.....	50
III.7.1 Pre-processing and Holder exponent estimation algorithms	50
III.7.2 Discussion of the result of the Holder exponent algorithm	51
III.7.3 Multifractal spectrum estimation	51
III.7.4 Multifractal spectrum First database.....	52

III.7.5 Multifractal spectrum Second database	53
III.8 Step to classification.....	54
III.8.1 Discussion First database result	57
III.8.2 Discussion second database result	60
III.8.3 Discussion of the pertinent parameters	61
III.9 Conclusion.....	61
General Conclusion And Perspectives	62
General Conclusion	63
Perspectives in future works.....	64
References	65

List of figure

Figure 0- 1: (A) Incidence of thyroid cancer in Algeria, 2014-2017, (B) Incidence of thyroid cancer in Algeria, 2020.	xviii
Figure 0- 2: The region of interest ROI on the femoral neck of the bone.	xx
Figure 0- 3: The tables designate the calculation windows for different boxes $i=1(a)$, $i=3(b)$ and $i=5(c)$	xx
Figure 0- 4: (A) and (B) illustrate MRI images with windows indicating ROIs. (C) Figure showing a trabecular bone texture ROI.	xxi
Figure 0- 5: The formulations of measures used in this research.	xxi
Figure 0- 6: System overview of multifractal analysis of tissue images used.	xxiii
Figure I- 1: Four types of human tissue [15].	5
Figure I- 2: Sectioning fixed and embedded tissue [11].	6
Figure I- 3: Tissue Embedded in paraffin [17].	6
Figure I- 4: Paraffin sections form “ribbons” during the sectioning process [17].	7
Figure I- 5: Mounting tissue sections [17].	7
Figure I- 6: (A) Light Microscopy, and (B) Electronic Microscopy [22] [24].	8
Figure I- 7: thyroid gland anatomy [27] [26].	9
Figure I- 8: Thyroid Follicles and thyroid parafollicular or C cells [30].	10
Figure I- 9: T3, T4, and TSH secretion systems [32].	11
Figure I- 10: Thyroid nodules in the thyroid gland [36].	11
Figure I- 11: Thyroid Scan [43].	14
Figure I- 12: (A) the macroscopic and (B) microscopic appearance of a follicular adenoma [46].	16
Figure I- 13: (A) the macroscopic and (B) microscopic appearance of a papillary carcinoma [46].	17
Figure II- 1: (A) and (B): baderne of Apollonius, (C) Albrecht Dürer pentagons,(D) and (E) represent a new geometry by Karl Weierstrass and Henri Poincaré respectively [48].	20
Figure II- 2: artificial fractals from (A) to (H) respectively (Cantor dust, Giuseppe Peano curve, David Hilbert curve, Paul Lévy curve, Gaston Julia and Pierre Fatou fractal image, the Sierpinski triangle, Karl Menger 3D extension of the Cantor collection) [1].	21
Figure II- 3: (A) length of British shores quantified in different size of the ruler, (B) Mandelbröt set [48] [54].	21
Figure II- 4: Self-similarity of Von Koch curve [64].	22
Figure II- 5: the six first iterations of the CANTOR SET structure [66].	23
Figure II- 6: the four iterations of the KOCH Curve [66].	23
Figure II- 7: the four iterations of the KOCH Snowflake [66].	23
Figure II- 8: Mandelbrot set: (A) the set appears in black, with the fractal boundary alive with color,	24
Figure II- 9: Examples illustrating the distinctions between topological and Euclidean dimensions [69].	25
Figure II- 10: Fractal dimension estimation applied to the Koch Curve [73].	25

Figure II- 11: Example of the box-counting method in binary images. The binary image is divided into increasingly fine boxes, and for each, the number of boxes needed to cover black pixels is calculated [86].	27
Figure II- 12: Graphical presentation of the principle of (A) DBCM and (B) XCM [81].	28
Figure II- 13: Illustration of the Triangular prism method. Where σ is the grid size, S1, S2, S3, and S4 represent the areas of four triangles. (i, j), (i, j+1) and (i+1, j+1) are, respectively, the coordinates of the four points of the triangular prism, h(0) denotes	29
Figure II- 14: The greyscale image (left) and its corresponding intensity histogram (right) [109].	32
Figure II- 15: The α -image. The α -range for each measure is different: [0.0000, 0.4808] for max measure, [0.0000, 0.9354] for inv-min measure, [1.7917, 2.3315] for sum measure, and [0.0000, 2.1694] for Iso measure [109].	34
Figure II- 16: α -histogram. The distribution of α -values has a bell-shaped curve, and is skewed and translated along the α -axis respectively [109].	34
Figure II- 17: Schematic representation of a multifractal spectrum [116].	35
Figure III- 1: Summary of calculating the Hölder exponent and multifractal dimension.	42
Figure III- 2: Some images from the first database. Some images from the database (a. First database, b. Second Database).	43
Figure III- 3: Python logo [2].	44
Figure III- 4: OpenCV logo [5].	45
Figure III- 5: NumPy logo [5].	45
Figure III- 6: matplotlib logo.	46
Figure III- 7: math logo.	46
Figure III- 8: scipy logo.	46
Figure III- 9: The processing steps.	47
Figure III- 10: Application of the pre-processing python program for a healthy thyroid image.	47
Figure III- 11: the tables designate the calculation windows for different window sizes in red color $w_0=1$ (A), $w_0=3$ (B) $w_0=5$ (C) and $w_0=7$ (D).	48
Figure III- 12: Holder images for different classes (a) (b) and (c).	48
Figure III- 13: Holder images for different classes of carcinoma (a) (b) and (c).	49
Figure III- 14: Box-counting method that uses different box sizes ϵ .	49
Figure III- 15: Example of multifractal spectrum obtained using holder images for the first and the second database.	50
Figure III- 16: Preprocessing and Holder exponent-Samples from first Database (A: healthy thyroid; B: follicular adenoma; C: papillary carcinoma).	50
Figure III- 17: Preprocessing and Holder exponent-Samples from second Database (A: medullary carcinoma; B: papillary carcinoma; C: vesicular carcinoma).	51
Figure III- 18: The multifractal spectrum of healthy thyroid holder images.	52
Figure III- 19: The multifractal spectrum of follicular adenoma holder images.	52
Figure III- 20: The multifractal spectrum of papillary carcinoma holder images.	53

Figure III- 21: The multifractal spectrum of medullary carcinoma holder images.	53
Figure III- 22: The multifractal spectrum of papillary carcinoma holder images.	53
Figure III- 23: The multifractal spectrum of vesicular carcinoma holder images.	54
Figure III- 24: Excel diagrams of the f_{α} data as a function of alpha of the selected healthy thyroid images.	55
Figure III- 25: Excel diagram of the mean multifractal spectrum for the selected healthy thyroid images.	55
Figure III- 26: Excel diagrams of the f_{α} data as a function of alpha of the selected follicular adenoma images.	55
Figure III- 27: Excel diagram of the mean multifractal spectrum for the selected follicular adenoma images....	56
Figure III- 28: Excel diagrams of the f_{α} data as a function of alpha of the selected papillary carcinoma images.	56
Figure III- 29: Excel diagram of the mean multifractal spectrum for the selected papillary carcinoma images...	56
Figure III- 30: Excel diagram of the mean multifractal spectra for different classes of the first database.....	57
Figure III- 31: Excel diagrams of the f_{α} data as a function of alpha of the selected medullary carcinoma images.	58
Figure III- 32: Excel diagram of the mean multifractal spectrum for the selected medullary carcinoma images.	58
Figure III- 33: Excel diagrams of the f_{α} data as a function of alpha of the selected papillary carcinoma images.	59
Figure III- 34: Excel diagram of the mean multifractal spectrum for the selected papillary carcinoma images...	59
Figure III- 35: Excel diagrams of the f_{α} data as a function of alpha of the selected papillary carcinoma images.	59
Figure III- 36: Excel diagram of the mean multifractal spectrum for the selected papillary carcinoma images...	60
Figure III- 37: Excel diagram of the mean multifractal spectra for different classes of the second database.	60

List of tables

Table I- 1: stratification of the risk of malignancy according to (TI-RADS) score [26].....	14
Table I- 2: Thyroid cytopathology: Bethesda system 2010 [40] [34].	15
Table II- 1: Differences between Gaston Julia set and the Mandelbrot set [48].	24
Table II- 2: Some differences between topological and Euclidean dimensions [69] [71].....	25
Table II- 3: Similarity dimension calculation [76].....	26
Table III- 1: Different alpha range of the classes for the first database.	61
Table III- 2: Different alpha range of the classes for the second database.....	61

General Introduction

Context and problematic

Humans acquire three-quarters of their information visually. In addition to the importance of vision to a person's existence and in many aspects of their life, in medicine, vision is emerging as the preferred diagnosis method. The digital creation and processing of high-quality images are therefore of paramount importance, and this is the purpose of medical imaging, the medical specialty that consists of producing and interpreting images of the living human body for diagnosis, treatment (interventional imaging), or monitoring of disease progression. Thus, the main purpose of medical imaging is to obtain images of the interior of the human body using various physical concepts to enable clinicians to examine the human body and thus provide increasingly accurate diagnoses (a direct understanding of physiology and pathology). In general, image processing uses two methods. The first is image enhancement, which includes visualization and sometimes-manual interpretation by a human expert. The second approach is computer vision, which involves implementing automated interpretation procedures similar to those of the human visual perception system.

Histology, or the examination of cells, tissues, and organs under the microscope, is one of the most dynamic and complex disciplines of medicine. Recent advances in medical imaging allow doctors generally and especially pathologists today to identify and diagnose diseases that were previously inaccessible one of them the thyroid tumors present as a thyroid nodule and can be benign (thyroid adenoma) or malignant (thyroid carcinoma). More than 100 different types of cancer have now been discovered. According to the statistics collected, and through the following figures, we review the statistics on thyroid cancer in Algeria. The first figure (Figure 0- 1 (A)) presents an increased incidence of thyroid cancer over a three-year period (incidence of thyroid cancer in Algeria, 2014-2017); we notice through it that the group most at risk of developing thyroid cancer is the elderly. Thyroid cancer is the third most prevalent cancer diagnosis in Algerian women in both the east and west, according to the Algerian Journal of Health Sciences 2017. In the figure (Figure 0- 1 (B)), the statistics show the prevalence of various types of cancer in Algeria in the year 2020; thyroid cancer is the third most common cancer. The evaluation of a thyroid nodule is one of the most common and difficult challenges that pathologists face.

Diverse cancer kinds may have significantly different morphology, size, texture, and color distributions, making it difficult to design a standard pattern for tumor identification that can be applied to thyroid nodules. Furthermore, because individual histology images are so large, the histopathology image dataset is considered large-scale, which increases processing complexity and complicates image analysis. These are the key obstacles in automatic analysis of digital histopathology images. Difficulties and uncertainty exist, notably in evaluating the possibility of malignancy and the effective therapeutic strategy. As a result, researchers use a variety of methods to expand visual perception to study the relationship between structure and function in human cells and tissues. One such method is medical image analysis, which includes image compression, image synthesis, image segmentation, and tissue analysis. In addition, the Histological characterization presents an intensive research field in medical and histological image analysis that aims to complement the visual observation of histological images with quantitative information about histology.

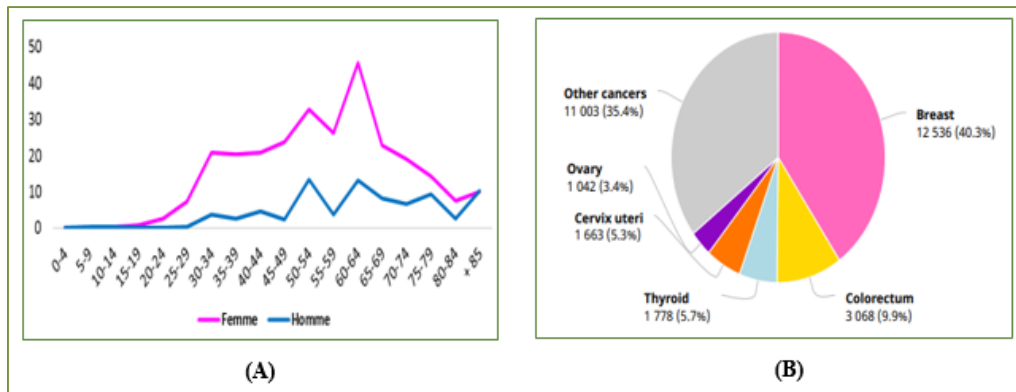


Figure 0- 1: (A) Incidence of thyroid cancer in Algeria, 2014-2017, (B) Incidence of thyroid cancer in Algeria, 2020.

Fractal geometry and multifractal analysis

The tools of Euclidean geometry make it difficult to describe the complexity of natural objects. This geometry has the ability to evaluate elements with simple structures. Natural images have an extremely complex structure that is built on irregular forms. As in the case of tissues and cells. Therefore, performing such complex tasks necessitates techniques that are more advanced than traditional image analysis methods. After the discovery that Natural geometry or fractal geometry by the mathematician Mandelbrot in the 70s, who proposed new concepts for understanding certain complex phenomena. There is no longer any doubt about the regularity of nature: behind all chaos and all-hazard hides an order. There is a set in mathematics called the Julia set, which paved the way for fractal geometry, in which the scientist Mandelbrot chose a small set within the Julia set and obtained the Mandelbrot set, from which Mandelbrot derived began to establish the science of fractals or fractal geometry. The Mandelbrot set is distinguished that the more you zoom in, the more copies of the first figure you will find, and this is the most important characteristic of fractal shapes. Fractals can be compared to matryoshkas, which are famous Russian dolls that are similar to each other. Complex patterns of repeating geometric patterns result in shapes that repeat infinitely in smaller and smaller sizes, and this is what makes fractal geometry more complex. This notion allows for a straightforward geometrical interpretation and is used in a wide range of domains, including geophysics, biology, medicine, and fluid mechanics.

A fractal dimension is a non-integer number proposed by fractal theory that allows the object's more or less tortuous aspect to be quantified. The fractal dimension can be defined in a variety of ways, including the Minkowski or Hausdorff definitions. Fractal dimension can be used to describe natural scenes; however, when the studied image is sufficiently irregular, this type of analysis is no longer effective. When examining signals with a large fluctuation in regularity from point to point, multifractal analysis is recommended. Multifractals could be seen as an extension of fractals. A multifractal object is more complex in the sense that it is always invariant by translation, although the dilatation factor needed to be able to distinguish the detail from the whole object depends on the detail being observed.

Fractal analysis has experienced significant growth in recent years, it has been the subject of many applications in very varied fields both theoretically (development of multifractal analysis). In the multifractal approach, the image model is not determined using a transformation function, such as the filter function, but the image is modeled using one or more measures, which we will denote by (μ) .

This approach allows emphasizing the fundamental role that resolution plays in multifractal image analysis. Then, the most significant difference between the classical and multifractal approach is in the way of treating irregular details. While classical methods use different techniques to try to rid the image of irregularities, the multifractal approach draws information about the image from irregularities (singularities). In addition, most classical methods use relative (normalized) gray pixel levels as basic information when analyzing an image. The multifractal method uses the degree of Hölder regularity of a point measure as basic information. Quantitative description of multifractals is usually done through the so-called. Multifractal spectrum $f(\alpha)$. The procedure begins with the determination of Hölder's exponent α , which describes the degree of regularity of the structure at each of its points, and then determines the distribution of α value in the structure, i.e. multifractal spectrum $f(\alpha)$.

Finally, it is important to point out that multifractal analysis does not assume anything in terms of image structure and regularity. Namely, the image does not have to be either "fractal" or "multifractal", whatever that means, in order to be analyzed. Instead of making and proving any assumptions, the multifractal method is simply applied to the image, and then based on the results; there are different conclusions can be drawn about the structure and regularity of the image.

State of the art

Recently, several important developments in multifractal analysis have had a major impact on applications of image processing and analysis. These applications, among others, show that multifractal analysis has resolutely passed over the past few years from the descriptive stage to the operational stage. The capacity of multifractal analysis algorithms to classify medical images in general, and especially histological images, has been shown in multiple published papers during the past decade. In addition, several studies showed the interest of extracting from histological images fractal or multifractal parameters, potentially related to the fractal or multifractal behavior of tissues in space and time. Several outstanding works in medical imaging [1, 2, 3]. We will also mention some interesting research in histological image characterization and classification, but first, we will cite some works from various modalities (we take CT-Scan and Magnetic Resonance imaging as examples).

- **CT-Scan**

Among the outstanding works in medical imaging by CT-Scan, we can cite those **R. Korchiyne and others** [4] proposed a powerful method for the characterization and segmentation of medical images based on fractal geometry. In which they developed a method based on the Hausdorff multifractal spectrum to characterize CT-Scan medical images. In this study, the group of researchers analyzed two CT-Scan bone images corresponding to two different subjects. A healthy subject whose densitometric analyzes showed the absence of pathologies linked to osteoporosis, the other osteoporotic (Figure 0- 2).

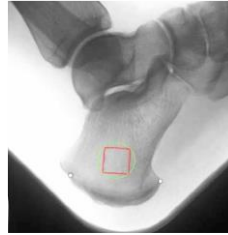


Figure 0- 2: The region of interest ROI on the femoral neck of the bone.

The steps of their multifractal algorithm:

- Grayscale image → Normalize the image to full scale → Consider an arbitrary pixel and its neighboring porches (Figure 0- 3)→ Consider the maximum(minimum) measurement of each box → Calculate the logarithm of the maximum values of the box → Plot the linear regression line "Log (Max)" as a function of the "Log (i)" of the dimension of the box. → The slope of the linear regression is the value→ same procedure for all pixels → Find Hölder's image. → Plot the multifractal spectrum.

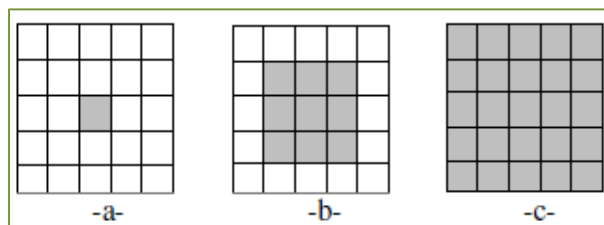


Figure 0- 3: The tables designate the calculation windows for different boxes $i=1(a)$, $i=3(b)$ and $i=5(c)$.

Results of the research:

- Holder images (images according to A) make it possible to distinguish the image of a healthy subject from a diseased image.
- Hausdorff spectra allow to accurately deriving a lot of statistical information about the microarchitecture of the bone.
- The texture becomes more irregular as α value increases.
- The minimum values of the Hölder exponent have a maximum spectrum $f(\alpha)$ close to two (dimension of a surface).
- In the healthy subject, the signal decreases regularly in an angular way while the other spectrum decreases differently in three zones.

- **Magnetic Resonance Imaging**

Among the outstanding works in medical imaging by magnetic resonance, we can cite those of **Mohamed Khider** [5] the researcher implemented fractal and multifractal analysis methods after that proposed classification procedures. The data used are radar images taken in three different regions: Sétif (Algeria), Bordeaux (France), Melbourne (United States) and medical images of the MRI and CT scanner type. In the case of medical images, the database used is made up of 40 images from different imagers (MRI and CT scanner) collected at the CHRU in Lille (Figure 0-4). They concern regions of interest (rectangular and various sizes) positioned by clinicians on each native image to cover strictly trabecular territories. They are coded on 8 bits in BMP format.

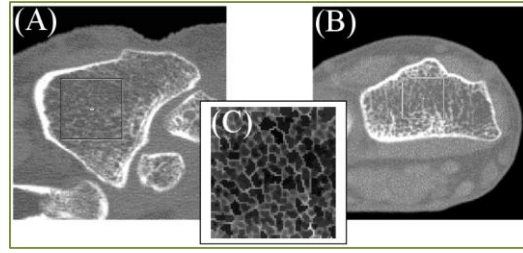


Figure 0- 4: (A) and (B) illustrate MRI images with windows indicating ROIs. (C) Figure showing a trabecular bone texture ROI.

The multifractal analysis method used for image classification:

The grain spectrum and large deviation method were used to classify bone texture with 10 images of MRI type.

The preliminary results obtained on 10 images are very satisfactory.

- **Microscope**

Among the outstanding works in medical imaging by microscope we can cite the applications of multifractal analysis in histological images for some organs:

- **Liver and prostate cancer**

Chamidu Atupelage and others [6]. In this paper, they proposed a texture descriptor to observe the histologic texture into highly discriminative feature space. The data used (20x magnification) and visualized using a tool called Nano-Zoomer (the tool visualizes each data sample in 8-different magnifications: 1.25x, 2.5x, 5.0x, 10x, 20x, 40x, 63x, and 100x) and experienced pathologists annotated the cancer regions of each of the data samples. Based on this annotated data sample, for each organ (liver and prostate), then researchers constructed 24 categories of experimental datasets (three sizes of image patches: 64×64, 128×128, and 256×256 pixels with eight magnifications). Each category consists of around 300~400 sample patches.

Multifractal characterization method used:

In this work, they extract texture characteristics in the multifractal domain as α and $F(\alpha)$, which correspond to each pixel of a given image. They empirically defined six local singularity characteristic measures to construct the multifractal feature descriptor. The formulations of these measures are illustrated in (Figure 0-5).

Maximum	$\mu_i(m, n) = \max_{(k,l) \in \Omega} g(k, l)$
Minimum	$\mu_i(m, n) = \min_{(k,l) \in \Omega^*} g(k, l)$
Sum	$\mu_i(m, n) = \sum_{(k,l) \in \Omega} g(k, l)$
Modified differential box counting	$\mu_i(m, n) = \left(\max_{(k,l) \in \Omega} g(k, l) - \min_{(k,l) \in \Omega} g(k, l) \right) / i$
Gradient magnitude	$\mu_i(m, n) = \sqrt{(\nabla_{x,\delta} \otimes g(m, n))^2 + (\nabla_{y,\delta} \otimes g(m, n))^2}$
Gradient angle	$\mu_i(m, n) = \tan^{-1} \left(\frac{(\nabla_{x,\delta} \otimes g(m, n))}{(\nabla_{y,\delta} \otimes g(m, n))} \right)$

Figure 0- 5: The formulations of measures used in this research.

Results of the research:

The use of multifractal characteristics to characterize histologic texture is more effective. For both the liver and prostate data sample datasets, the suggested feature descriptor has a good classification rate (Around a 95% of classification rate for both liver and prostate data samples).

- **Large intestine (colon) cancer**

Natasa Zivic et al. [7] are analyzing images with the purpose of finding differences between medical images in order of their classifications in terms of separation of malign tissue from normal and benign tissue. Dataset used contain three groups of images tissues (Normal tissue of large intestine (colon), Tissue of large intestine (colon) with diagnose of malign tumors – cancer, Tissue of large intestine (colon) with diagnose of benign tumors – adenomas).

The steps of their multifractal analysis method:

1. Calculating parameters of multifractal analysis for all three group of images
2. Exploring if there are differences of statistical significant between multifractal parameters for previous mentioned groups of tissues. For multifractals analysis of digital medical images and gaining of parameters of multifractals analysis, they have used "FracLac" programs.

Results of the research:

- The reliability of classification between cancer and adenoma groups obtained using the program FracLac was a little bit lower (73%) compared to the obtained result obtained using the program FracLab.
- The parameters of multifractal analysis significantly differ for all three observed groups of normal tissue, cancer and adenoma

- **Breast cancer**

Ramakrishnan Mukundan et al. [8] explored the possibility of using multifractal methods for identifying the statistical characteristics of the image intensity distribution that are important for processing histopathological images. The data set used contained four histopathological image samples; each sample contributes to 250 sub image frames.

The steps of their multifractal analysis method:

The high-resolution high magnification histopathological images are sub-divided into small image frames of size 288*288 pixels.

The α -threshold comparison is applied to separate the sub image frames that contain epithelial type tissues from those containing non-epithelial type tissues.

After that, the system detects the mitosis cells and computes fractal spectrum of the epithelial sub-image frames (Figure 0- 6).

The mitotic cell detection is a method, which is based on the computed α -values within the cell region. They then explore if the NP and TF scores can be estimated from the multifractal spectrum.

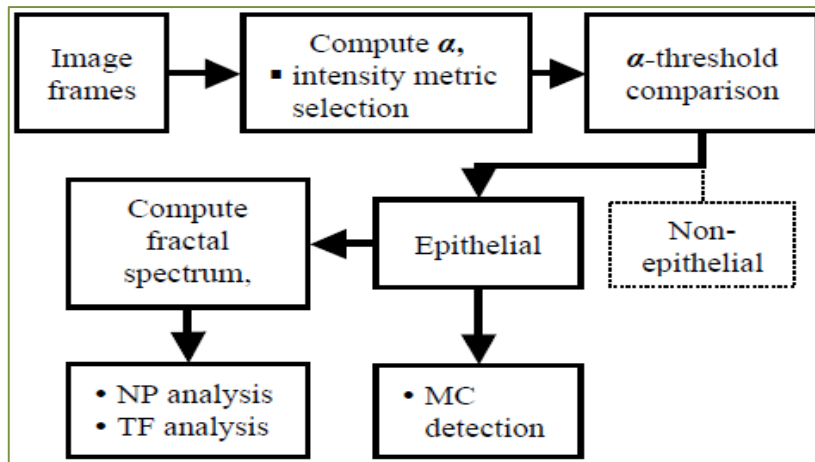


Figure 0- 6: System overview of multifractal analysis of tissue images used.

Results of the research:

- It has been shown that a multifractal decomposition of tissue images could be used for identifying mitotic cells, and for estimating the NP and TF scores.
- The proposed multifractal methods could be combined with algorithms for extracting cytological features for effective classification and segmentation of images of biopsy sections.

Goal of the present Work

The main goal of the present work is to apply the multifractal analysis method in the analysis of the histological images for **thyroid in particular** follicular adenoma and papillary carcinoma. Our program will be executed on the Python programming environment.

We propose a simple, efficient, and effective method using multifractal analysis applied to the characterization and classification of histopathology images. The advantages of our framework include:

- The ability to characterize the singularity of images locally and globally, which solves the problem of the complexity of the clinical feature representation.
- The unified framework on two different thyroid nodules types, demonstrating the efficacy and simplicity of our method.
- This automated analysis system helps pathologists in automatically classifying and differentiating histological images corresponding to follicular adenoma, papillary carcinoma, and healthy thyroid, as well as improving diagnostic efficiency and accuracy.

Work structure

We will present our work in the form of three chapters after a **general introduction**.

Chapter 1

The medical context represented by histology images and the thyroid gland will be defined in the first chapter. Therefore, we divided it into two sections: the first discusses the microscopic image acquisition technology, their methods and some notions of virtual slide technology. In the second part, we will touch on the medical approach to the thyroid gland, dealing with the structure and tissues of the healthy thyroid gland, as well as, we will touch on thyroid diseases, their classification systems such as TIRADS and Bethesda, and finally, we touch the two types of thyroid nodules that we interested on; the follicular adenoma and papillary carcinoma and their macroscopic and microscopic brief descriptions.

Chapter 2

In the second chapter, we define fractal geometry and the Multifractal analysis method (characterization). Thus, we divided this chapter into two sections: In the first one, we present the notions of fractal geometry and fractal analysis as a quick review of basic fractal geometry concepts. We emphasize its peculiarity in comparison to Euclidean geometry, specifically, that it allows us to examine non-rectifiable sets. This section's main objective is to provide a complete explanation of the fractal dimension. As a result, we will focus on the Hausdorff dimension as well as box dimensions. In the second part, we are interested in the Multifractal analysis technique; in the first instance, we will examine its foundations: its uniqueness in relation to measurement theory; the fundamental concept of singularity as measured by Hölder's exponent, the concept of multifractal or singularity spectrum, which provides information on the geometric distribution of singularities.

Chapter 3:

The third chapter presents the work, and each steps we are going to describe the algorithms implemented for multifractal analysis. In addition, we will discuss the result that we obtained. Before this, we will present the database of thyroid samples that we will work on as well as the programming environment and then the general approach proposed.

We conclude by a **general conclusion** with perspectives for improving our work and suggestions for future work are presented.

Chapter I

Medical context

Content

I.1 Introduction..... 4

I.2 Histological techniques and Histology imaging technologies..... 4

 I.2.1 History..... 4

 I.2.2 Histology Definition..... 4

 I.2.3 Histological techniques 4

 I.2.4 The microscope 7

I.3 The Thyroid gland 8

 I.3.1 Anatomy..... 9

 I.3.2 Histology..... 9

 I.3.3 Thyroid Gland Function 10

 I.3.4 Thyroid nodules 11

 I.3.5 Types of thyroid nodules..... 11

 I.3.6 Thyroid nodule diagnostic tools and evaluation methods 12

 I.3.7 Bethesda Classification of Thyroid cytopathology 14

 I.3.8 Follicular adenoma and papillary carcinoma 16

I.4 Conclusion 17

I.1 Introduction

Advances in medical imaging have allowed for the early detection and diagnosis of a variety of ailments in various areas that were previously unattainable. Therefore, in our research project, we are interested in the analysis of histological images of the thyroid with nodules as a pathology. As a point of organization, we have split this chapter into two sections:

The first part introduces histological science; we must have some basic knowledge of histology, one of the most active and technologically advanced fields in medicine. Wherein, it is the study of cells, tissues, and organs as seen through the microscope.

Through the second part, as we are interested in the tissue characterization of histological images for the Thyroid gland. We are going to present the thyroid medical approach to place the application we are working on in its proper context.

I.2 Histological techniques and Histology imaging technologies

I.2.1 History

Malpighi was the "Father of Histology" (1628-1694). The next man to be dubbed the "Father of Histology" was Marie F.X. Bichat, who in 1801, without using a microscope, described 21 different types of tissues. Then, Carl Mayer, a professor of anatomy in Bonn, was the first to use the term "histology" in 1819 [9].

Histology has undergone three revolutions in the last two centuries: the founding revolution based on optical microscopy and cell theory, the revitalizing revolution based on electron microscopy, and the definitive revolution based on molecular biology.

These three critical stages in the history of this field correspond to a dive into ever-finer scales of observation, corresponding to increasingly elementary levels of living organisms [10].

I.2.2 Histology Definition

Histology is the study of the human body's tissues and their arrangement to constitute organs. This subject covers all elements of tissue biology, with a focus on how the structures and arrangements of cells optimize organ-specific activities [11].

I.2.3 Histological techniques

As molecular cell biology and histopathology of biopsied specimens are of the highest importance nowadays, histological techniques are key steps in histology, cell biology, and histopathology.

As mentioned in the definition Histology is the scientific study of tissues. This science studies the anatomy of different tissues using microscopes. Histology, a microscopic biological science, aided in the classification of plant and animal tissues as well as the identification of their detailed structures

Tissue

A tissue, in biology, is a group of similar cells (contributing to the same function) and of the same origin. The assembly of biological tissues constitutes an organ. There are four basic types of tissue: epithelial tissue, connective tissue, muscle tissue, and nervous tissue (Figure I- 1) [12].

Types of human tissue

a) Epithelial tissue (or epithelium): They form the epidermal layer of the skin, which covers the whole surface of the body. Moreover, it covers the surface of organs (e.g., the inner lining of the digestive system). Thus, they protect the organ from external factors, such as injury, and loss of fluids. It also fulfills a variety of functions within the body including secretions and absorption [13].

b) Connective tissue: The main function of connective tissues, as its name implies, is to connect. In addition, protection of soft tissues (e.g., the Skull), transmission of mechanical stress (e.g., the Fascia), also transport (e.g., the Blood), besides, the storage process (e.g., the White fat) [13].

c) Muscle tissue: The ability to contract is the prevailing feature among all muscle tissue. The muscular tissue is classified into three sections (skeletal, cardiac, and smooth). Each sort of muscle cell has its distinct characteristics. Skeletal muscle tissue is necessary for generating forces for movement and locomotion. The heart wall and the proximal sections of the aorta include cardiac muscle tissue .In addition, the walls of blood vessels and visceral organs such as the digestive, urinary, and reproductive systems, a prominent component of which is smooth muscle tissue [13] [14].

d) Nervous tissue: Neurons, or nerve cells, are the cells in nervous tissue that create and conduct impulses. Nerve tissue makes up the brain, spinal cord, autonomic ganglia, peripheral nerves, and portions of sensory organs [13] [14].

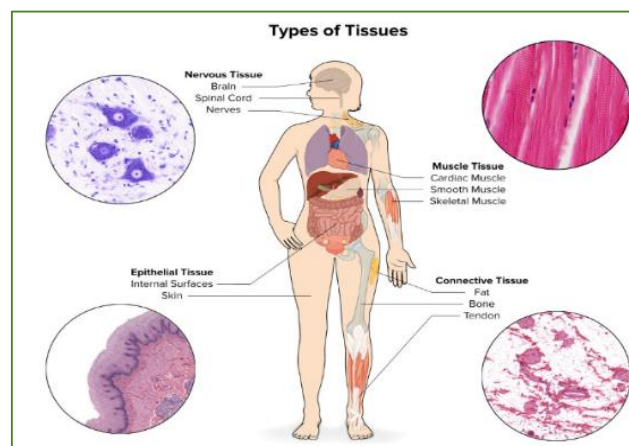


Figure I- 1: Four types of human tissue [15].

Histology Tissue preparation procedures and analysis

The histopathological approach is based on a semiological analysis that compares healthy tissues with pathological tissues. The preparation of tissue slices or sections' is a method employed in histological research.

To examine the tissue's cellular nature, samples must be processed in such a way that microscopic details may be viewed, the basic technique involves several steps: Fixation, Dehydration, Clearing, Infiltration, Embedding, and Trimming (Figure I- 2) [11].

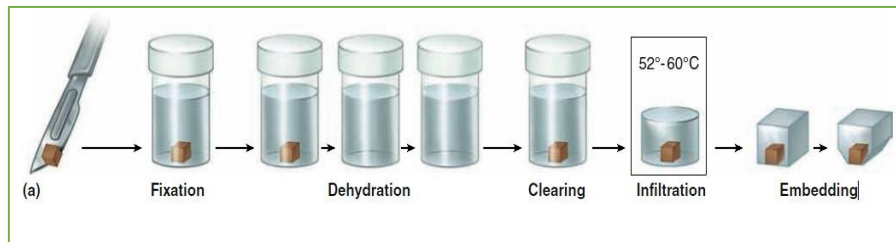


Figure I- 2: Sectioning fixed and embedded tissue [11].

a) Fixation

It is realized by placing small pieces of tissue in solutions of chemicals that cross-link proteins and inactivate degradative enzymes, which is essential to preserve cell and tissue structure, it must be immediate or at least very quickly started after obtaining the Small pieces [11].

Fixation takes between 2 and 5 hours for a biopsy and 48 hours for an operative specimen, depending on the size of the sample. Add the most commonly used fixative for light microscopy is buffered formalin [11].

The samples having completed their fixation are deposited in plastic cassettes, directly if they are biopsies or if they are surgical specimens.

b) Tissue Processing

Processing tissues into thin microscopic sections is usually done using a paraffin block, as follows:

Dehydration: The tissue moved through a sequence of progressively concentrated alcohol solutions. Ethanol (alcohol) is miscible with water in all proportions so that the alcohol progressively replaces the water in the specimen. A series of increasing concentrations is used to avoid excessive distortion of the tissue [11] [16].

Clearing: We use an intermediate solvent that is fully miscible with ethanol and paraffin wax. This solvent will displace the ethanol in the tissue, and then this, in turn, will be displaced by molten paraffin wax. The reagent used is called a "clearing agent", which removes a substantial amount of fat from the tissue [11] [16].

Infiltration: The tissue is then immersed in melted paraffin until it is entirely infiltrated with it [11].

Embedding: The specimen must now be shaped into a "block" that can be clamped into a microtome for section cutting after it has been extensively penetrated with paraffin (Figure I- 3) or plastic wax [11] [17].

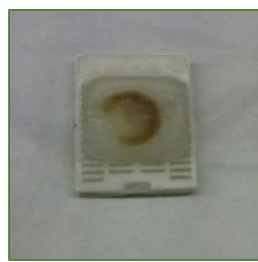


Figure I- 3: Tissue Embedded in paraffin [17].

c) Sectioning

A microtome is a precision cutting instrument that slices sections from a block of embedded tissue. For frozen sections, the section thickness typically ranges from **8 - 15 μm** , for wax sections 4–10 μm , and 0.5–3 μm for plastic histological sections (Figure I- 4). With each pass of the tissue past the knife, it advances the tissue block a preset amount [17].

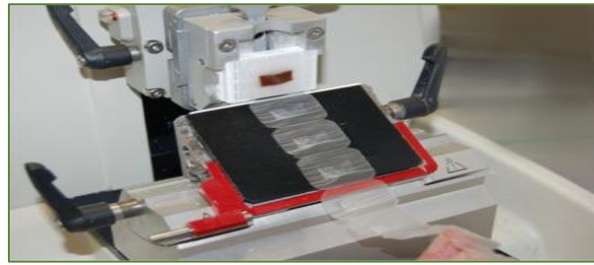


Figure I- 4: Paraffin sections form “ribbons” during the sectioning process [17].

Mounting Tissue Sections: The tissue ribbons transferred carefully to a warm water bath after cutting (Figure I-5). They are allowed to float on the surface before being scooped up and placed on a slide beneath the water level. The best slides for this method are charged slides, which promote tissue adhesion to the glass and limit the risk of sections washing off the slide during staining [18]. After clearly labeling the slides, they should be dried upright at 37°C for a few hours to slowly melt the extra paraffin wax while leaving the tissue segment intact [18].

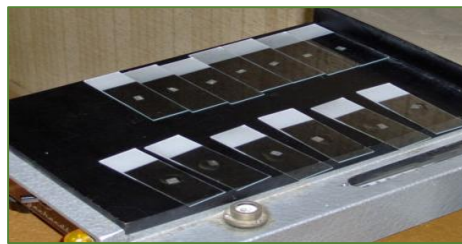


Figure I- 5: Mounting tissue sections [17].

d) Staining and Coverslipping

When not stained, most cells are translucent and seem practically colorless. Histochemical stains (usually hematoxylin and eosin) are used to create contrast to tissue slices, allowing tissue features to be seen and evaluated more easily. After staining, an optical grade glue is used to attach a coverslip over the tissue specimen on the slide to protect it [18].

I.2.4 The microscope

Microscopy is a set of imaging techniques at the microscopic scale is a science that studies the structure and morphological organization of cells using an instrument called the microscope. The word microscope is the source of two Greek words (micros: meaning small, skopos: meaning watcher thus) [19]. The microscope is an extremely useful tool. There are many small objects or details of objects that cannot be seen with the naked eye. The microscope produces images of small objects with high clarity and magnification as well as studies morphological properties at micro- and Nano-scale lengths [20].

The eyepieces, microscope tube, nosepiece, objective, mechanical stage, condenser, coarse and fine focusing knobs, and light source are the essential components of the microscope [21]. There are different microscopes categories available essentially Light and Electronic Microscopy.

Light Microscopy

Light microscopes, also known as optical microscopes, are necessary for histology investigations because they allow us to see cells and morphological characteristics of tissues (Figure I- 6 (A)). To magnify tissue samples, a light microscope uses glass lenses and visible light. It was invented in the sixteenth century [22].

Most microscopes are light microscopes, which illuminate the specimen with a light bulb. The resolution of a light microscope is restricted to 3 micrometers (magnification up to 1500X). After then, two items that are close together no longer appear to be separate [23].

Electronic Microscopy

An electron microscope is an optical tool that magnifies things using a beam of electrons for a more detailed view. Thus, the use of electrons as a source of illumination produces high-resolution images in electronic microscopy (Figure I- 6 (B)). The resolution is around 0.01 nanometers (magnification up to 300,000X) [22] [23].

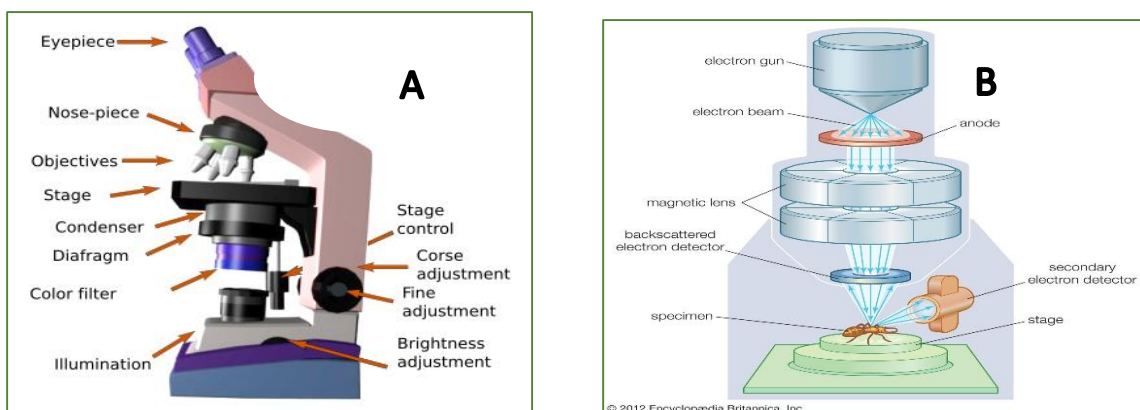


Figure I- 6: (A) Light Microscopy, and (B) Electronic Microscopy [22] [24].

I.3 The Thyroid gland

Histologic tissue characterization is an area of intensive research, aiming at complementing the visual observation of histological images with quantitative information about the tissues.

In this project, we are interested in the tissue characterization of histological images for the Thyroid gland.

The thyroid is an endocrine gland; it releases hormones that regulate metabolism, or the body's energy utilization. Thyroid hormones control many important bodily functions, including (Respiration, heart rate, central and peripheral neurological systems...etc.) and other factors are all important.

The thyroid gland can be affected by a variety of disorders, including nodules, hyperthyroidism, hypothyroidism, thyroiditis, and hyperthyroidism [25].

I.3.1 Anatomy

The thyroid is a butterfly-shaped gland that sits low in the front of the neck (just below Adam's apple). It has two side lobes (left and right) of elongated shape connected by an isthmus (Figure I-7). These lobes are attached to the lateral surfaces of the larynx and the trachea. They are enveloped by a conjunctive capsule dependent on cervical Aponeurosis. A third, inconstant lobe is located on the anterior surface of the trachea it is called the Lalouette pyramid [26] [27].

The thyroid, weighing 20 to 30 g, is a lobulated-looking gland, architecturally organized into follicles or vesicles. Its volume is highly variable among individuals, depending on morphotype, age, sex, and iodine load. The consistency of the gland is soft and elastic, also characterized by its reddish color [28].

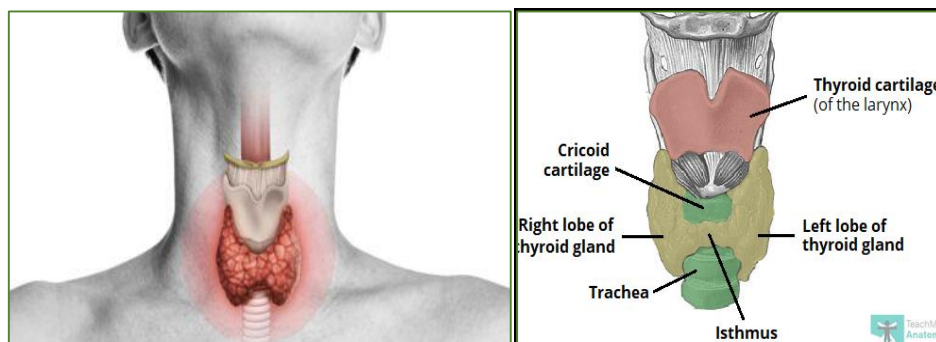


Figure I- 7: thyroid gland anatomy [27] [26].

I.3.2 Histology

A thin capsule, made of fibrous connective tissue, covers the thyroid and penetrates the glandular parenchyma, which divides the thyroid gland into lobules by incomplete partitions. Each thyroid lobules contains 20 to 40 round to oval follicles [29] [25].

Thyroid vesicles or follicles are responsible for the synthesis and release of thyroid hormones. Furthermore, they are spheres containing a homogeneous colloid, bounded by a simple epithelium (follicular cells), representing the structural and fundamental units of the thyroid parenchyma. In addition, a thin connective tissue stroma containing lymphatic vessels, blood vessels, and nerves separate the thyroid follicles [29].

Thyroid is the source of Thyroid hormones (T3 and T4) by follicular cells (also called thyroid epithelial cells or thyrocytes). Add, Calcitonin (hypocalcemic hormone) by C cells, clear cells, or parafollicular cells. These hormones are necessary for all cells of the body to function normally [29].

Thyroid vesicles (Follicles)

Thyroid vesicles are the functional units of the gland. These have a lining and glandular epithelium formed of a single layer of cubic, squamous, or columnar cells, heir structure varies depending on where they are located in the gland and what function they perform. Regardless of regional differences, thyroid activity can be determined by the appearance of all vesicles. The epithelium of the vesicles is made up of follicular and parafollicular cells (Figure I- 8) [29].

a) Follicular cells

Follicular cells form small round structures called follicles, in which, the thyroid hormone is stored in a material called colloid that fills the center of the follicles. These cells are in contact with the colloid on one side and the capillaries on the other (polarized) [29].

The iodine in the blood is absorbed by the follicular cells, which then produce the hormones T4 (thyroxine) and T3 (triiodothyronine). These two hormones are secreted under the dependence of the pituitary hormone TSH (Thyroid Stimulating Hormone). The latter is under the control of TRH (Thyrotropin-Releasing Hormone) [29].

b) Parafollicular cells or C cells

The clear cells, also known as C cells or calcitonin cells are the thyroid's second type of endocrine cells. Between the follicular epithelium and the basement membrane. These cells their nucleus is pale and ovoid, their cytoplasm is clearer than that of follicular cells, hence their name. Furthermore, C cells are embedded in the follicular epithelium but never meet the colloid. In addition, in the usual histological preparations, the C cells are difficult to recognize [29].

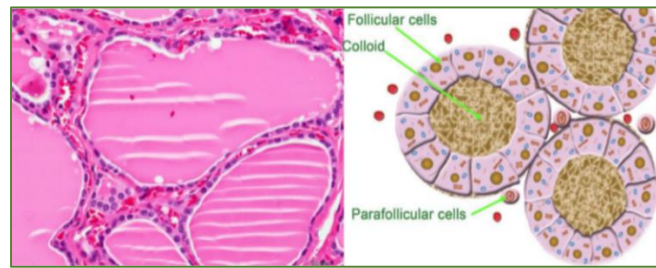


Figure I- 8: Thyroid Follicles and thyroid parafollicular or C cells [30].

I.3.3 Thyroid Gland Function

The thyroid is part of the endocrine system, which consists of glands that produce, store, and release hormones that regulate metabolism, or the body's energy utilization. Thyroid hormones control a number of important bodily functions (Respiration, heart rate, central and peripheral neurological systems, and other factors are all important, etc.). The thyroid gland uses iodine to produce two main hormones: Triiodothyronine (T3) and Thyroxine (T4) [31].

It is critical that T3 and T4 levels are not excessively high or excessively low. The hypothalamus and pituitary glands in the brain communicate to keep T3 and T4 levels balanced. TSH-releasing hormone (TRH) is produced by the hypothalamus and signals the pituitary to tell the thyroid gland to produce more or less T3 and T4 by increasing or decreasing the release of thyroid-stimulating hormone (TSH) [31]. When T3 and T4 levels in the blood are low, the pituitary gland secretes more TSH, which signals the thyroid gland to produce more thyroid hormones (Figure I-9). Conversely, when T3 and T4 levels are high, the pituitary gland sends less TSH to the thyroid gland, slowing the hormone's production [31]. Calcitonin is a hormone produced by thyroid C cells that helps regulate blood calcium levels. It accomplishes this by slowing calcium release from the bones and increasing calcium excretion into the urine by the kidneys [31].

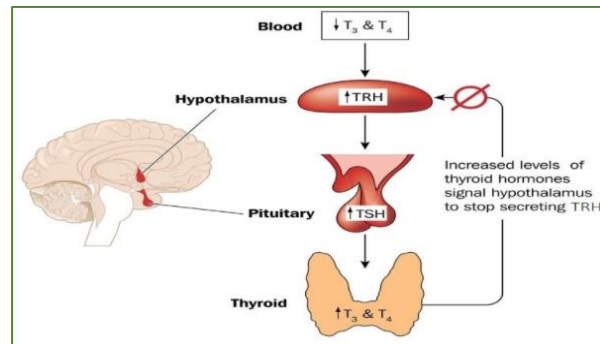


Figure I- 9: T_3 , T_4 , and TSH secretion systems [32].

I.3.4 Thyroid nodules

The thyroid gland affected by a variety of disorders (Thyroid nodules, hyperthyroidism, hypothyroidism, thyroiditis, and hyperthyroidism... etc.). Thyroid nodule genesis may be considered as an amplification of thyroid heterogeneity. Lumps or growths of the thyroid (Figure I-10), usually made up of normal thyroid tissue or fluid, frequently discovered on routine physical examination or imaging tests [33] [34].

Thyroid nodules are tumors of the thyroid gland that can be benign or malignant (cancer). They occur frequently and their frequency increases with age. Undoubtedly, the prevalence of nodular thyroid disease has increased over time, because of advancements in imaging technology. Likewise, the four major components of thyroid nodule assessment: clinical history and examination; serum thyroid-stimulating hormone (TSH) measurement; ultrasound; and fine-needle aspiration (FNA) if needed [34].

Most benign nodules have no known cause, however, they are frequently observed in members of the same family. Iodine deficiency is a common cause of nodules all over the world. Thyroid nodules grow increasingly common, as people get older [35].

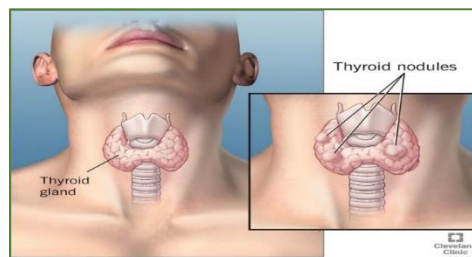


Figure I- 10: Thyroid nodules in the thyroid gland [36].

I.3.5 Types of thyroid nodules

Thyroid nodules are classified into five types with distinct histological features: hyperplastic, neoplastic, colloid, cystic, and thyroiditis nodules [37]. In general, thyroid nodules may be a benign nodules or malignant nodules.

Hyperplasia: Nodular thyroid hyperplasia is a non-cancerous development that affects the thyroid gland. One-half of the gland (one lobe) or the entire gland can be affected by abnormal growth (both lobes and the isthmus). This type is the most common cause of nodules in the thyroid gland [37].

Neoplastic: Neoplasms are abnormal mass of tissue that form when cells divide too fast or die too soon. Thyroid neoplasm might be classified as benign (non-cancerous) for example Thyroid adenoma, or malignant (cancer) such as papillary, follicular, and medullary. Malignant neoplasms can spread to other parts of the body through the blood and lymph systems [37].

Colloid: There are one or more overgrowths of normal thyroid tissue. These growths are benign (non-cancerous). They may grow to be enormous, but they never expand beyond the thyroid gland [37].

Cystic: These growths are filled with fluid or partly solid and partly filled with fluid. Overall, these growths are benign (non-cancerous) [37].

Thyroiditic: Nodular lymphocytic thyroiditis (NLT) is an inflammation of the lymphatic system in the thyroid, which grows as a nodule in a hyperplastic or normal gland. It can be associated with other nodular diseases of the thyroid such as papillary thyroid carcinoma and lymphoma [37].

Depending on whether or not they generate thyroid hormones, thyroid nodules are classified into three types: cold, warm, or hot: cold nodules do not produce Thyroid hormones. Warm nodules act as normal thyroid cells. Thyroid hormones are overproduced in hot nodules [38] [39].

I.3.6 Thyroid nodule diagnostic tools and evaluation methods

When a doctor examines a mass or nodule in the neck, the main purpose is to rule out the possibility of cancer. However, the doctor would want to ensure that the thyroid is functioning appropriately. Several examinations are available to determine the exact nature of the thyroid nodule.

Therefore, the doctor might recommend one or more of the following tests:

Anamnesis and clinical examination

The clinician will carefully examine the anterior cervical region, as well as the lymph node areas. He will note the location of the nodule, its consistency and size. The doctor will also look for any signs and symptoms of an overactive thyroid, such as tremors, hyperactive reflexes, and a fast or irregular heartbeat.

Moreover, he will also check for signs and symptoms of hypothyroidism, such as a slow heartbeat, dry skin, and facial swelling [40]. Upon this, the doctor must use a blood test to determine the irregularity in terms of secretory hormones.

Laboratory tests

Tests that measure levels of **thyroid-stimulating hormone (TSH)** and hormones produced by the thyroid gland in the blood, which indicate whether the patient has hyperthyroidism or hypothyroidism. In the case of patients who are consulting for thyroid nodules, it has been shown that the risk of cancer is higher if the TSH is within the high values of normal (normal values; 0.4 à 4 mUI/l.), and lower in the case of low normal values [40] [34].

Although not systematically recommended, the detection of **antiperoxidase antibodies** makes it possible to exclude chronic thyroiditis.

The **thyroglobulin** assay isn't recommended in the development of thyroid nodules but is only useful in the follow-up of patients operated on for thyroid cancer. **Calcitonin** is useful in the initial evaluation of thyroid nodules and before surgery. If calcitonin is higher than normal, a calcium stimulation test will help refine the diagnosis [40] [34].

However, the blood tests are not enough to test for thyroid cancer. To gather more information about the nodule, the doctor might recommend one or more of the following tests.

Thyroid ultrasound

Ultrasonography (US) is a reference test for the investigation of thyroid morphology, particularly nodules. Clinicians can use them to differentiate cysts into solid nodules or to determine if there are multiple nodules. They may also use them as a guideline during a fine-needle aspiration biopsy.

The role of the ultrasonography in the case of the nodular pathology is for a more accurate diagnosis and study the adjacent thyroid parenchyma, look for other associated subclinical nodules, and specify the characteristics of the nodular formations detected [34].

There are three modes of medical ultrasonography (US). The first one is the B-Mode, which measures the acoustic impedance and displays the anatomy. The second mode is the Doppler, which measures the motion and displays the vascular flow. The last mode is Elastography, which measures the mechanical properties and displays tissue stiffness [34].

The technique used in ultrasonography imaging of the thyroid nodules is that the operator use a lower frequency probe (10–15 MHz) to measure a large goiter or to study endothoracic extension. The examination includes a study in three modes mentioned above [34]. The operator must be educated and trained in thyroid ultrasound to provide detailed and informative reports that contain (location, nodule size in three dimensions, nodule sonographic features: “composition, echogenicity, shape, margin, halo, calcification, and vascularity”). With which, the clinician can assess the risk of a cancerous nodule [39] [34] [41].

The ultrasound study completes the clinical, biological and possibly scan evaluation of the nodules. It does not allow, or rarely, to affirm independently of the other evaluations the nature of a nodule [34].

Thereby appeared the *thyroid imaging reporting and database system* (TI-RADS). It has then been adapted, refined, and evaluated in order to be easily usable in routine by radiologists and clinicians; this system describes six categories of nodules (Table 1), associated with an increasing level of malignancy risk [34] [42].

Table I- 1: stratification of the risk of malignancy according to (TI-RADS) score [26].

TI-RADS score	Signification	Risk of malignancy (%)
TI-RADS 1	Normal exam	
TI-RADS 2	Benign	≈ 0
TI-RADS 3	Most likely benign	0.25
TI-RADS 4A	Low suspicion of malignancy	6
TI-RADS 4B	Strong suspicion of malignancy	69
TI-RADS 5	Practically definitely malignant	≈ 100

Additional medical examinations may be recommended based on the results.

Thyroid scan

For hot nodules with low TSH, a scan to visualize the functioning of the thyroid and detect if the nodule secretes thyroid hormones [39].

The scintigraphy will show the distribution of the tracer and will guide the gesture of the puncturer (Figure I-11), who will avoid stinging in hot and/or hyperfixing areas, which will give an automatically very cellular cytopuncture [34].

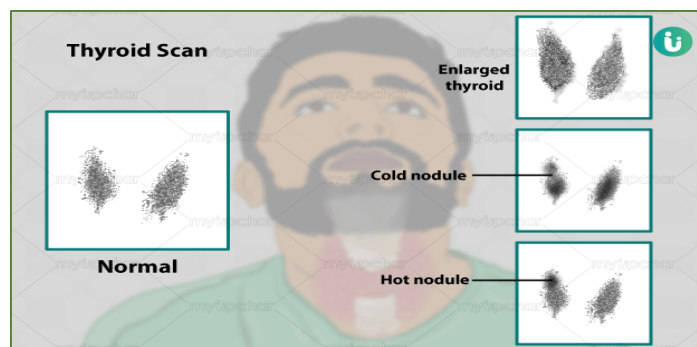


Figure I- 11: Thyroid Scan [43].

Fine-needle cytopuncture

For cold nodules with normal TSH, simple medical surveillance or cytopuncture (biopsy) of the nodule using a fine needle to remove cells from the nodule and analyze them in the laboratory [39]. Thyroid cytology helps distinguish benign thyroid nodules from thyroid cancer [40].

I.3.7 Bethesda Classification of Thyroid cytopathology

Thyroid cytologies are classified according to a six-category system established in 2007 at Bethesda [40] [34].

Each category contains a number of cytological diagnostic orientations, each of which is associated with an individual's risk of developing cancer. This classification accounts for the ambiguities of cytology and has the benefit of directing the clinician's therapeutic decision [40] [34].

Table I- 2: Thyroid cytopathology: Bethesda system 2010 [40] [34].

Categories (prevalence)	Subcategories	Risk of cancer	To behave
Bethesda I Sampling unsatisfactory / non-diagnostic (< 15 %)		Not evaluated	Solid nodule: 2 nd cytopuncture at 3 months Cystic nodule: to be correlated with the clinic and ultrasound (cytopuncture).If suspicious areas remain
Bethesda II Benign (60 %)	Vesicular adenoma Vesicular colloid nodule hyperplasia Thyroiditis	0 - 3%	Simple ultrasound control at 6-18 month intervals for 3 to 5 years
Bethesda III Significance follicular Lesion indeterminate (< 7 %)		5- 15%	2 nd cytopuncture within 3 to 6 months under ultrasound guidance
Bethesda IV Follicular tumor (neoplasm) (6-11 %)		15-30 %	Surgical control (lobectomy)
Bethesda V suspected of malignancy (2-8 %)	Papillary carcinoma Medullary carcinoma Poorly differentiated carcinoma	60-75 %	Surgical control (total thyroidectomy or lobectomy)
Bethesda VI Malignant (5-8 %)	Anaplastic carcinoma Metastases Lymphomas	97-99 %	Surgical control (total thyroidectomy) or specific medical treatment (radiotherapy ± chemotherapy)

Thyroid nodules are common diseases presented in the clinic, and their pathological types are complex.

This research project sheds light on the classification of two types of nodules, which are follicular adenoma and papillary carcinoma.

Therefore, we describe the histological aspect as well as the characteristics of these two nodules in order to do this.

I.3.8 Follicular adenoma and papillary carcinoma

A follicular adenoma is a benign tumor of the thyroid that is entirely enclosed by the capsule. A carcinoma is a thyroid tumor that has invaded the capsule and is malignant.

Follicular adenoma

Follicular cancers (Benign tumor of thyroid) are cancers of follicular origin, not having the characteristics of papillary cancer, and which can resemble the normal thyroid (Figure I-12). Follicular cancer is often unifocal, lymph node metastases are infrequent, and distant metastases are located in the lungs and bones. Hürthle cell cancer is composed of more than 75% oxyphil (or oncocytic) cells; the malignancy criteria are the same as for follicular cancers, and the prognosis is determined by the same factors as for follicular cancers. It is a firm tumor, homogeneous or oval surrounded by a thin fibrous capsule [44].

Microscopically, it is a very well encapsulated tumor, enveloped by a thin fibrous capsule. In addition, the tumor is composed of closely packed follicles. Furthermore, there are different patterns, like Normofollicular (the follicles will be of normal size), micro-follicular (follicles will be very small), also known as the fetal type. Macrofollicular (the follicles are large and colloid-filled). Moreover, the lining epithelial cells are low cuboidal to columnar and have a regular nucleus. Also, the surrounding thyroid will show compressed follicles [45].

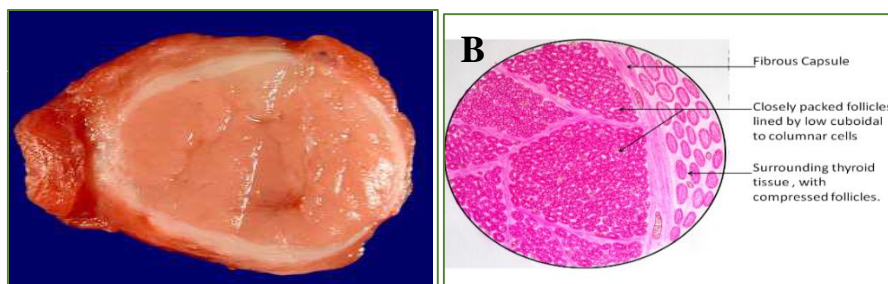


Figure I- 12: (A) the macroscopic and (B) microscopic appearance of a follicular adenoma [46].

Papillary thyroid carcinoma (PTC) is the most frequent type of malignant thyroid tumor, accounting for around 80% of all thyroid cancers. Histologically, papillary thyroid carcinomas can have a papillary, solid, or follicular architecture [47].

According to the WHO (World Health Organization) definition, papillary carcinoma is a malignant epithelial tumor of the vesicular strain with unique nuclear features (Figure I-13) [33].

Macroscopically, papillary carcinomas are variable in shape and size ranging from less than a millimeter to several centimeters and can be uni or multifocal. They are frequently firm, grainy in appearance, greyish-white, or buff for the oxyphilic forms, and poorly limited [33].

Microscopically, as the WHO definition states, the nuclei of the cells constituting the papillary carcinomas have characteristic aspects. They have sinuous contours and an appearance with edges that are not round. These nuclei appear as 'coffee beans' and accumulate as 'roof tiles', they are enlarged, rounded, and oval or elongated. Concerning the nuclear membrane, chromatin condensation thickens it irregularly and nuclei pressed on it [33].

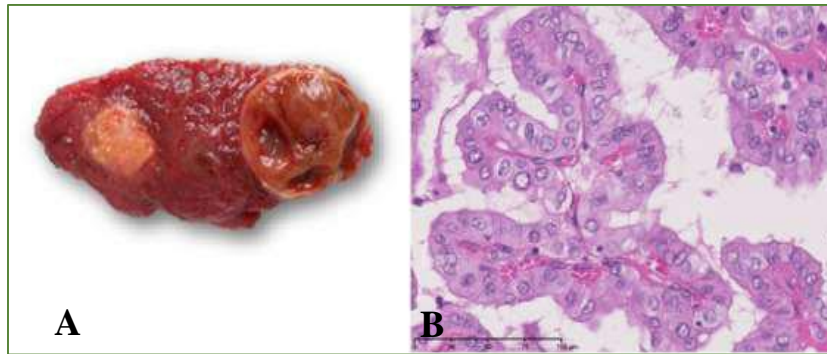


Figure I- 13: (A) the macroscopic and (B) microscopic appearance of a papillary carcinoma [46].

I.4 Conclusion

In this first chapter, we presented our medical context. After an introduction to the chapter, and a brief history of histology, its definition, and its techniques, we have detailed the technique for preparing histological samples. We talked about the microscope. Thus, we presented in the second part the thyroid gland and its histology, and we presented the nodules and their method of diagnosis. Finally, we addressed the two types of pathology that we had selected namely follicular adenoma and papillary carcinoma.

In this project, we are interested in the tissue characterization of histological images for the Thyroid gland. Histologic tissue characterization is an area of intensive research, aiming at complementing the visual observation of histological images with quantitative information about the tissues. Tissue and cell image analysis is difficult and time-consuming. Because they have irregular shapes; they are different sizes and have different orientations. As a result, performing such complex tasks necessitates techniques that are more advanced than traditional image analysis methods. As a reason, we will use a novel method of analysis called Multifractal analysis that we will discuss in the following chapter.

Chapter 2

Fractal Geometry and Multifractal Analyses of images

Content

II.1 Introduction	20
II.2 Fractal geometry and dimensions.....	20
II.2.1 History of Fractal geometry.....	20
II.2.2 Fractal geometry and Fractal objects.....	22
II.2.3 Properties of fractal objects	22
II.2.4 Examples of some famous fractal structures	23
II.2.5 Fractal and dimensions	24
II.2.6 Fractal dimension computing methods.....	26
II.3 Multifractal Analysis.....	30
II.3.1 Multifractal History	30
II.3.2 Methods of multifractal analysis	31
II.3.3 Concept of measure	31
II.3.4 Hurst exponent and fractal dimension	31
II.3.5 Local behavior: Hölder exponent (α -value).....	32
II.3.6 Multifractal measures	32
II.3.7 Holder image (α -image)	33
II.3.8 Global behavior: Multifractal Spectrum (Singularity spectrum).....	34
II.3.9 Methods for Multifractal Spectrum calculation.....	35
II.4 Conclusion.....	37

II.1 Introduction

Traditional object descriptions based on the well-known Euclidean geometry are incapable of expressing a variety of natural objects and events. The mathematician Benoît Mandelbröt in about 1970 invented a new geometry, which is Fractal geometry that facilitates the study of objects that has complex geometric shapes.

Fractal geometry is widely used in medical image analysis problems, as it finds different applications and provides diverse results. Specifically, it is used in the analysis of histological images, where the analysis of tissues and cells is difficult and time-consuming due to their complex and irregular shapes, which requires more advanced techniques than traditional image analysis methods. This chapter attempts to review fractal geometry and Multifractal analysis. As a point of organization, we have split this chapter into two sections: in the first one, we present the fractal objects, their notion of dimensions, and their methods of calculation. Through the second part, we are interested in the Multifractal analysis.

II.2 Fractal geometry and dimensions

II.2.1 History of Fractal geometry

Geometry derived from the Greek words "geo" (meaning earth) and "metrein" (meaning "to measure"). Euclidean geometry is the traditional way of studying geometrical shapes and figures formed by the use of lines and circles. "Euclid geometry." named after the Greek mathematician **Euclid d'Alexandrie** (around 300 BC) [48]. **Apollonius** in the 3rd century BC came up with the notion of merging three circles into a fourth. Then, when space permitted, he fills it with more tangent circles, etc., in an attempt to fill the "contained" circle, which is impossible to do. He thus touched infinity. In doing so, he uncovered the "baderne of Apollonius," the earliest known fractal object in human history [48] [49] [50]. **Albrecht Dürer** published another fractal artwork in 1520 that specifies how to make his pentagons, and Sierpinski will pick up where he left off [51].

Johannes Kepler realized that the planets orbit the sun in ellipses rather than circles. Afterwards, **Edmond Halley** had assumed that these orbits could be explained by an analogy with light, using the inverse square law. Subsequently, **Isaac Newton** devised a new approach known as infinitesimals, and he came up with his renowned theory of universal gravitation in the end. Simultaneously, **Gottfried Leibniz** invented the most concise version of differential calculus, whose tools are differentiation and integration [48]. **Pierre-Simon Laplace** asserted that using this type of calculation in the case where the exact location of each known particle could predict the future of the entire universe. The differential calculation approach used on straight or curved lines. After that, **Karl Weierstrass**, **Georges Cantor**, and **Henri Poincaré** established a new geometry to study the irregular and rough characteristics [48](Figure II- 1).

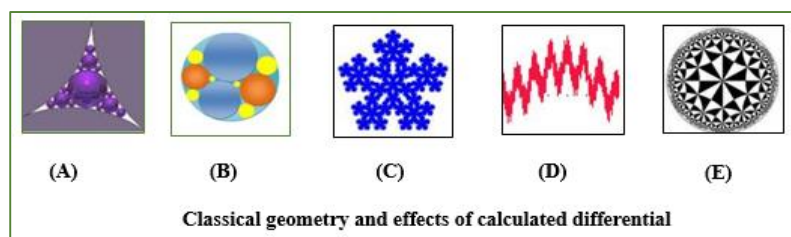


Figure II- 1: (A) and (B): baderne of Apollonius, (C) Albrecht Dürer pentagons, (D) and (E) represent a new geometry by Karl Weierstrass and Henri Poincaré respectively [48].

A huge number of mathematicians attempted to create artificial fractals bearing their names. In 1883, **Georg Cantor** discovered a set that was fractal in nature and named after him (Cantor dust). The curve of Peano is one of the fractals shape. In 1891, an analysis professor **Giuseppe Peano** found a curve that covered all of space. It does not omit any points of the plane. In 1900, **David Hilbert** designed his curve, which is a one-dimensional curve that fills an entire two-dimensional space. Following that, in 1904, **Helge von Koch** designed The Koch Snowflake, which is a fractal curve. After that, **Paul Lévy** proved that dimension is a continuous topological invariant in 1911. In addition, he described the properties of self-similarity and showed its geometry [48]. A few years after, separately in about 1914, **Gaston Julia** and **Pierre Fatou**, they researched the translation of the plane of complex numbers using iterative functions. The transformation results in an image of the initial position. Their work is known as the Julia set. In 1916, **Vaclav Sierpinski** proposed a new fractal: the Sierpinski triangle also called Sierpinski gasket or Sierpinski sieve. In 1919, **Felix Hausdorff** pioneered a new method of thinking about dimensions, introducing the fractal dimension, which accepts non-integer values. In 1926, **Karl Menger** made a 3D extension of the Cantor collection or the Sierpinski [48](Figure II- 2).

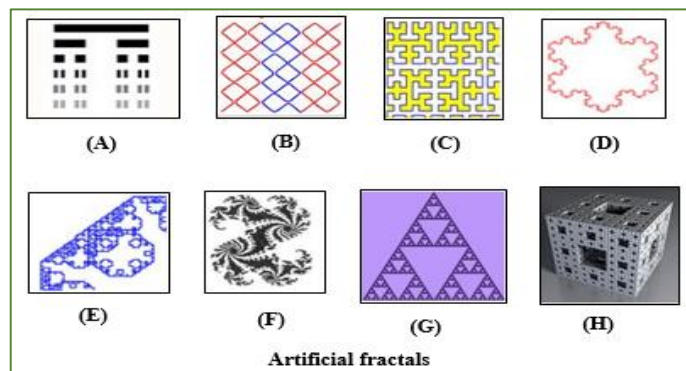


Figure II- 2: artificial fractals from (A) to (H) respectively (Cantor dust, Giuseppe Peano curve, David Hilbert curve, Paul Lévy curve, Gaston Julia and Pierre Fatou fractal image, the Sierpinski triangle, Karl Menger 3D extension of the Cantor collection) [1].

Lewis Fry Richardson was interested in the length of British shores in 1926. He concluded that it depended on the size of the ruler. The length will be unlimited if the size of the ruler is infinitely small. In fact, the length of the boundary is fractal. This work related to fractals and a method for solving a system of linear equations known as the modified Richardson iteration [48].

The history of fractals dates back to 1975 when **Benoît Mandelbrot** The father of fractal geometry coined the word fractal. He discovered that the errors were fractal in nature. Furthermore, he was acquainted with Julia and Fatou's works and used computers to exploit them [48]. Benoît Mandelbröt used the concept of fractals to demonstrate that irregular objects and chaotic phenomena, in general, are interesting and can be studied in a non-reductive way that takes into account their complexity [52] [53](Figure II- 3).

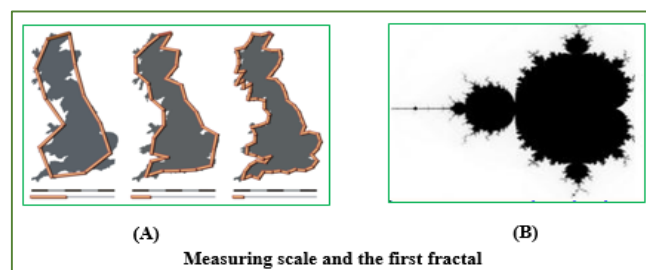


Figure II- 3: (A) length of British shores quantified in different size of the ruler, (B) Mandelbröt set [48] [54].

II.2.2 Fractal geometry and Fractal objects

As fractal geometry belongs to the geometric field, then, it is concerned with the study of the shape and spatial relationships of points, lines, surfaces, volumes, etc., which are referred to as "objects" or "sets". In the context of image analysis, these sets are a collection of points from a binary image, i.e., we can say whether or not a point in the image belongs to the set (the spatial distribution of the points that comprise the object) [55].

Fractal geometry provides a powerful tool for exploring the world of non-integer dimensions. Monofractals, Multifractals, and self-affine fractals are the three most prevalent fractals. A monofractal object is a simple self-similar fractal with only one scaling factor, whereas a Multifractal object is a complicated fractal system with at least two scaling factors for separate regions. A self-affine fractal has various scaling factors in different development directions or at different scale levels, as well as, they are frequently classified as Multifractals [56].

Fractal is coined from the Latin word fractus. The Latin verb "frangere" correspondent stands for "to break:" to create irregularly shaped fragments. In addition to "fragmented," fractus should also mean "irregular," with both meanings preserved in fragment. The proper pronunciation is frac'tal, the stress being placed as in frac'tion [52].

"Bottomless wonders spring from simple rules, which are repeated without end." – *Benoît Mandelbröt*

A fractal is an object composed of several sub-objects, or a mathematical object, such as a curve, an irregular surface, or even a volume, results from an iterative process and, presents a character self-similarity. Moreover, can be built using accurate or random rules [51] [57].

"Fractal is a structure, composed of parts, which in some sense similar to the whole structure" – *Benoît Mandelbröt*

II.2.3 Properties of fractal objects

The term fractal, which can be geometrical or statistical, is the fundamental idea of fractal geometry. According to Mandelbrot's theory, fractal objects have the following characteristics: Primarily, they have self-similar behavior; it is the most important property of fractals [58] [59] [60]. It defines structures that appear very similar at different scales. This means that when a portion of the structure is removed and compared to the entire structure, they are identical (Figure II- 4). As well as, they do not have a specific (finite) length; the object's level of detail is infinite. Besides, it is far too irregular to be described in traditional Euclidean geometric terms, either extremely interrupted or fragmented. What is more, it has a recursive and easy definition, and its dimensions are not integers. Because of their complications, computers are required for their studies [61] [62] [63].

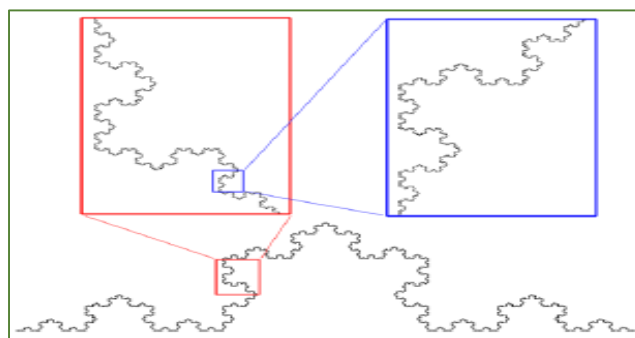


Figure II- 4: Self-similarity of Von Koch curve [64].

II.2.4 Examples of some famous fractal structures

These irregular geometrical objects can be classified into two distinct categories. The first category is deterministic fractals; these fractals are pure mathematics and self-similar. The second one is probabilistic fractals, which are fractals created by random processes [48]. In the following we will give some examples of deterministic fractals.

a) The Cantor set

Georg Cantor discovered this fractal set in 1883, many fractal figures, such as the Cantor dust and the Koch curve, as well as the Sierpinski triangle, have their origins in the Cantor set. The method followed to create it is given in the following steps mentioned: Take a segment, and remove its central third. Then, take the central third of each of the two remaining segments and remove it. Etc. (Figure II- 5). Continuing, we form dust of points, there is an infinity of them and the total length is zero. However, the quantity of dashes increases until it becomes uncountable like the infinity of real numbers [48] [65] [66].

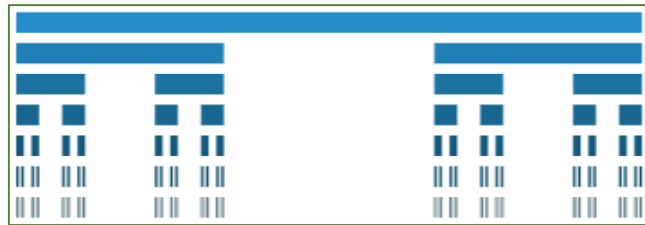


Figure II- 5: the six first iterations of the CANTOR SET structure [66].

b) Von Koch curve

Helge von Koch designed the snowflake curve in 1904, a transformation rule: The **Koch curve** corresponds to the transformation of a single segment (Figure II- 6), created by substituting a single straight-line segment with a pattern of several line segments. Then, the pattern's line segments are then substituted with the same pattern [66].

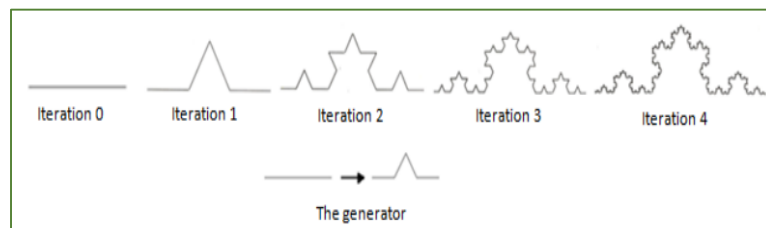


Figure II- 6: the four iterations of the KOCH Curve [66].

Regarding the **Koch snowflake** is the figure formed on an initial equilateral triangle (Figure II- 7), created by Replacing the middle third of each segment with an equilateral triangle with no base. In which this operation is repeated on the figure obtained; and, this, as a number of times needed [48] [65] [66] [67].

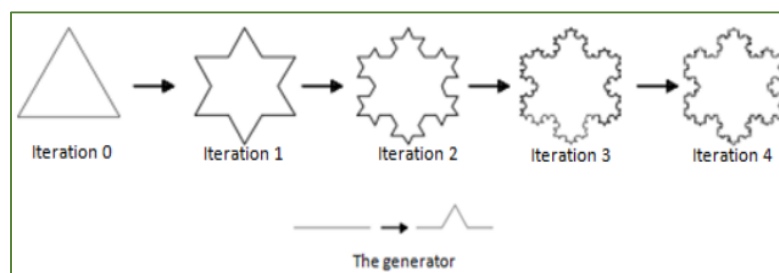


Figure II- 7: the four iterations of the KOCH Snowflake [66].

c) The Julia and Mandelbrot sets

Gaston Julia (French mathematician born in Algeria) published his work in 1918: research on the iteration of rational functions. Through it, he underscores what is known today as Julia sets. He had imagined them but had never seen them for lack of means of calculation such as computers. Julia becomes famous, but his works will wait about fifty years before being exploited by B. Mandelbrot in 1975 [48].

The Mandelbrot set is the most famous object in modern mathematics. It is also a breeding ground for the world's most famous fractals. B. Mandelbrot represented this set for the first time in 1978. The set itself is an infinite swarm of odd-shaped points clustered on "complex number plane". This classic fractal figure, obtained very simply, it describes the convergence of the recursive function used by Julia [48] [68]:

$$Z_n = Z_{n-1}^2 + C \tag{1}$$

The function's new value (Z_n) is equal to the function's old value (Z_{n-1}) squared plus a constant ($C = A + i B$).

If $Z_0 = \text{zero}$ The Mandelbrot set is the set of complex plane points C such that the sequence does not tend to infinity (Table II-1)(Figure II- 8).

Table II- 1: Differences between Gaston Julia set and the Mandelbrot set [48].

	Gaston Julia set	the Mandelbrot set
We fix	C	Z_0
The recursive function used	$Z_n = Z_{n-1}^2 + C$	$Z_n = Z_{n-1}^2 + C$
scan all the values of	Z_0	C
sometimes, the value of Z_n bounded	We draw Z_0 all the points for which the sequence is bounded.	We draw C all the points for which the sequence is bounded.

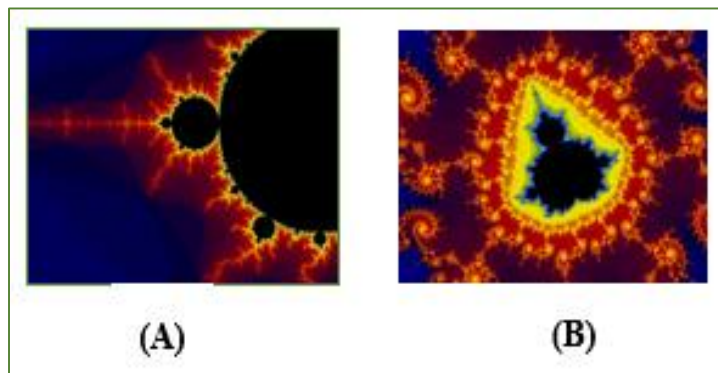


Figure II- 8: Mandelbrot set: (A) the set appears in black, with the fractal boundary alive with color,

We will develop below some examples of fractal analysis tools such as fractal dimensions.

II.2.5 Fractal and dimensions

Dimensions are different measurements that have traditionally been used to describe objects and phenomena. When we talk about dimensions in antiquity, we mean the height, length or width of an object. The most well-known dimension is the Euclidean one D_E and the second is known as the topological dimension D_T . In most circumstances, they can be used as synonyms because many objects could be the same thing. However, we will briefly mention some differences (Table II-2) (Figure II- 9). The topological dimension is defined by how an observed object can be divided, whereas the Euclidean dimension is determined by the space filled by an object [69] [70].

Table II- 2: Some differences between topological and Euclidean dimensions [69] [71].

The topological dimensions D_T	The Euclidean dimensions D_E
The point topological dimension $D_T = 0$	The point Euclidean dimension $D_E = 0$
The line can be divided by dashed points $D_T = 1$	The straight line is one dimensional $D_E = 1$
To divide surfaces, curves are necessary $D_T = 2$	The curve line lying in the plane $D_E = 2$
To divide space, surfaces are necessary $D_T = 3$	The complex curve in space is three-dimensional $D_E = 3$

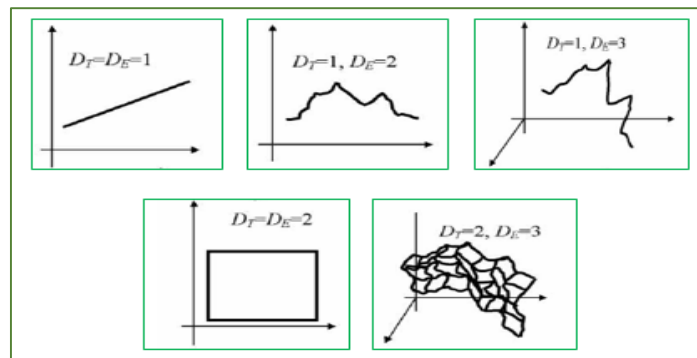


Figure II- 9: Examples illustrating the distinctions between topological and Euclidean dimensions [69].

Returning to our running examples, when dealing with the self-similarity of fractals with intricate and irregular geometric structures, classical geometry or an integer dimension are not suitable. In this case, a new mathematical method is used to evaluate the complexity of geometric figures using a single parameter, known as “fractal dimension D_F ” or “Hausdorff dimension D_H ” also called “Self-similar dimension D_S ;” is a concept applicable only to deterministic self-similar fractals [72] [69].

A fractal dimension “Hausdorff dimension D_H ” is a number that quantifies the degree of irregularity and fragmentation of a geometric set. It characterizes the self-similar behavior of the surface. Furthermore, it estimates the change in a set's size based on the unit of measurement [73] [74]. Fractal dimension can be defined as follows. Let d be the dimension of a fractal object in the Euclidian space. We cover this object with balls of diameter r such that each point of the object is inside one of the balls. We estimate that this requires at least $N(r)$ balls. If, for a sufficiently small r , $N(r)$ satisfies the power law [72] [69] [75].

$$N(r) = r^{D_F} \quad \text{or likewise} \rightarrow \quad D_F = \frac{\log(N)}{\log(r)} \quad (2)$$

Where D_F is called the fractal dimension or fractal capacity of the object. In addition, $N(r)$ number of balls with linear diameter r used to cover the object (Figure II- 10).

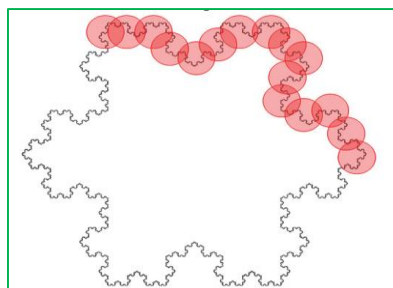




Figure II- 10: Fractal dimension estimation applied to the Koch Curve [73].

Fractal dimension accepts integer values for simple geometric objects like a point, a straight line, or a smooth two-dimensional surface (equivalent to $D_F = 0, 1, 2$), and non-integer values for self-similar fractal objects with a highly irregular shape. In general, there is a relationship between fractal and topological dimension; While D_T is always an integer ('2' for an object in the plane and '3' for an object in space), D_F is a decimal number ranging between '1' and '2' (for an object in the plane) or '2' and '3' (for an object in space) [72] (Table II-3).

Table II- 3: Similarity dimension calculation [76].

Example sets	D_T	$N(r)$	r	$D_s = \frac{\log(N)}{\log(r)}$
The Cantor set 	0	2	3	0.631
The Koch curve 	1	4	3	1.261

II.2.6 Fractal dimension computing methods

Fractal analysis is a collection of methods (most of which are computer-based) for assigning a fractal dimension and other fractal features to a dataset in all areas of research, including medical image processing, to better understand its complexities [77]. The fractal dimension quantifies the irregularity of complex objects and can characterize the complexity and inhomogeneity of porous media. For all of these reasons, the fractal dimension is commonly employed to describe a texture. There are numerous techniques for calculating it, each with its own theoretical foundation, which frequently results in different dimensions being obtained by different methods for the same object. Although they are all different, a basic principle is always respected. It is summarized by the three phases below [78] [79, 80]: Use various "measurements" to calculate the quantities represented by the object. Then, plot the logarithm of the quantities measured as a function of the logarithm of the sizes and use linear regression to estimate this line. ultimately, estimate the Fractal Dimension as the slope of the obtained line.

Below, we provide and categorize the most commonly used literature approaches, which are divided into three categories: box-counting methods, fractional Brownian motion (fBm) methods, and area measurement methods.

a) Box counting methods

The first methods developed were those known as "box-counting." We cite three methods in this class that share the following steps: Each approach in this class needs a meshing of the signal, the formulation of a probability in each created box, and the estimate of the Fractal Dimension by least-squares linear fitting as the final step. Their theory is reasonably simple and straightforward to construct. However, they have certain drawbacks [64] [79] [81].

✓ Box-counting method (BCM)

The box-counting dimension is an estimate of fractal dimension obtained using the box-counting method for image purposes or natural situations. Russel et al. (1980) defined this method. It consists in dividing an image into a set of equal squares, and then count the number of squares that contain one or more pixels of the object [82, 81].

Its principle is to cover a signal or an image with boxes of size r and calculate the fractal dimension. For example, consider an image of size $N \times N$ with each pixel either black (foreground) or white (background) to demonstrate the method for binary images. Starting, the image is covered with a grid of r -sized boxes. The number of boxes $N(r)$ required to cover the black pixels (foreground) is then calculated [82] [83] [84] [85] [86] (Figure II- 11). The box-counting dimension is defined as follows for different values of r :

$$D_B = - \lim_{r \rightarrow 0} \frac{\log(N(r))}{\log(r)} \quad (3)$$

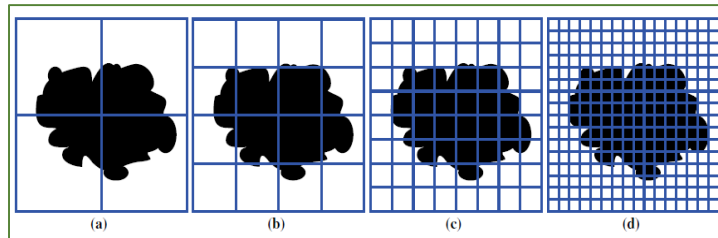


Figure II- 11: Example of the box-counting method in binary images. The binary image is divided into increasingly fine boxes, and for each, the number of boxes needed to cover black pixels is calculated [86].

Because $N(r)$ is computed over a range of r , fractal objects have a linear relationship between $\log(r)$ and $\log(N(r))$. This linear relationship can be seen as a line on a scatter plot with the x and y axes representing $\log(r)$ and $\log(N(r))$, respectively. Box-counting dimension can thus be calculated using the slope of the line created by $\log(N(r)) * \log(r)$.

Anyhow, this method has several limitations, as it requires the use of a binary image. It is sensitive to box size and is only valid for self-similar images. Other solutions are provided, as we are going to mention below, to address some of the drawbacks of the Box-counting dimension method.

✓ Differential box-counting method (DBCM)

The differential box-counting method (DBCM) is a box-counting method adaptation that Chaudhuri and Sarkar (1995) suggested it. It has the advantage to work with greyscale images, thus eliminating the binarization step. The basic idea behind this method is as follows: The signal is divided into r -sized boxes, and $N(r)$ is calculated like the difference between the minimum and highest grey levels in the $(i, j)^{th}$ box. This procedure is then performed for each box, and the fractal dimension is estimated using the equation (3) [82].

The choice of box size is a significant constraint of the box-counting algorithms. Many researches were conducted in order to determine the upper and lower constraints for the box size. Among the researchers' findings, that with a too-small box size, the maximum number of boxes above the grid would be greater than the number of available intensity levels. As a result of the unaccounted boxes, fractal dimension would be underestimated. Similarly, given an excessively large box size, the number of boxes would be significantly smaller than the number of intensity levels [82] [87] [88].

✓ « Extended counting » method (XCM)

As an alternative to the BCM, the extended counting method "XCM" (Sandau and Kurz, 1997) was presented. The XCM principle can be expressed as follows: The BCM is applied to numerous subsets of a fractal set, and the maximum dimension of the subsets is considered as the set's FD. The BCM, on the other hand, is considerably simple when used for subsets [82] [81] (Figure II- 12).

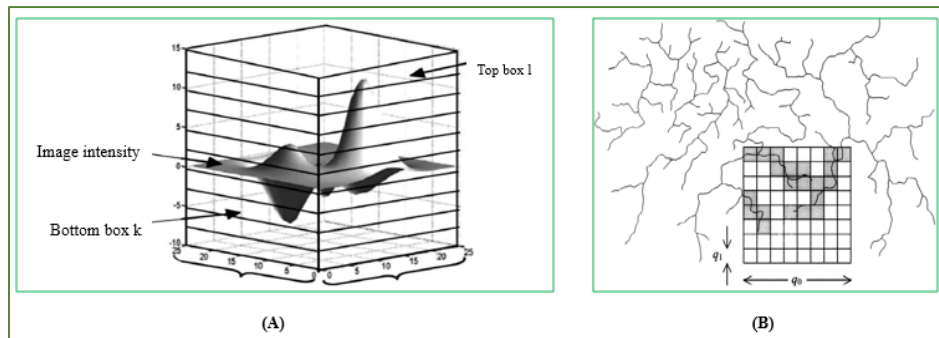


Figure II- 12: Graphical presentation of the principle of (A) DBCM and (B) XCM [81].

b) Fractional Brownian motion (fBm) methods

A fractal model based on fBm is a non-stationary model that is frequently used to describe random phenomena. According to Pentland (1984), the majority of fractals observed in physical models are fractal Brownian functions (fBfs). Two approaches are typically used to estimate the Fractal Dimension of an image believed to be a 2D fractal Brownian function. They are based on the image's variogram or Fourier transform [82].

✓ Variogram method

The variogram method is based on statistical Gaussian image modeling. Given an Fractal Dimension, fractional Brownian motion modeling can be used to generate a corresponding image. Given an image, the Fractal Dimension is approximated using the assumption that it is formed from a fractional Brownian motion.

This algorithm generates reliable Fractal Dimension estimates. Its applicability to erratically distributed data sets is one of its main features. However, it was demonstrated that partitioning a signal into an insufficient number of clusters allows the variogram approach to estimate the Fractal Dimension, but when a sufficiently enough number of clusters is utilized; a very abrupt decrease toward the correct value is detected, followed by delayed convergence [82, 81].

✓ The power spectrum

The power spectrum approach is based on fractional Brownian motion's power spectrum dependence. Each image line is Fourier processed in this method, the power spectrum is evaluated, and the power spectra are then averaged. The slope is used to calculate Fractal Dimension. The Fourier approach is appropriate for self-affine surface analysis and modeling. Unfortunately, the procedure is time-consuming and necessitates the use of gridded data. The key disadvantage is that the method is only effective on surfaces having an exponential power spectrum. In general, this constraint on the shape of the power spectrum is invalid, and it may lead to inaccuracies in the calculation of Fractal Dimension [82, 81].

c) Area measurement methods

Area measuring methods employ structuring elements of varying scales r to compute the area $A(r)$ of the signal intensity surface at a given scale (r). The slope of the best fitting line at the points $(\log(r), \log(A(r)))$ yields the Fractal Dimension. Three algorithms are the most commonly utilized in this techniques class [82]:

✓ Isarithm method (IM)

The Isarithm method's concept is to determine the complexity of the isarithm or contour lines required to approximate the complexity of a surface. This approach is only defined for the two-dimensional scenario. On the image, a series of isarithms (e.g., contours) are created depending on the data values. The walking divider method

can be used to estimate the Fractal Dimension of each isarithm, and the Fractal Dimension of the image is the average Fractal Dimension of the isarithms plus one. Most importantly, unlike other approaches such as BCM, it is only applicable to self-similar surfaces. This approach is useful for estimating the Fractal Dimension of non-similar surfaces. Its main drawbacks are Isarithm dependence, applicable for only 2D cases and dependence on directions: rows, columns, cardinal [82, 89].

✓ **Blanket method (BM)**

Peleg et al. (1984) developed the blanket approach to determine the area of a gray level surface and consequently the Fractal Dimension of a 3D structure. The algorithm is based on Mandelbrot's approach, which in turn is based on Minkowski's sausage logic. They examined all the points in 3D space at a distance 'e' from the surface in the method, covering the surface with a "blanket" of thickness 2e. This blanket has two surfaces, one on top and one on the bottom (defined by dilatation and erosion of the image). One of the method's advantages is its resistance to fluctuations in gray levels and applicable for 3D case. Another advantage of using asymmetric structuring components was that anisotropic structures within the picture could be identified. Moreover, its main drawback is that Fractal Dimension is restricted to relatively low theoretical Fractal Dimensions [90, 91, 82].

✓ **Triangular prism method (TPM)**

Clarke introduced this method in 1986; it compares the surface areas of triangular prisms with the pixel's area in log-log. The aim is then to compute the surface of the triangle prism of each analysis window of size s, and then to calculate the surface A(s), which corresponds to the sum of all the triangular prism surfaces acquired. Thus, the approach derives a relationship between the surface area of triangular prisms formed by the image's grey-level values and the grid step size used to measure the prism surface area [82, 92] (Figure II- 13). The advantage of this method is that it is fastest and more accuracy and its main drawbacks include fractal dimension underestimation and sensitivity to noise or extreme gray-level [81].

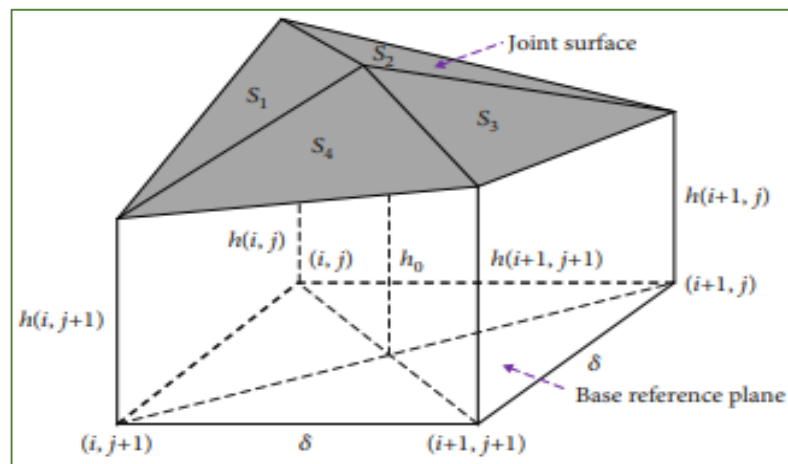


Figure II- 13: Illustration of the Triangular prism method. Where σ is the grid size, S_1 , S_2 , S_3 , and S_4 represent the areas of four triangles. (i, j) , $(i, j+1)$ and $(i+1, j+1)$ are, respectively, the coordinates of the four points of the triangular prism, h_0 denotes.

Fractal analysis is no longer effective when the object is very complex and presents a punctual regularity that varies greatly from one point to another. Its dimension cannot be characterized by itself. It is therefore necessary to calculate its local fractal dimension to describe its irregularity at every point. The multifractal analysis covers the study of these objects, their local behaviors, and their scale invariance properties.

II.3 Multifractal Analysis

Beyond mathematical models for understanding invariance of scale, a series of analysis approaches known as Multifractal analysis has been created. Where, multifractal analysis can be applied to any object in order to characterize and understand changes, fluctuations in local regularity. This new paradigm shift, which focuses on fractal methods rather than fractal objects, has been critical in the advancement of multifractal research.

Multifractal analysis is a useful method for processing biomedical images. Several researchers have advocated employing multifractals for segmentation, classification, signal analysis, and other purposes. The multifractal spectrum can provide the statistical characterization of intensity fluctuations in an image structure. Despite the complexity of the tissue and cell pictures' extremely irregular shape, multifractal analysis can resolve local densities and depict the statistical features of shapes with complicated spatial arrangements.

This section discusses the technique for calculating the Hölder exponent, often known as the α -value, as well as variations in the local density of the image. Furthermore, the many kinds of multifractal measures. As well as it is shown how to generate a multifractal spectrum, which describes an image's fractal dimension.

II.3.1 Multifractal History

Multifractal analysis, which was developed in the 1980s to explain turbulence signal findings, has provided new tools for the study and modeling of signals from a variety of scientific domains. **Kolmogorov** created the theory of homogeneous and isotropic turbulence in 1941, which paved the way for the history of multifractals. The turbulent velocity signals appear to be quite erratic in some locations and considerably less so in others, with no obvious borders to these regions. This "multi-scale" complexity is too similar to fractals. Multifractal analysis first developed in physics to better comprehend and analyze such complicated functions, as well as to offer new quantitative characteristics that allow their classification [93].

In fact, the beginnings of multifractal analysis are in the various energy cascade models proposed by **Mandelbrot** (1974) in fully developed turbulence: "Intermittent turbulence in self-similar cascades: divergence of high moments and dimension of the carrier", which were formalized in 1985 by **Parisi** and **Frisch** in their investigation of experimental data. Mandelbrot's multifractal ideas were revisited in a broader context developed and clarified in a work by theoretical physicists **Halsey et al**: "Fractal Measures and their Singularities" in 1986. Simultaneously, **Kadanoff** and his collaborators at the University of Chicago laid the foundations of this approach in the context of invariant measures of dynamical systems [94, 95].

According to Mandelbrot (1988), the concept of self-similarity can be extended to measures (such as spreading mass or probability) distributed on Euclidean support (e.g., a point set). In this context, fractal sets may be characterized by a function or a spectrum of interlinked fractal dimensions rather than simply one fractal dimension (as seen in the preceding section). These fractal sets are referred to as multifractal. Thereupon, multifractal analysis can be seen as an extension of fractal analysis [96].

By 1992, two studies had been published that validated the Multifractal Formalism for two types of measures that showed some degree of self-similarity: {Gibbs' states on hyperbolic cookie-cutters in \mathbf{R} (Rand); Moran's self-similar measures in \mathbf{R}^d (Cawley & Mauldin)} [94].

II.3.2 Methods of multifractal analysis

Multifractal analysis can be seen as an extension of fractal analysis. A multifractal object is more complex in that it is always invariant under dilation, and the factor required to distinguish the detail from the entire object depends on the observed detail. There are several ways and approaches for performing multifractal analysis. As an example, we quote the following [97]:

- The structure-function approach was pioneered by Parisi and Frisch [98].
- The generalized dimension method of Hentschel and Procaccia uses the box-counting algorithm [99].
- The method of moments was pioneered by Halsey and all [100].
- The Barabasi and Vicsek method based on the HHCF (Height Height Correlation Function) technique [101].
- Use the box-counting method with the BDC (Differential Box-Counting) algorithm on grayscale images by Sarkar and Chaudhuri [102].
- The method of multifractal analysis based on a direct method without recourse to multifractal formalism by Chhabra and Jensen [103].
- 2D wavelet transform modulus maxima lines (2D-WTMM) is a multifractal formalism that is based on the continuous wavelet transform proposed by Arneodo and all [104].
- Peng and others first proposed the multifractal detrended fluctuation analysis method and then developed for higher orders by Kantelhardt and others [105].
- The dominant coefficients method that uses the discrete wavelet transform [106].
- Maximum coefficients of Discrete Wavelet Transform for 2D Multifractal Analysis proposed by Ouahabi [107].
- The large deviation spectrum method proposed by Mandelbrot, and used by Hentschel and Procaccia [108].

II.3.3 Concept of measure

A measure of a bounded subset S of R^n , expressed as $\mu(S)$, is frequently regarded as a type of mass distribution. Consider spreading a small handful of sugar on a bounded surface; the mass sugar distribution on the surface at a given point corresponds to the measure.

In the context of image processing, the most natural choice is to consider that the measure carried by a region is the sum of the light intensities of each point of the region's support. On an image, the points where the light intensity is non-zero constitute the measure's support, while the points where it is zero are considered "outside the object" [76].

II.3.4 Hurst exponent and fractal dimension

A fractal object, as defined in the previous section on fractals, is one whose fractal dimension differs from its topological dimension and is invariant with respect to the scales of analysis. We define another parameter, the exponent of Hurst, to distinguish between the fractal dimension and the topological dimension. The relation that binds it to the fractal dimension is given by $D_F + H = D_T$ where D_T denotes the object's topological dimension.

Hurst exponent can be calculated using various methods for example; box counting method, the method of variation, the probabilistic method, the method of spectral analysis in the Fourier domain, the morphological method, etc. [72].

II.3.5 Local behavior: Hölder exponent (α -value)

A multifractal object is more complex in that it is always invariant under dilation, and the factor required to distinguish the detail from the entire object depends on the observed detail. Therefore, the Multifractal’s main parameter is **Holder’s exponent** also known as the **local singularity coefficient** or says the **local Hurst exponent** so verifies the relation locally. Together with the multifractal spectrum, this scaling exponent can be used to characterize statistically the overall image structure. Multi-fractal analysis can also be used to provide local information and to isolate particular fractal dimension regions [72, 109].

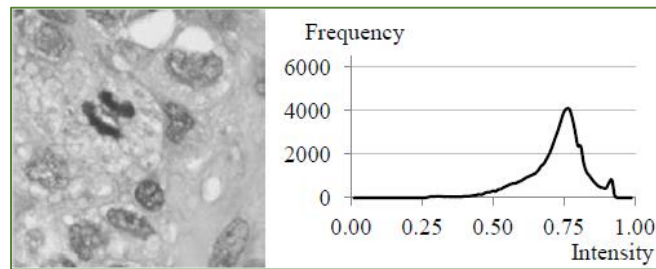


Figure II- 14: The greyscale image (left) and its corresponding intensity histogram (right) [109].

Using a grayscale image as an example (Figure II- 14), each pixel has an intensity value that is represented as a multilevel gray value. These grey values are interpolated linearly from black to white. The local singularity coefficient, also known as the Hölder exponent or α -value, reflects the local behavior of a function $\mu_p(w)$ around the pixel, as given in Equation(4).

$$\mu_p(w) = Cw^{\alpha_p}, \quad w=2k+1, \quad k=0,1,2,3,\dots m. \tag{4}$$

$$\log(\mu_p) = \alpha_p \log(w) + \log(C), \tag{5}$$

Where w stands for the window size centered at the pixel p . In addition, C is an arbitrary constant, and m is the total number of boxes used in the computation of α_p . The slope of the linear regression line can be used in a log logarithmic plot where $\log(\mu_p(w))$ is plotted against $\log(w)$ to estimate the value of α_p [110, 111, 109]. The Hölder exponent is computed for the entire data set. The range of values $[\alpha_{min}, \alpha_{max}]$ may vary depending on the nature of the studied process. In some cases, it is limited to a narrow value range, whereas in others, it can range from zero to infinity [112].

The following are some commonly used multi-fractal intensity measures for calculating the Holder exponent.

II.3.6 Multifractal measures

In multifractal analysis, there are four types of intensity measures: maximum measure, inverse-minimum measure, summation measure, and Iso measure [113]. The function of a multifractal measure is denoted as $\mu_w(x, y)$. Let $g(k, l)$ represent the intensity value at pixel (x, y) , and Ω be the set of all pixels within the measured neighborhood of a square window size w .

a) maximum measure (max measure)

The maximum intensity value within the square region $\mu_w(m, n)$ is represented by the max measure. In ways it is the measure with the highest intensity value found in the window w centered on the pixel p . If all pixels are black with an intensity value of exactly zero, a problem may develop.

This may result in a mathematical error while computing $\log(0)$. To avoid this issue, fully black pixels are treated as background and are ignored in max measure [109].

$$\text{Maximum : } \mu_w(x, y) = \max g(k, l), \quad (k, l) \in \Omega \quad (6)$$

b) Inverse-minimum measure (inv-min measure)

The minimum measure determines the lowest intensity value and gives it to $\mu_w(x, y)$. Hemsley proposed an inverse-minimum measure based on the positive difference between $\mu_w(x, y)$ and one. The subtraction from one is needed to ensure that the measure's value does not drop as the window size increases. If all pixels are white with an intensity value of exactly one, a problem may develop. This may result in a mathematical error while computing $\log(0)$. To avoid this issue, fully white pixels are treated as background and are ignored in inv-min measure [109].

$$\text{Inverse-minimum : } \mu_w(x, y) = 1 - \min g(k, l), \quad (k, l) \in \Omega \quad (7)$$

c) Summation measure (sum measure)

The sum measure adds together all of the pixel intensities in the neighborhood. Similarly, if all pixels are black, Equation (8) will encounter an error for calculating $\log(0)$. As a result, completely black pixels are treated as background and will not be used in sum measure computations [109].

$$\text{Summation : } \mu_w(x, y) = \sum g(k, l), \quad (k, l) \in \Omega \quad (8)$$

d) Iso measure

The Iso measure, as shown in Equation (9), counts the number of pixels in the neighborhood that have identical intensity values to the centered pixel. If the central pixel is the sole pixel in the region with a unique intensity, then $\mu_w(x, y)$ equals one. Because the probability that the pixels in a neighborhood to have the same intensity value is quite low, the Iso measure can be tweaked to accept a 5% degree of precision. This adjustment permits more pixels with similar intensity values to the central pixel to be included in the multifractal measurement [112, 109]. (Note that # is the number of pixels)

$$\text{Iso: } \mu_w(x, y) = \#\{(k, l) \mid g(x, y) \cong g(k, l), (k, l) \in \Omega\}, \quad (9)$$

II.3.7 Holder image (α -image)

The local singularity is computed for the entire original image, and the resulting image is called the α -image. (Figure II- 15) shows the results of utilizing several multifractal measures, while (Figure II- 14) shows the original greyscale image. For display purposes, the original image in (Figure II- 14) and the α -images in (Figure II- 15) are normalized to [0.0, 1.0], black to white. Furthermore, the α -histogram for each multifractal measure demonstrates that the distribution of α -values has a bell-shaped curve, is skewed, and is translated along the α -axis (Figure II- 16) [109].

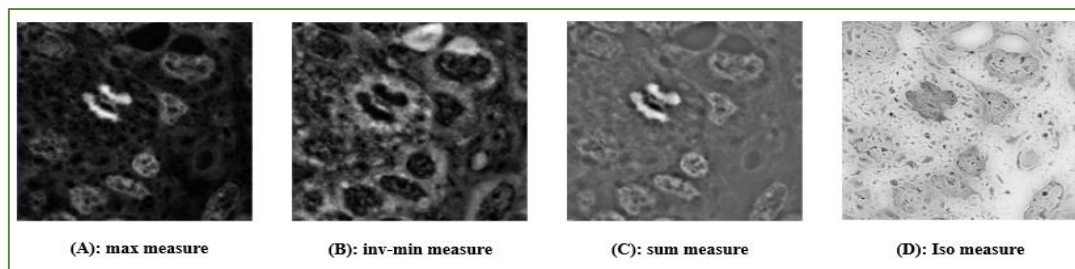


Figure II- 15: The α -image. The α -range for each measure is different: $[0.0000, 0.4808]$ for max measure, $[0.0000, 0.9354]$ for inv-min measure, $[1.7917, 2.3315]$ for sum measure, and $[0.0000, 2.1694]$ for Iso measure [109].

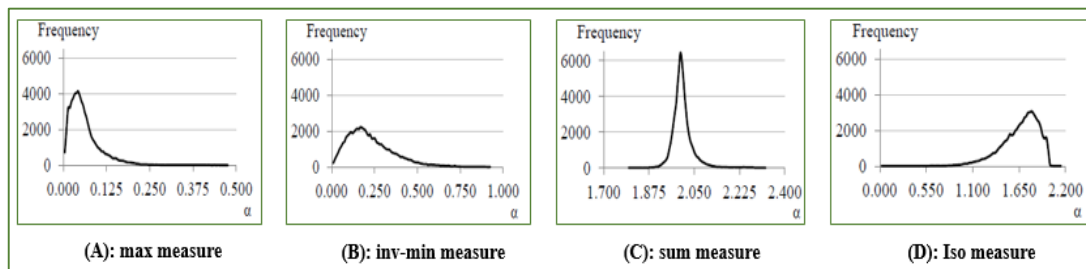


Figure II- 16: α -histogram. The distribution of α -values has a bell-shaped curve, and is skewed and translated along the α -axis respectively [109].

II.3.8 Global behavior: Multifractal Spectrum (Singularity spectrum)

A multifractal spectrum is a function that describes the geometrical property of the α -image. The Hölder exponent provides a local approach to the images. This only gives useful information about the image's local singularity. To define a multifractal image description, it is important to be able to characterize points of the same singularity and discern the different local behaviors in an image. Then we consider that each value of the defined Hölder exponent corresponds to a fractal set $E(\alpha)$, the fractal dimension of which we will calculate and that the support of the image X is therefore formed by the union of fractal sets of different dimensions [109, 114].

$$S_i = E(\alpha_i) = \{(x, y) \mid \alpha(x, y) = \alpha_i\}, \quad X = \cup_i E(\alpha_i) \quad (10)$$

$E(\alpha_i)$ can be interpreted as the subset of points having the same scaling behavior described by α .

Furthermore, the information provided by the Hölder function $\alpha(x, y)$ is either difficult to obtain or impossible to obtain in several cases. In this case, it is preferable to consider simplified high-level information, which consists of describing the distribution of the image's Hölder exponents from a geometrical or statistical point of view; this approach is known as multifractal analysis [109]. Hausdorff dimension is one of the box-counting-based methods for calculating fractal dimension. Each value α of the Hölder exponent defines a fractal set $E(\alpha)$ [115]. The Hausdorff fractal dimension is defined as follows with α_i represent the Hölder exponent of the subspace S_i . $N_\lambda(\alpha_i)$ is the number of boxes S_i containing the value α_i

$$f_\lambda(\alpha_i) = -\frac{\log(N_\lambda(\alpha_i))}{\log(\lambda)} \quad (11)$$

The multifractal spectrum $f(\alpha)$ is found by the limited value:

$$f(\alpha) = \lim_{\lambda \rightarrow 0} f_\lambda(\alpha_i) \quad (12)$$

The pair $(\alpha, f(\alpha))$ provides both local (via α) and global (via $f(\alpha)$) information. It is referred to as the Hausdorff spectrum of the image X [114] (Figure II-17).

The Hausdorff spectrum provides a global geometric characterization of signal singularities. It thus measures the global distribution of the various Hölder exponents.

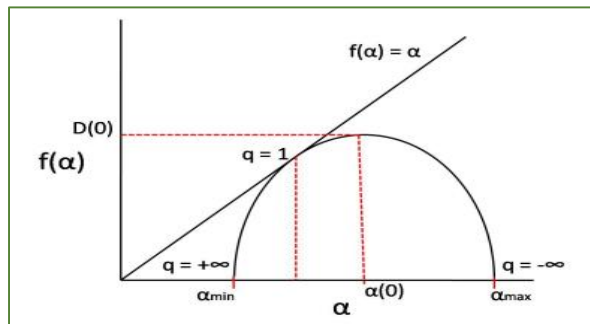


Figure II- 17: Schematic representation of a multifractal spectrum [116].

II.3.9 Methods for Multifractal Spectrum calculation

There are several methods for approximating the multifractal spectrum. They are divided into two categories: those based on box counting and those based on wavelets.

3.1.1.9.1 Box counting methods

To characterize the structure of some scaling processes, an unlimited number of fractal dimensions are required. Box counting techniques are ‘extensions’ of (monofractal) box counting methods that are used to describe multifractals. This class's methods are built on the same principles as the techniques for fractal dimension assessment shown in the preceding section. The signal is meshed using various box sizes, r , and a normalized measure is calculated in each box.

1) Generalized fractal dimensions and multifractal spectrum

To analyze point sets, standard box-counting techniques are used. An infinite number of generalized dimensions D_q , ("generalized" in the sense that they are defined using the variable q), which are also known as "Renyi's dimensions", and the associated spectrum of singularities given by $f(\alpha)$, describes each set. The definition of D_q as a function of q is provided by the expression [117, 118]

$$D_q = (q - 1)^{-1} \lim_{N \rightarrow \infty} \left[\sum_i \frac{p_i^q}{\ln N} \right] \quad (q \neq 1) \tag{13}$$

Here $p = \int box \, d\mu$, with μ being the probability measure of the multifractal set, and $i = 1, 2, \dots, N$ (where N is the number of boxes). In addition, i is the index of a box that belongs to a grid that covers the set.

where, the sequence of mass exponents τ_q , which is a function relating the probability moments to the radius length of the covering areas gives the relationship between the spectrum of generalized fractal dimensions, D_q , and the multi-fractal spectrum, $f(\alpha)$, by the expression [119, 79]:

$$\tau_q = (q - 1) D_q \tag{14}$$

By using the Legendre transform described by the relations, the previous expression can be used to obtain the multifractal spectrum $f(\alpha)$ [120].

$$\alpha_q = -d\tau_q/dq \tag{15}$$

$$f(\alpha_q) = q\alpha_q + \tau_q$$

With α being the holder exponent.

These methods have the same limitations as box-counting methods, although numerous computational improvements have been documented. Aside from issues that arise when the boxes contain few points, the algorithms are characterized by low statistics, which are accentuated by the negative exponents ($q < 0$); this causes the measure to diverge rapidly [79].

2) The “sand box” or cumulative mass method

The sandbox approach, created by Vicsek (1990) and introduced by Tél et al. (1989), is effective for assessing generalized fractal dimensions for both positive and negative moment orders, q , allowing reconstruction of the entire multifractal spectrum [121].

The Sandbox approach takes into account the mass (total of sample measurements), $M(R)$, inside a region i of a certain radius R (i.e. a 3D sphere) centered on the fractal. Using arbitrary points as centers, the average mass and their q^{th} moments over randomly dispersed centers can be calculated as $\langle [M(R)]^q \rangle$, where q is the probability moment order [119]. The benefit of this method is that the boxes are centered on the structure, so no boxes have too few elements (i.e. pixels) within. Indeed, for $q < 0$, boxes with a limited number of elements (because they barely overlap with the cluster) contribute abnormally huge amounts [79].

3) The large-deviation multifractal spectrum

The form of the multifractal spectrum is always concave when estimated using the methods outlined above. The large-deviation multifractal spectrum has the advantage of not being inherently concave, resulting in less information loss. However, far more numerical effort is necessary, making the method difficult to apply in both 2D and 3D. In fact, the methodology necessitates the calculation of two limits rather than only one as in the previous two methods [79]. Let μ be a function of measure, and $N_r(\alpha)$ the number of boxes, which satisfies [97]:

$$N_r(\alpha) = \#\{\text{covering with intervals of size } r \text{ such that } \mu(I) \geq r^\alpha\}$$

in the previous expression expresses "the number of", α is the exponent of the singularity.

The relation expresses the Multifractal spectrum of large deviations (of grains) of the measurement μ :

$$f_c(\alpha) = \lim_{\varepsilon \rightarrow 0^+} \lim_{r \rightarrow 0^+} \frac{\log^+(N_r(\alpha + \varepsilon)) - N_r(\alpha - \varepsilon)}{-\log(r)} \quad (16)$$

Where r represents the measurement scale.

B. Wavelets methods

Concerning the methods of approximation of the spectrum of singularities, specifically which of Legendre, three formalisms based on the transform in wavelets using three different methods. Some methods are based on the discrete wavelet transform, while others on the continuous wavelet transform we mentioned them: Methods based on the discrete wavelet transform, the wavelet transform modulus maxima (WTMM) method, and the wavelet leaders' method [79, 122].

1) Methods based on the discrete wavelet transform

We begin with the first technique for multifractal spectrum computation in wavelet methods, which uses the Discrete Wavelet Transform. Intuitively, there appear to be some parallels between these mathematical devices. Jaffard established the properties of the multifractal formalism (based on discrete wavelet coefficients) (1997). Meyer (1998) demonstrated that under conditions of moderate regularity on the paths of the process $x(t)$, the local Hölder exponent can be calculated from size estimates of the wavelet coefficients $W_{j,k}$ [123, 79].

Discrete wavelet transform enables signal investigation at many resolutions and locations, which is closely connected to multifractal analysis. The discrete or dyadic wavelet transform is used in this method. The structure function and multifractal spectrum are derived from the coefficient modules of this transform [123, 79].

$$\alpha(t_0) = \lim_{k2^{-j} \rightarrow t_0} -\frac{1}{j} \log_2 |W_{j,k}| \quad (17)$$

Where $k2^{-j} \rightarrow t_0$ means that t_0 belongs to $[2^{-j}k, 2^{-j}(k+1)]$ as $j \rightarrow +\infty$

2) The wavelet transform modulus maxima (WTMM) method

This analysis allows for the characterization of data's multifractal aspect (whether 1D, 2D or 3D). This method is also based on the wavelet concept in general, and specifically on the use of the continuous wavelet transform. Thus, rather than studying the signal directly, the method proposes studying its wavelet transform, whose local maxima reveal the singularities [122, 79].

Here we remind the definition of a singularity of the signal s at x in the form of the Holder exponent h .

$$|s(x) - p(a)| \sim a^{h(x_0)} \quad (18)$$

The wavelet transform of s

$$T[s](x_0, a) \sim a^{h(x_0)} \quad (19)$$

The spectrum of singularities using the Legendre transform is given by the equation (20):

$$f(\alpha) = \min_q (q\alpha - \tau(q)) \quad (20)$$

3) The wavelet leaders method

This is a relatively new approach. It is founded on the discrete wavelet transform's notion of wavelet leaders [79].

II.4 Conclusion

In this chapter, we have described a new geometrical model created and proposed by the mathematician Mandelbrot to describe the complexity of irregular shape objects, which subsequently came to be known as “fractal geometry”. When fractal analysis is no longer effective when the object is very complex and has a very variable fine regularity from one point to another. Accordingly, the use of multifractal analysis in this case is the solution. The multifractal analysis approach aims to characterize complex structures and images locally; using the holder exponent, and globally; using multifractal spectrum.

There are three kinds of multifractal spectra, each of which is calculated using a different algorithm:

- The Hausdorff spectrum.
- Legendre's spectrum.
- The spectrum of large deviations.

In the next chapter, we will present the implementation our project method based on multifractal analysis of histological images, and results obtained.

Chapter 3

Application of the multifractal analysis method

And Results

Contents

III.1 Introduction.....	40
III.2 Image processing and analyzing generalities.....	40
III.3 Proposed approach	42
III.4 Data Acquisition.....	43
III.5 Programming Environment	44
III.6 Method description	47
III.6.1 First part: Prepossessing	47
III.6.2 Second part: Holder exponent estimation.....	48
III.6.3 Third part: Multifractal spectrum estimation.....	49
III.7 Application and results.....	50
III.7.1 Pre-processing and Holder exponent estimation algorithms	50
III.7.2 Discussion of the result of the Holder exponent algorithm.....	51
III.7.3 Multifractal spectrum estimation.....	51
III.7.4 Multifractal spectrum First database	52
III.7.5 Multifractal spectrum Second database	53
III.8 Step to classification.....	54
III.8.1 Discussion First database result.....	57
III.8.2 Discussion second database result	60
III.8.3 Discussion of the pertinent parameters.....	61
III.9 Conclusion.....	61

Chapter III Application of the multifractal analysis method and Results

III.1 Introduction

Because of the variability and morphological complexity of tumors, histological images are difficult to interpret. Even well trained pathologists strain to make a precise diagnosis. Our research aids in the identification of thyroid diseases such as follicular adenoma and papillary cancer. Pathologists will benefit from this approach, which is based on the analysis of histological images of the thyroid and the automatic classification of the latter into three classes: follicular adenoma of the thyroid, papillary carcinoma of the thyroid, or normal thyroid.

In the previous chapter, we have mentioned some method to estimate multifractal spectrum, in this chapter we propose a box-counting method for analyzing histological images of the thyroid based on multifractal analysis. The method is composed of three main steps: pre-processing the input image, finding the image of Holder (α -image), and estimating the multifractal spectrum. Pre-processing operations to improve the characteristics of an image are required before the main analysis and information extraction. In the second step, we propose a local characterization method of the pre-processed image. The third step aims at the global characterization of the image. However, before proceeding with these steps, we will first present the general approach proposed then we present the databases of thyroid samples that we will work on.

III.2 Image processing and analyzing generalities

1. Medical image

A medical image is the materialization of anatomical or functional information in vivo of elements (organs, tissues, cells) of the human body, as well as the data collected or generated from these elements, in the form of images. These images are obtained to answer a medical requirement (a clinician's issue) by employing acceptable technical imaging methods while reducing the patient's risks and expenditures [124].

2. Digital image

Derived from the two Latin words [125]; the word "image" is derived from the verb "imitari," which means, "to imitate." On the other hand, digital is derived from "digitalis," which means "relative to a finger" and is the result of the combination of two words: "digitus," which means "finger," and the suffix "-al," which means "relative to."

A digital image is a virtual image that only exists in computer memory or as a binary number sequence (1-0) that specifies the image as it should appear on a computer monitor. Digital images are divided into two categories: Images in bitmap format and Images in a vector format [126]. A digital image is made up of a finite set of elements, called picture elements, or pixels (3D voxels). The dimensions (height and width) of an image are related to the number of pixels, where the number of pixels in image is (height multiplied by width) [127]. A pixel is a point in an image that has a particular on a specific shade, opacity, or color. (The integers represent the intensity of red, green, and blue). RGBA; this is an extension of RGB with the addition of an alpha field that represents the image's opacity [127].

3. Medical imaging

Medical imaging refers to several different technologies that are used to obtain images of the interior of the human body. It employs a variety of physical principles (US, X-Ray, Gama Rays). In addition, it enables physicians to investigate the human body and make diagnosis that is more exact as a result (direct understanding of physiology and pathology) [128]. It is an essential tool in diagnosis and treatment [129].

Chapter III Application of the multifractal analysis method and Results

4. Medical image processing

The objective of image processing is to remove irrelevant data so that important information may be extracted and manipulated for image analysis. The three fundamental steps for implementing this system are as follows [130]:

- **acquisition and digitization**

The first step in digital image processing is image acquisition, which involves converting an image into a number. In another way, an optical device captures an unprocessed image of an object or scene and converts it into a manageable format for processing and analysis purposes [131].

- **pre-processing**

Processing, also known as pre-processing, is a technique for enhancing image quality. Various techniques are used to link the concept of quality to the achievement of an objective: (Restoration, Compression, and segmentation...) [132].

- **analysis and interpretation**

The process of extracting meaningful information from images, such as finding shapes, counting objects, identifying colors, or measuring object properties, is known as image analysis. As same, the process of examining images and identifying and judging their significance by considering their location and extent is known as image interpretation. Expertise in image interpretation develops over time as a result of practice [133, 134].

5. Classification of medical images

Automatic Image Classification is a pattern recognition application that uses a classification system to automatically assign a class to an image. Object classification, scene classification, texture classification, face recognition, fingerprint recognition, and character recognition are all examples of current applications.

Depending on the information available about the data to be classified, there are two main types of machine learning: supervised machine learning and unsupervised machine learning.

- supervised methods

The analyst must first select training areas where he/she knows what is on the ground and then digitize a polygon within that area using supervised classification (Each image in the supervised approach is assigned a label that describes its class membership.)

- unsupervised methods

The data available in the unsupervised (or clustering) approach does not have labels, so the system must extract a rule of membership for each image in a given group.

Many different algorithms are used in machine learning; the classifier is the procedure that performs this task, as an example we cite the Support Vector Machine algorithm:

Support Vector Machine (SVM)

SVMs are a type of machine learning algorithm that can be used to solve problems like classification, regression, and anomaly detection. They are known for their strong theoretical guarantees, great flexibility, and ease of use, even if you do not know much about data mining [135].

The training data is represented as points in space, separated into categories by a clear gap as wide as possible in a support vector machine. Then we accomplish classification by locating the hyper-plane such that all the points of the same class are on the same side of the hyper-plane [136].

Chapter III Application of the multifractal analysis method and Results

- **Linear SVM**

This type is used for linearly separable data, which means if a dataset can be classified into two classes by using a single straight line, then such data is termed as linearly separable data, and classifier is used called as Linear SVM classifier.

- **Non-linear**

Non-Linear SVM is used for non-linearly separated data, which means if a dataset cannot be classified by using a straight line, then such data is termed as non-linear data and classifier used is called a Non-linear SVM classifier.

III.3 Proposed approach

Medical imaging is one of the medical fields that embrace image processing and analysis. Our work is based on a multifractal analysis approach to characterize locally and globally the histological medical images of the thyroid by proposing attributes from the image of singularities and the multifractal spectrum.

In our study, we are interested in the analysis of different histological image samples of the thyroid corresponding to different pathologies. Healthy samples (healthy thyroid tissue), the second samples contain the follicular adenoma (benign pathology), the third samples contain the papillary carcinoma (malignant pathology) and the last one contains different types of carcinoma (papillary, medullary, and vesicular carcinoma).

Fractal geometry analysis of digital images is based on seeing the image as a surface in three-dimensional Euclidean space, where (x, y) denotes the pixel position and the gray level is the third component [137]. The proposed approach is based on the analysis of fractal components of the image.

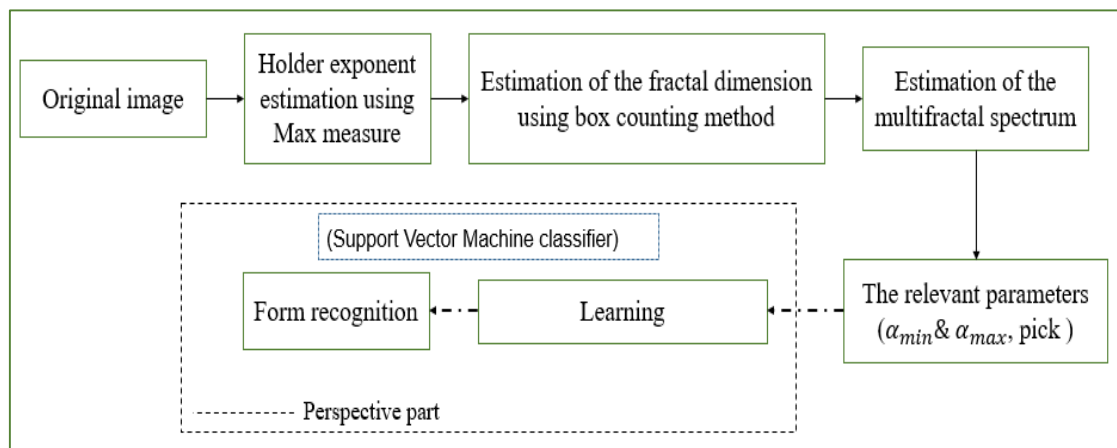


Figure III- 1: Summary of calculating the Hölder exponent and multifractal dimension.

The steps of our multifractal algorithm are (Figure III- 1):

- Grayscale image then normalize the image to full scale the next step is to consider an arbitrary pixel and its neighboring porches after that consider the maximum measurement of each window and calculate the logarithm of the maximum values of the window.
- Plot the linear regression line "Log (Max)" by the function of the "Log (i)" of the dimension of the window. The slope of the linear regression is the value α . Repeat the same procedure for all pixels
- Find the Hölder image (α -image).

Chapter III Application of the multifractal analysis method and Results

- The α -values within the α -intervals are obtained by subdividing the range of α -values $[\alpha_{min}, \alpha_{max}]$ into a pre-specified number of sub-intervals.
- The size of box ε starts from half the size of the input image of size N and recursively reduces until one.
- Plot the linear regression line $\log(n(\varepsilon))$ against $\log(\varepsilon)$. The slope of linear regression is the multifractal spectrum $f(\alpha)$

$$f(\alpha) = -\frac{\log(n(\varepsilon))}{\log(\varepsilon)} \quad 3 - 1$$

$$n(\varepsilon) = \#\{\Omega \mid \alpha_i \leq \alpha(k, l) < \alpha_{i+1} \mid, (k, l) \in \Omega\}$$

Where # is the number of pixels.

- Plot the multifractal spectrum
- Find the relevant parameters to characterize the multifractal spectrum.
- *The classification using the classifier "support vector machine" (perspective part).*

III.4 Data Acquisition

The first step of our end of studies project work was the acquisition of the base of histological microscopic images from the slides containing the thyroid tissue (normal thyroid, follicular adenoma, and papillary carcinoma). Thanks to the kind contribution of Dr. Pathologist BELARBI Omar who provided us with this database, sufficient for a pilot study.

First real database of thyroid sample, acquired with Olympus microscope and DIP camera at Tlemcen University Faculty of Medicine. Finally, obtained images are color images in JPG (Joint Photographic Group) format. We selected 90 thyroid histological sections from this database, 2048x1536 in size at three magnifications of 10, 20, and 40. Among these images, 30 represent the case of the normal thyroid, 31 represent the case of the benign pathology, which is the follicular adenoma, and the other 29 represent the case of the malignant pathology, which is the papillary carcinoma Cases for analysis included (Figure III- 2.a).

Second real database of thyroid sample, acquired with Optika microscope and camera at El Bayadh Hospital. Finally, obtained images are color images in JPG (Joint Photographic Group) format. We selected 130 thyroid histological sections from this database, 1920x1080 in size at three magnifications of 4, 10, and 40. Among these images, 42 represent the case of the medullary carcinoma, 44 represent the case of the papillary carcinoma, and the other 44 represent the case of the vesicular carcinoma, which is the papillary carcinoma Cases for analysis included (Figure III. 2. b).

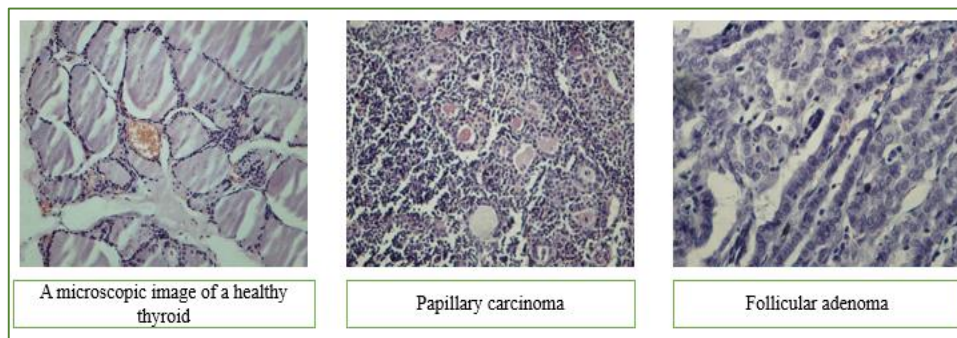
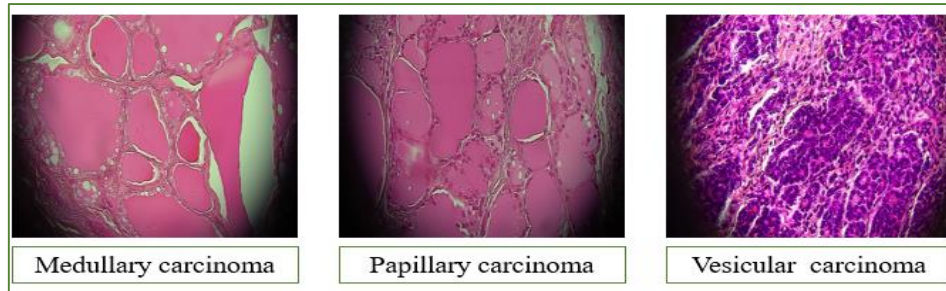


Figure III- 2: Some images from the first database. Some images from the database (a. First database, b. Second Database).



b. Samples from Second Database

III.5 Programming Environment

○ Equipment used

Model	Lenovo IdeaPad 330
Processor	Intel(R) Celeron (R) CPU 3867U @ 1.80 GHz
RAM	4.00 GO
System used	Windows 10 Professional

○ Programming language (Python)

Today, the Python programming language enables a wide range of software applications, many of which have a significant impact on our everyday lives. Python, invented by Guido van Rossum and first released in 1991, has experienced continuous refinement and has evolved into a powerful yet flexible and easy-to-learn "Swiss Army knife" for programmers [138, 139]. The Python version 3 (python 3.10 (64-bit)) programming environment is used to implement our program (Figure III- 3).



Figure III- 3: Python logo [2].

Python is an object-oriented programming language that is open source and multi-platform. It contains high-level data structures that are efficient and a basic but effective approach to object-oriented programming [140]. Python provides the following educational advantages [141]:

- Portable, accessible across all systems (from Unix to Windows);
- Python has a straightforward syntax. Python statements are extremely similar to pseudocode algorithm statements, while Python expressions employ algebraic notation.
- Python's semantics are safe. Any phrase or statement whose meaning deviates from the language's definition generates an error notice.
- Python is scalable. Straightforward Python applications are simple to write for novices.

Chapter III Application of the multifractal analysis method and Results

- Python is a free programming language that is widely used in the industry. Python has a vast user community, and knowledge in Python programming is highly valued on resumes.

It is a simple and versatile language for expressing ideas about computing, suitable for both beginners and specialists, due to specialized libraries, and is utilized in a wide range of applications, including software development, data analysis, and infrastructure management. Among them, we use in our project (OpenCV, NumPy, Matplotlib, Math, scipy ...)

- **OpenCV**

Initially developed by Intel, the first version of OpenCV (Open Computer Vision) in June 2000; it is a free graphics library that specializes in real-time image processing [142]. This package has a wide range of features that allow you to create programs that start with raw data and end with basic GUIs. It supports the majority of low-level image processing activities. It can read, write, and display photos, as well as compute grayscale and color histograms, smooth and filter images, and perform image thresholding (Otsu method, adaptive thresholding), segmentation (connected components), and mathematical morphology [143].

The focus of OpenCV has been on matrices and operations on them since version 2.1. The matrix is, in fact, the fundamental structure. A matrix of pixels can be thought of as an image. As a result, all of the basic matrices operations are available, including transpose, inversion determinant calculation, and multiplication (by a matrix or a scalar) (Figure III- 4).

You must initially import the OpenCV package with the following instruction:

```
import cv2
```

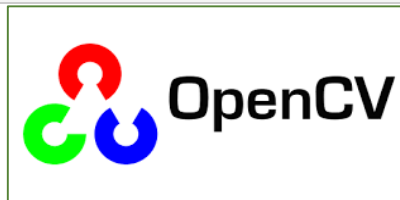


Figure III- 4: OpenCV logo [5].

- **Numpy**

NumPy is a Python library for manipulating arrays. Travis Oliphant created NumPy in 2005. It also has functions for working with linear algebra, the Fourier transform, and matrices. This Python package allows us to manipulate matrices and multidimensional arrays as well as mathematical algorithms that operate on them.

This free and open-source software library offers a variety of functions, including the ability to create directly a table from a file or, conversely, save a table in a file, as well as manipulate vectors, matrices, and polynomials [144] (Figure III- 5).

You must initially import the numpy package with the following instruction [145]:

```
import numpy as np
```



Figure III- 5: NumPy logo [5].

Chapter III Application of the multifractal analysis method and Results

- Matplotlib

In the Python programming language, Matplotlib is a library for plotting and presenting data in the form of graphs. It may be used in combination with the scientific computing Python packages NumPy and SciPy. It also has an object-oriented API that enables graphics to be incorporated into programs using GUI tools like Tkinter, wxPython, Qt, or GTK [146](Figure III- 6).

You must initially import the numpy package with the following instruction

```
from matplotlib.pyplot as plt
```



Figure III- 6: matplotlib logo.

- Math

Python math module is defined as the most famous mathematical functions, we can use throughout code for more complex mathematical computations which include trigonometric functions, representation functions, logarithmic functions, etc. Furthermore, it also defines two mathematical constants, i.e., Pie and Euler number, etc. This library is not useful when dealing with complex mathematical operations like the multiplication of matrices (Figure III- 7).

```
import math
```

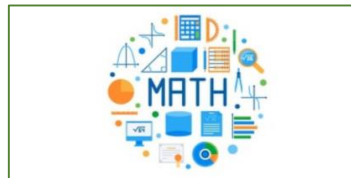


Figure III- 7: math logo.

- scipy

A scientific Python library is open-source, BSD-licensed math, science, and engineering library. It consists of a set of mathematical algorithms. NumPy, which allows convenient and quick N-dimensional array manipulation, is used by the SciPy package. The fact that SciPy is based on Python also means that a powerful programming language is accessible for creating sophisticated programs and customized applications (Figure III- 8).

```
from scipy import stats
```



Figure III- 8: scipy logo.

III.6 Method description

The processing steps are (Figure III- 9):

1. **Preprocessing** : (acquisition of the image, convert image to grayscale, normalized image)
2. **Characterization**: We use the holder exponent for local characterization and the multifractal spectrum based on the box counting method for characterizing the image globally.
3. **Learning**
4. **Form recognition**

The following diagram demonstrates the processing sequence to be followed in order to solve the project's problematic.

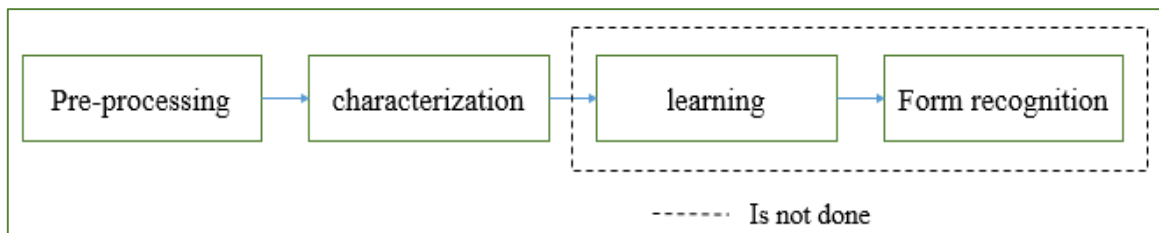


Figure III- 9: The processing steps.

III.6.1 First part: Preprocessing

- Input data; we start by reading the data.
- Transformation of the original image in grayscale level
- Resizing the grayscale level image
- Uses the median filter on a 3 x 3 neighborhood. as it is very effective in eliminating noise while preserving contours we use Median filtering to remove noise from images
- Normalization; the analysis focused on 256-level grayscale medical images with dimensions of 1522x1522 pixels for the first database and 1080x1080 pixels for the second database that contain three carcinoma classes.
- Plot all the images (Figure III- 10).

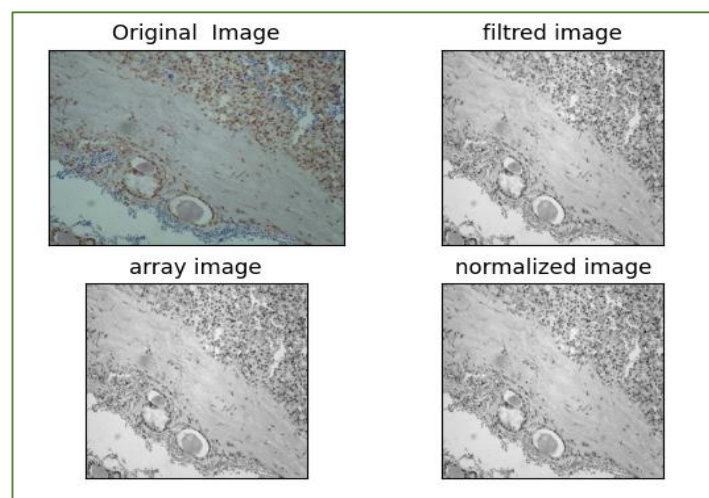


Figure III- 10: Application of the pre-processing python program for a healthy thyroid image.

Chapter III Application of the multifractal analysis method and Results

III.6.2 Second part: Holder exponent estimation

After we apply the first step in our project program to the frame image (pre-processing), the next step is to estimate the holder exponent allowing the following algorithm. There are various notions that can be used to estimate local Holder exponents. In our research, we use the log-log regression method. The holder exponent is a local measure in which at each neighborhood point we have a measure that we will present locally, we measure something like "fractal dimension", calculated by log-log regression performed at different scales (in our project we limited it in four scales "window dimension=[1, 3, 5, 7]").

According to the second chapter and among the multifractal measurements made to determine the holder image, we have chosen the max measure. The algorithm applied:

- Consider an arbitrary pixel "a central pixel" and its neighboring porches (Figure III- 11).
- After that, consider the maximum measurement of each window.
- Calculate the logarithm of the maximum values of each window.
- Plot the linear regression line "Log (maximum values)" by the function of the "Log (window dimension)".
- The slope of the linear regression is the value α "singularity coefficients".
- Repeat the same procedure for all pixels of the considered image.
- Find the Hölder image (α -image).

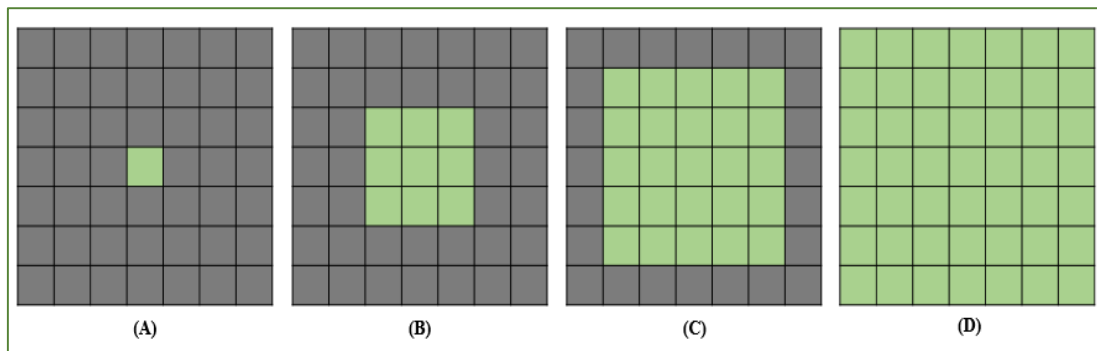


Figure III- 11: the tables designate the calculation windows for different window sizes in red color $w_0=1$ (A), $w_0=3$ (B) $w_0=5$ (C) and $w_0=7$ (D).

Example of Holder images obtained using images from the first database (Figure III- 12).

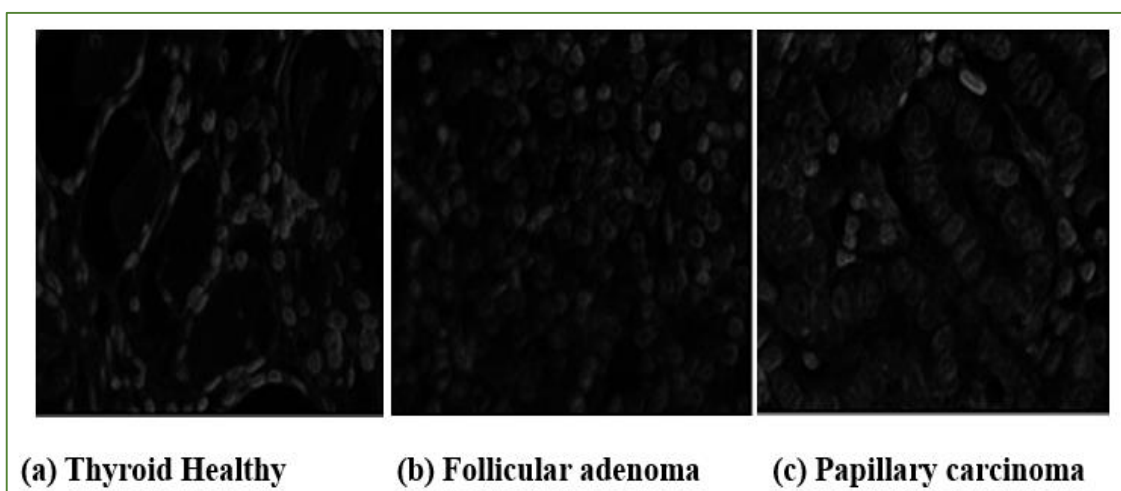


Figure III- 12: Holder images for different classes (a) (b) and (c).

Chapter III Application of the multifractal analysis method and Results

Example of Holder images obtained using images from the second database (Figure III- 13).

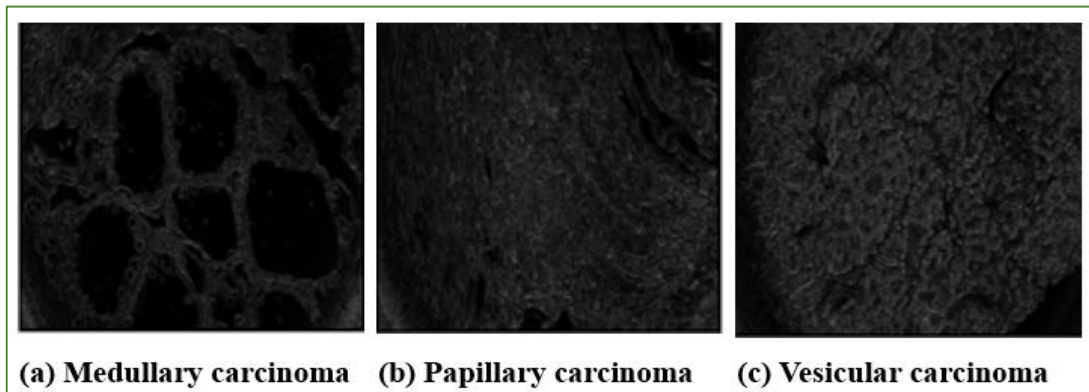


Figure III- 13: Holder images for different classes of carcinoma (a) (b) and (c).

III.6.3 Third part: Multifractal spectrum estimation

When the holder image has been estimated “the local characterization of the original image” then we will estimate the multifractal spectrum to characterize the intensity of this image “the global characterization”. This second part of the characterization in our multifractal analysis program is the calculation of the fractal dimension where sets of points have the same singularity coefficient alpha (Figure III- 14).

- Firstly, the α -values within the α -intervals are obtained by subdividing the range of α -values [$\alpha_{min}, \alpha_{max}$] into a pre-specified number of sub-intervals “with step is 0.1”.
- Therefore, the next step in the spectrum estimation is the application of the box-counting method seen in chapter two to determine the fractal dimension vector.
- Box-counting method counts the number of boxes, $n(\epsilon)$ with box size ϵ , that contain pixels with α -values within the α -interval, as shown in (Figure III- 14).
- Subdivision of the alpha image into boxes of different sizes.
- For each box size “epsilon”, calculate the number of boxes having at least one alpha value in the alpha interval; “if the box considered contains at least one pixel that have an alpha value in the range return number of boxes plus one”. Apply this step for all sub-intervals
- Calculate regression line between vectors $\text{Log}(\epsilon)$ and $\text{Log}(\text{number of boxes})$.
- Apply the algorithm until the number of max boxes is less then to the max of total number of boxes.
- Estimate the geometric multifractal spectrum by the equation (3 – 1) (Figure III- 15).

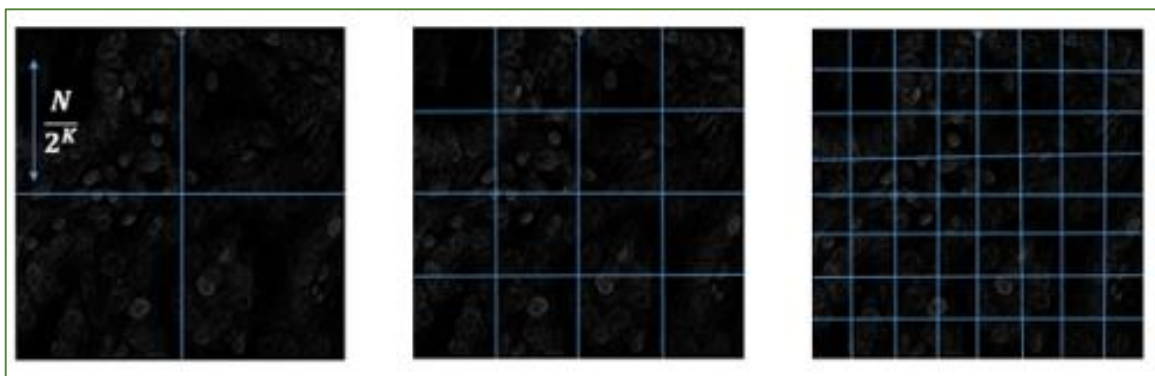


Figure III- 14: Box-counting method that uses different box sizes ϵ .

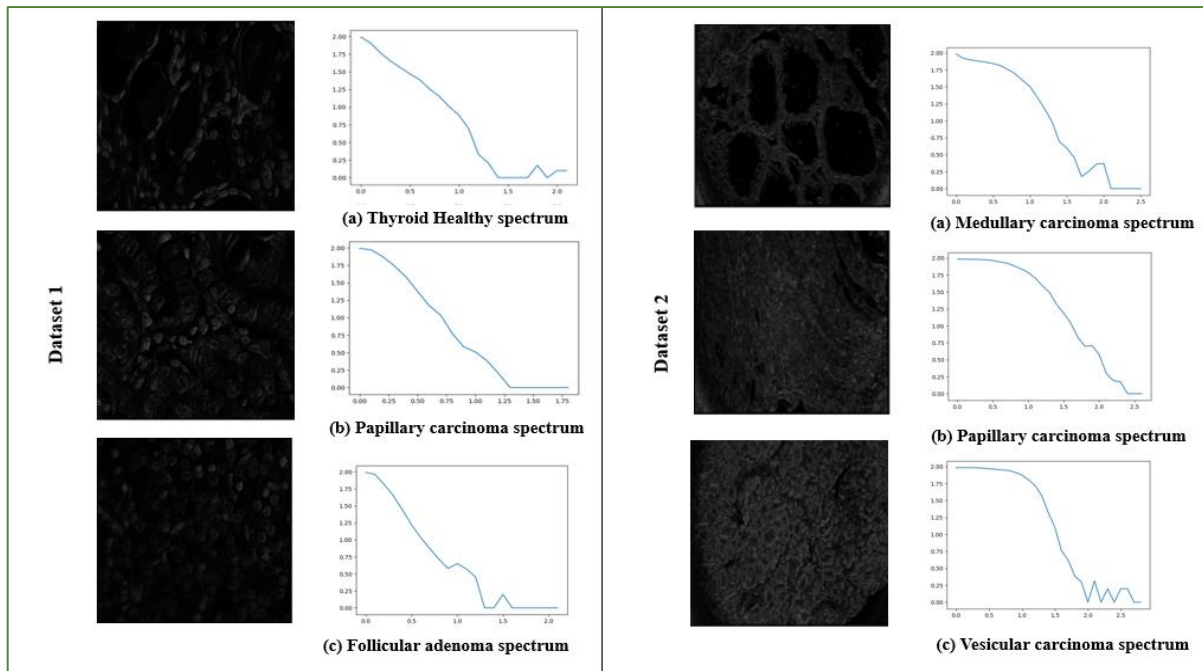


Figure III- 15: Example of multifractal spectrum obtained using holder images for the first and the second database.

III.7 Application and results

III.7.1 Pre-processing and Holder exponent estimation algorithms

We have selected 24 images from the two databases to be used in the application of our algorithm:

four images of a healthy thyroid, four images with follicular adenoma, and four images with papillary carcinoma (Figure III- 16), and from the second database, we have chosen four images with medullary carcinoma, four images with papillary carcinoma, and four images with vesicular carcinoma (Figure III- 17).

First database

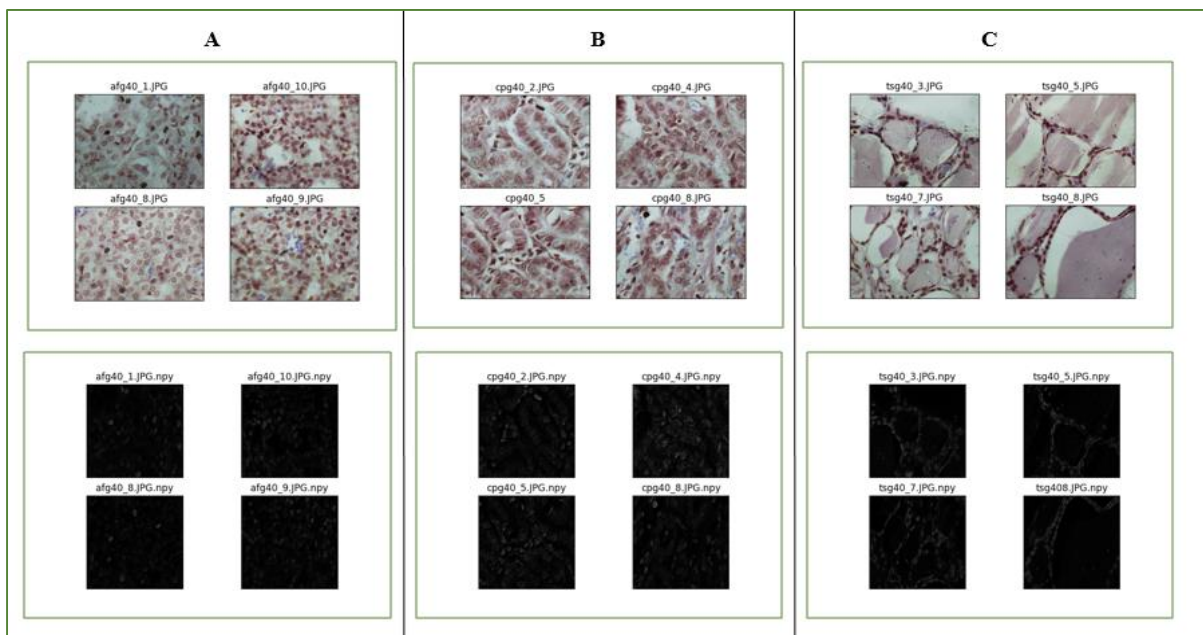


Figure III- 16: Preprocessing and Holder exponent-Samples from first Database (A: healthy thyroid; B: follicular adenoma; C: papillary carcinoma).

Chapter III Application of the multifractal analysis method and Results

Second database

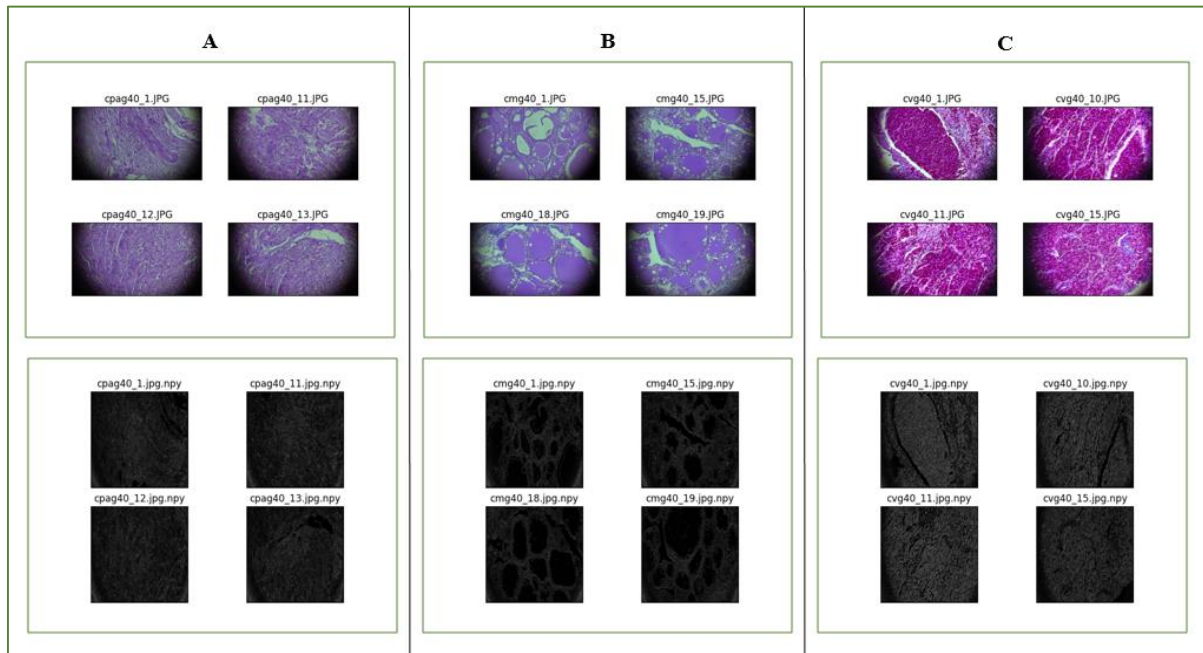


Figure III- 17: Preprocessing and Holder exponent-Samples from second Database (A: medullary carcinoma; B: papillary carcinoma; C: vesicular carcinoma).

III.7.2 Discussion of the result of the Holder exponent algorithm

- According to the Holder exponent of the images selected from the twice database in (Figure III- 16) and (Figure III- 17), Holder images make it possible to distinguish the image of a healthy subject from different diseased images.
- As indicated in (Figure III- 16) and (Figure III- 17) thyroid carcinoma tissues, and follicular adenoma tissues have a greater α -range of the α -image compared to healthy tissues in max measures.
- Based on these examples, we can conclude that the Holder exponent provides an efficient tool for detecting singularities.
- The choice of type of measure depends on what is to be detected: maximum measures in small environments can be used to detect all singularities.

III.7.3 Multifractal spectrum estimation

Until the holder image calculated, the estimation of the multifractal spectrum is the next step.

In the multifractal spectrum program that we use two vector are returned

- The first vector is named alpha vector contains α -values
- The second vector is named f alpha vector contains the fractal dimensions determined using the box counting method

The two vectors must be saved to be used in the rest analysis, in our case we save them in the first time as a python data type after that we use a program that convert them to excel data.

Chapter III Application of the multifractal analysis method and Results

Now we present in the following figures the results after the execution of the program on three classes of the previously obtained Holder images.

III.7.4 Multifractal spectrum First database

(Figure III- 18) shows multifractal spectrums of healthy thyroid holder images; (Figure III- 19) shows multifractal spectrums of follicular adenoma holder images; (Figure III- 20) shows multifractal spectrum of papillary carcinoma holder images.

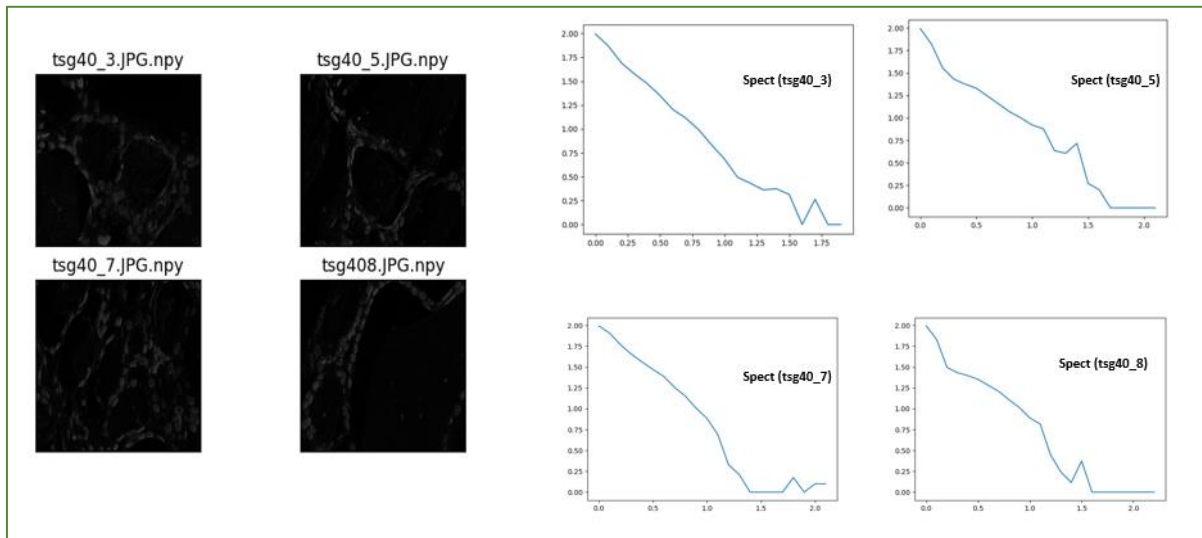


Figure III- 18: The multifractal spectrum of healthy thyroid holder images.

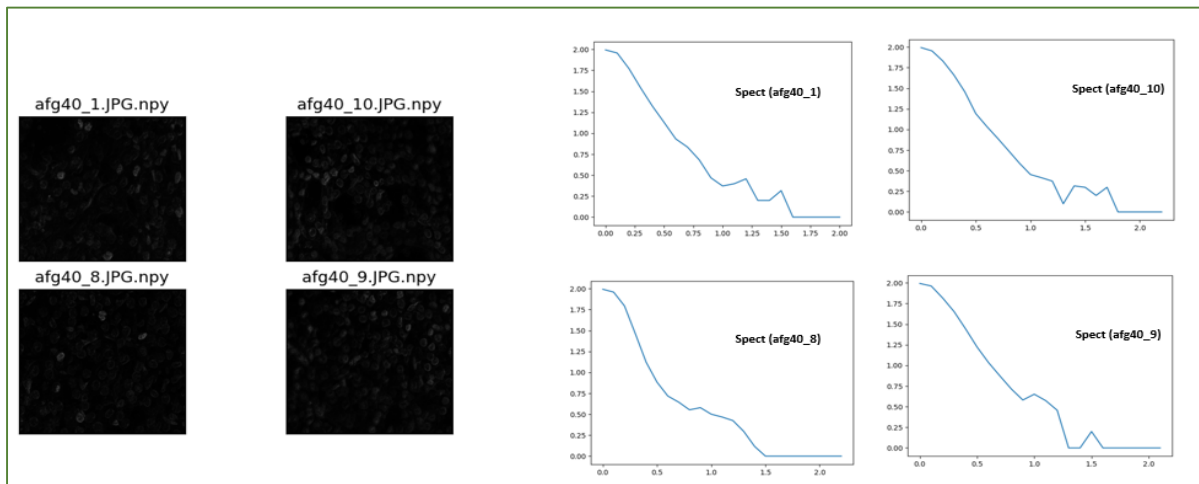


Figure III- 19: The multifractal spectrum of follicular adenoma holder images.

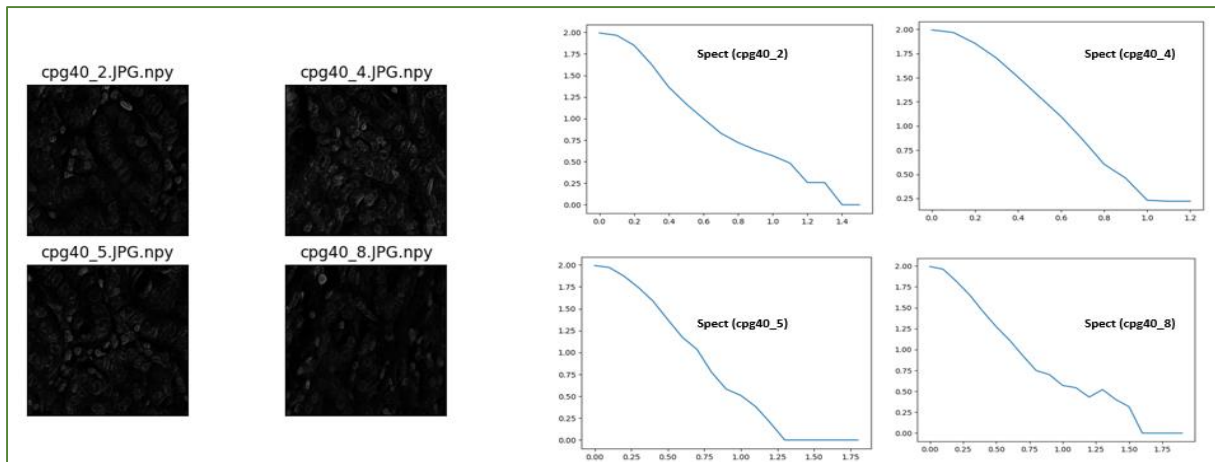


Figure III- 20: The multifractal spectrum of papillary carcinoma holder images.

III.7.5 Multifractal spectrum Second database

(Figure III- 21) shows multifractal spectrums of medullary carcinoma holder images; (Figure III- 22) shows multifractal spectrums of papillary carcinoma holder images; (Figure III- 23) shows multifractal spectrum of vesicular carcinoma holder images.

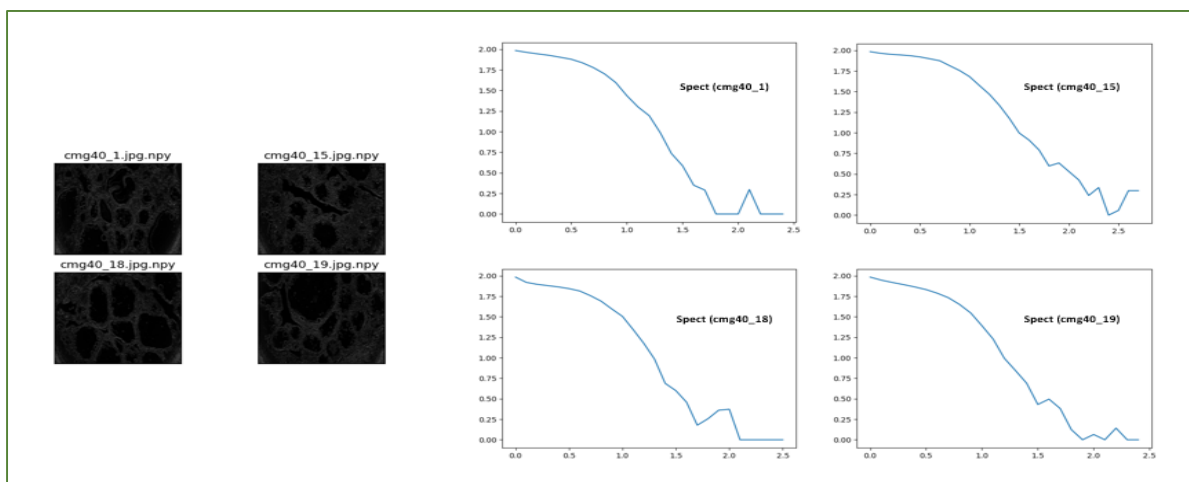


Figure III- 21: The multifractal spectrum of medullary carcinoma holder images.

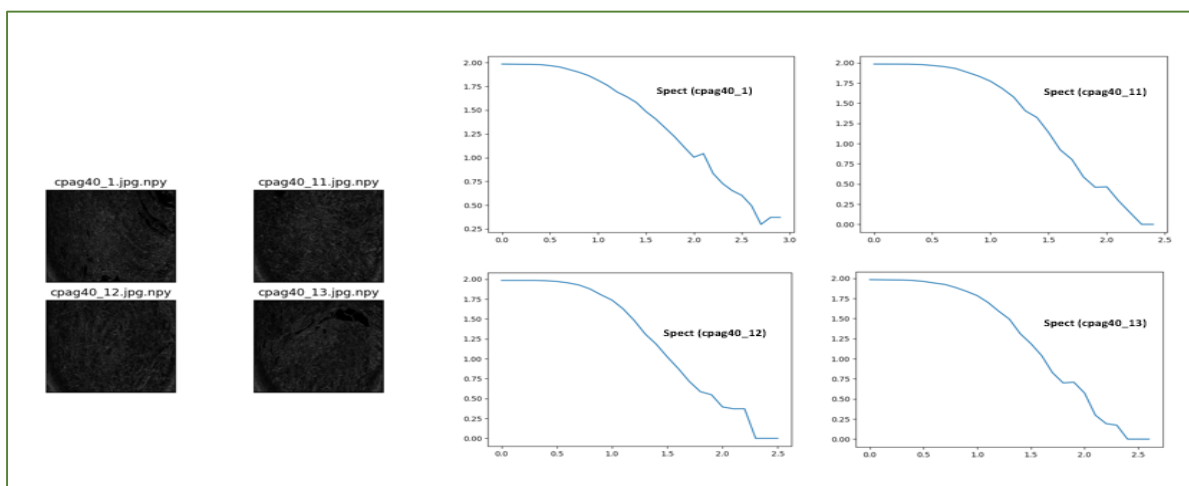


Figure III- 22: The multifractal spectrum of papillary carcinoma holder images.

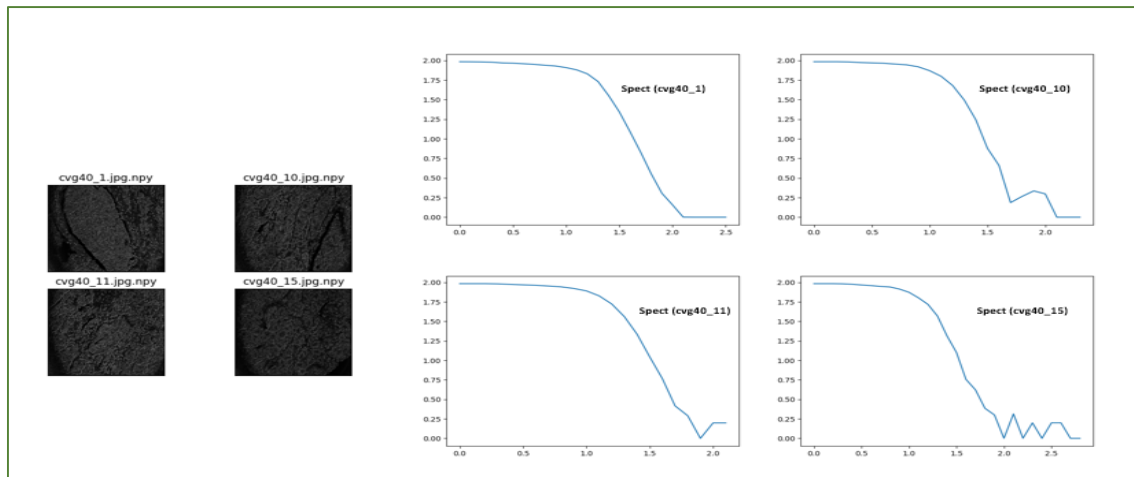


Figure III- 23: The multifractal spectrum of vesicular carcinoma holder images.

III.8 Step to classification

To compare different results obtained by the algorithm proposed we need to transform data save as python data to excel data for each class in first and second database after that we calculate the mean multifractal spectrum for each class. Finally, we present the means multifractal spectra corresponding to the three classes of the first database and three means specter of the second database.

- The first step is to load the data alpha and f_alpha saved previously as python data.
- The next step is to save data loaded to excel; for each image, we must save their data in a separable file.
- Then for each class, we have to concatenate Excel files for four images selected in one file.
- After that, as we need to plot all spectra of each class in one diagram the alpha minimum value for all images is zero and the maximum value is defined as the maximum value in four alpha vector.
- Then, we calculate and represent the mean spectrum for each class using Excel.
- Finally, for each database, we represent all mean spectra corresponding to the different classes in one diagram to compare their multifractal spectra.

Note

Here is the instruction that allows passing data from the python environment to excel which is a very easy tool to use.

```
#-----load the data alpha and f_alpha saved ----
with open ('path of the alpha data /name of data to open, 'rb') as f:
    alpha_vector1 = np.load (f)
with open ('path of the f_alpha data /name of the data to open','rb') as f:
    f_alpha1 = np.load (f)
#-----save to excel-----
df1 = pd.DataFrame ({'alpha_vector1': alpha_vector1, 'f_alpha1': f_alpha1})
df1.to_excel ("name the file 1.xlsx", index=True)
# ----- concatenate several Excel files -----
tout=[]
colonnes=[1,2] #here first and second colon of each file want to concatenate.
for f in glob.glob('path of files want to concatenate /*.xlsx'):
    df=pd.read_excel(f,usecols=colonnes)
    tout.append(pd.read_excel(f, usecols=colonnes))
df=pd.concat(tout, axis=1)
enregistrer=pd.ExcelWriter('path to save the result of the concatenation /name of
the file to save.xlsx')
df.to_excel(enregistrer, 'here put the name of the excel sheet')
enregistrer.save ()
```

Chapter III Application of the multifractal analysis method and Results

The following diagram represent the different multifractal spectra of the four images of **healthy thyroid class** (Figure III- 24).

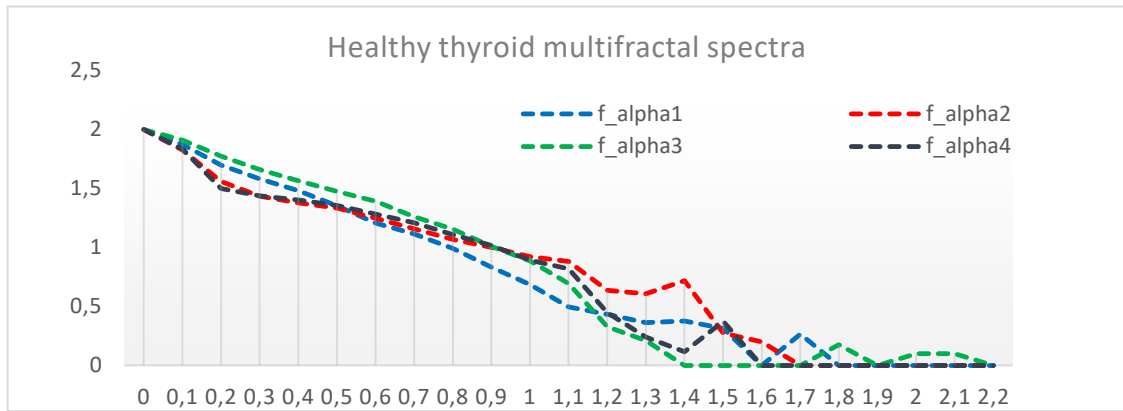


Figure III- 24: Excel diagrams of the f_{α} data as a function of α of the selected healthy thyroid images.

The following diagram represent the **mean multifractal spectrum** of the four images of healthy thyroid class (Figure III- 25).

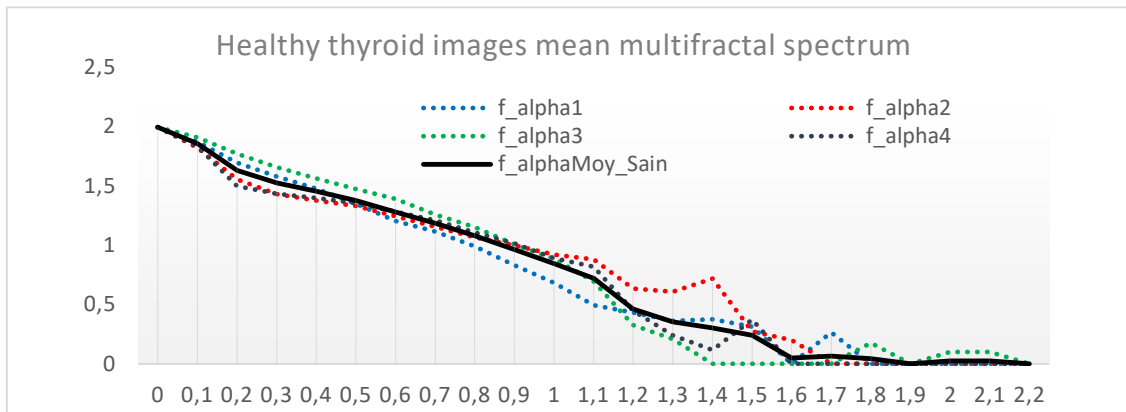


Figure III- 25: Excel diagram of the mean multifractal spectrum for the selected healthy thyroid images.

The following diagram represent the different multifractal spectra of the four images for **follicular adenoma class** (Figure III- 26).

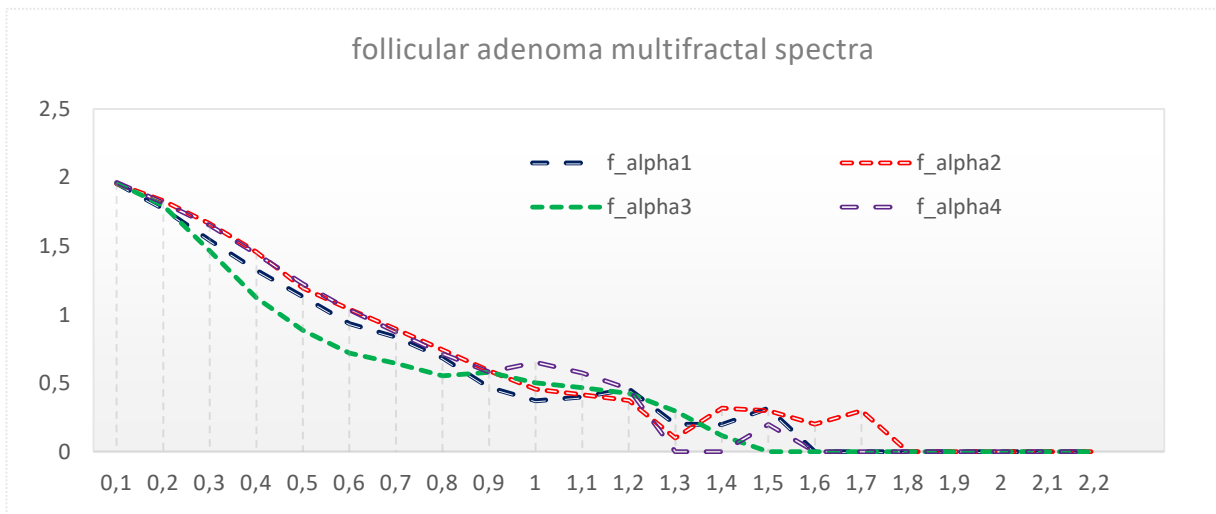


Figure III- 26: Excel diagrams of the f_{α} data as a function of α of the selected follicular adenoma images.

Chapter III Application of the multifractal analysis method and Results

The following diagram represent the **mean multifractal spectrum** of the four images of follicular adenoma class (Figure III- 27).

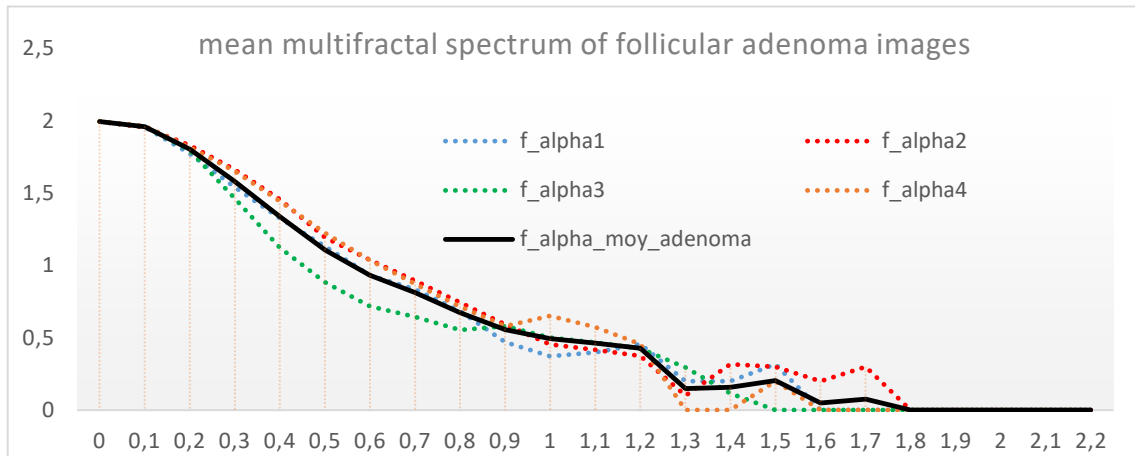


Figure III- 27: Excel diagram of the mean multifractal spectrum for the selected follicular adenoma images.

The following diagram represent the different multifractal spectra of the four images for **papillary carcinoma class** (Figure III- 28).

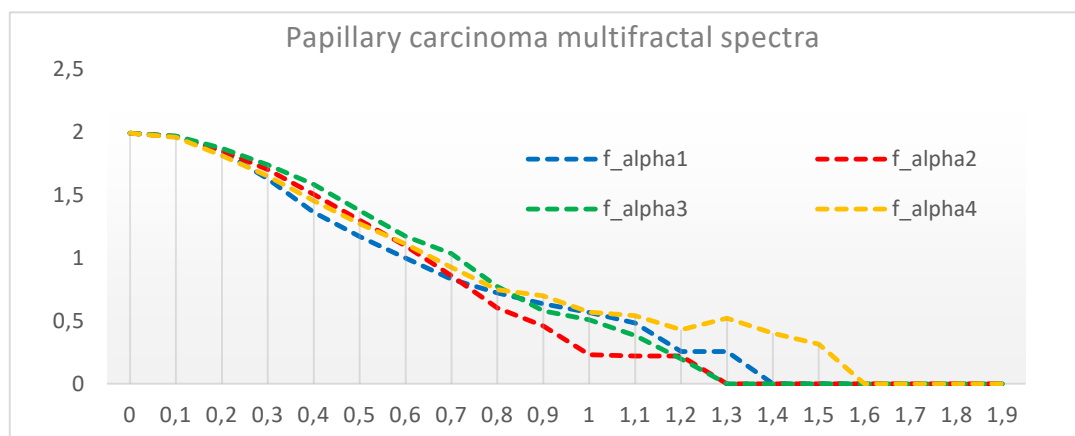


Figure III- 28: Excel diagrams of the f_α data as a function of α of the selected papillary carcinoma images.

The following diagram represent the **mean multifractal spectrum** of the four images of **papillary carcinoma class** (Figure III- 29).

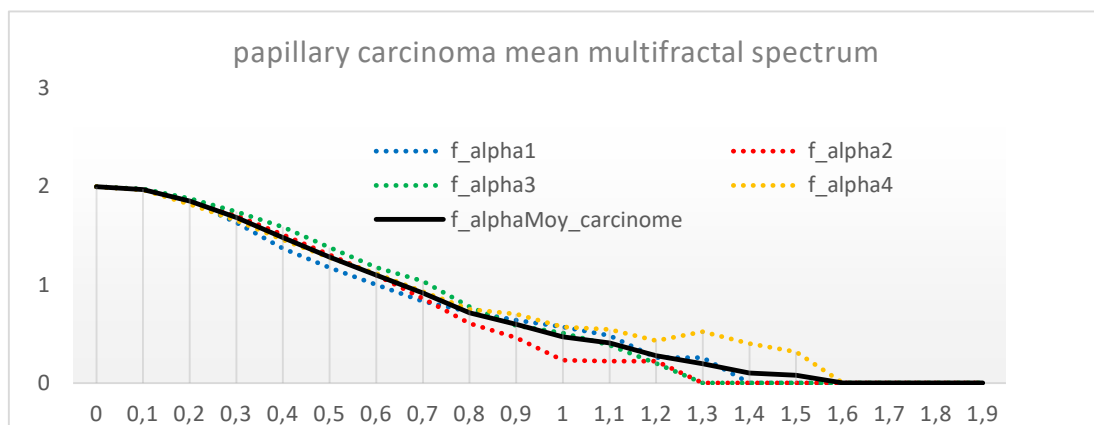


Figure III- 29: Excel diagram of the mean multifractal spectrum for the selected papillary carcinoma images.

Chapter III Application of the multifractal analysis method and Results

Multifractal mean spectra for different classes of healthy thyroid, follicular adenoma and papillary carcinoma from first Database (Figure III- 30).

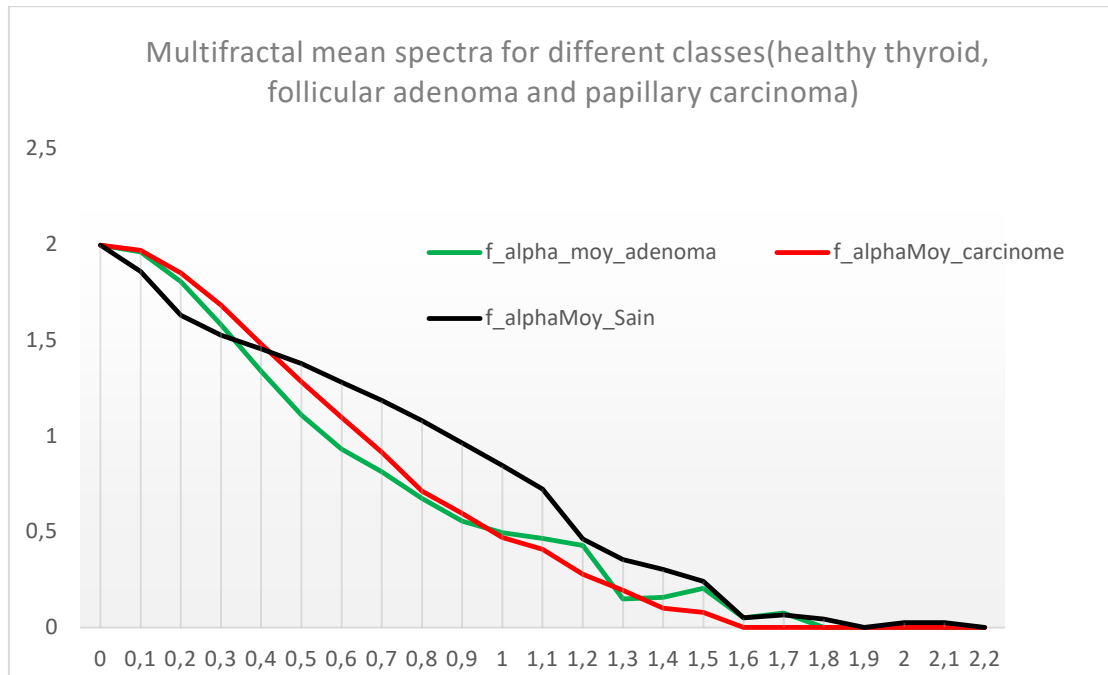


Figure III- 30: Excel diagram of the mean multifractal spectra for different classes of the first database.

III.8.1 Discussion First database result

- For the different three classes we noticed that the maximum values of the Hölder exponent “ f_{α} ” have a maximum mean spectrum $f(\alpha)$ close to two (dimension of a surface).
- In the healthy thyroid tissue images, the signal decreases regularly and reduced until it is zero (the signal in black color).
- In the case of the follicular adenoma signal (the signal in green color) compared with the healthy thyroid tissue signal, the follicular adenoma signal decreases differently in three zones, the first zone α in range $[0, 0.3]$ the signal is slowly changing then the healthy tissue signal, the second zone α in range $[0.3, 1]$ changing and decreases rapidly, the third zone α in range $[1, 1.8]$ changing in alternating form (increases and decreases).
- In the case of the papillary carcinoma signal (the signal in red color) compared with the healthy thyroid tissue signal, the signal decreases differently in three zones, the first zone α in range $[0, 0.4]$ the signal is more slowly decreasing then the twice described signals, the second zone α in range $[0.4, 1.6]$ changing and decreases rapidly, the third zone α in range $[1.6, 2.1]$ signal has a constant value of zero.
- According to the diagram of the variation of the obtained spectra in figure 31 and its discussion, we can say that the multifractal spectrum using box counting method can be used to classify the thyroid histological images and we can suggest the α in range $[0, 0.3]$ as the interested range.

Chapter III Application of the multifractal analysis method and Results

Second database

The following diagram represent the different multifractal spectra of the four images of **medullary carcinoma class** (Figure III- 31).

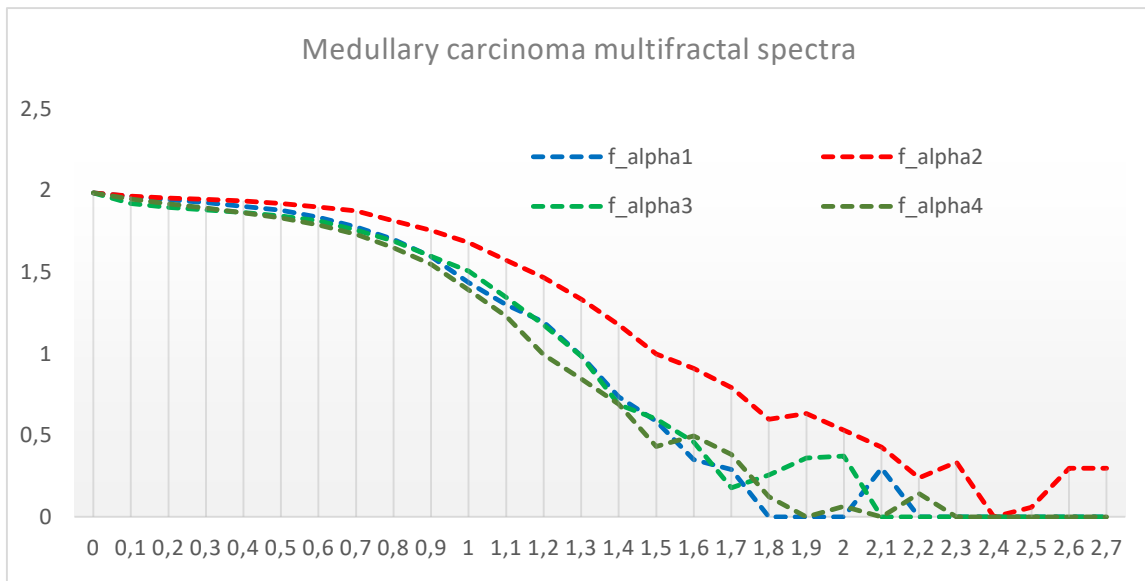


Figure III- 31: Excel diagrams of the f_{α} data as a function of α of the selected medullary carcinoma images.

The following diagram represent the **mean multifractal spectrum** of the four images of **medullary carcinoma class** (Figure III- 32).

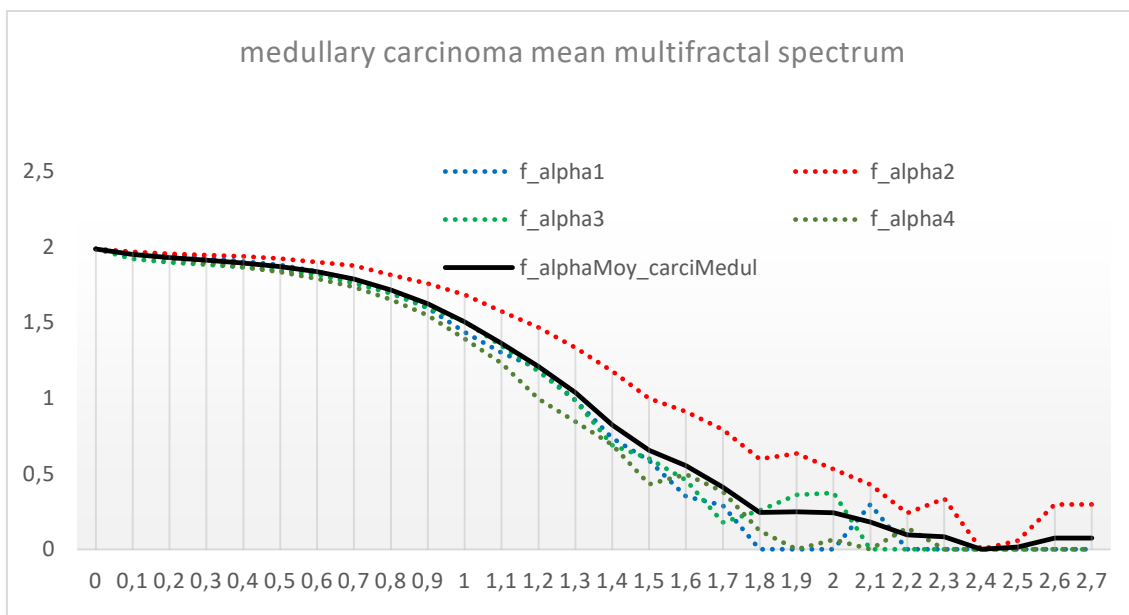


Figure III- 32: Excel diagram of the mean multifractal spectrum for the selected medullary carcinoma images.

Chapter III Application of the multifractal analysis method and Results

The following diagram represent the different multifractal spectra of the four images of **papillary carcinoma class** (Figure III- 33).

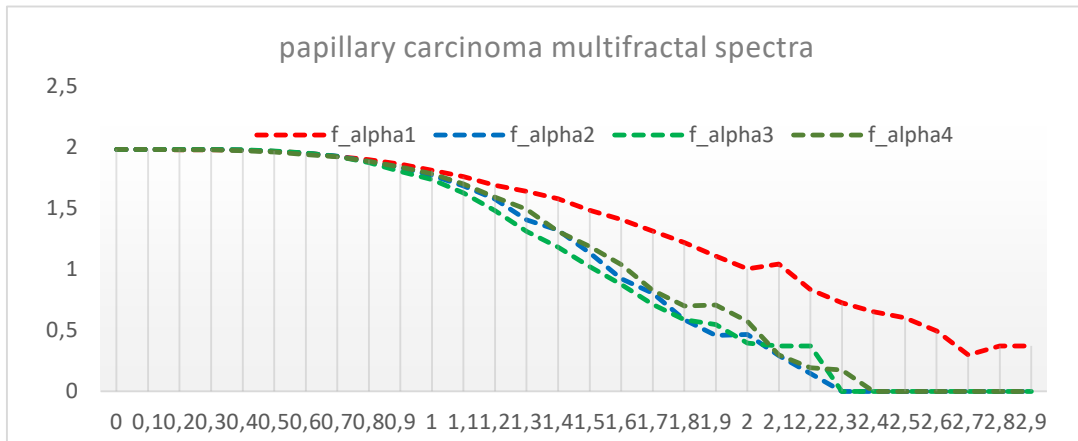


Figure III- 33: Excel diagrams of the f_{α} data as a function of α of the selected papillary carcinoma images.

The following diagram represent the **mean multifractal spectrum** of the four images of **papillary carcinoma class** (Figure III- 34).

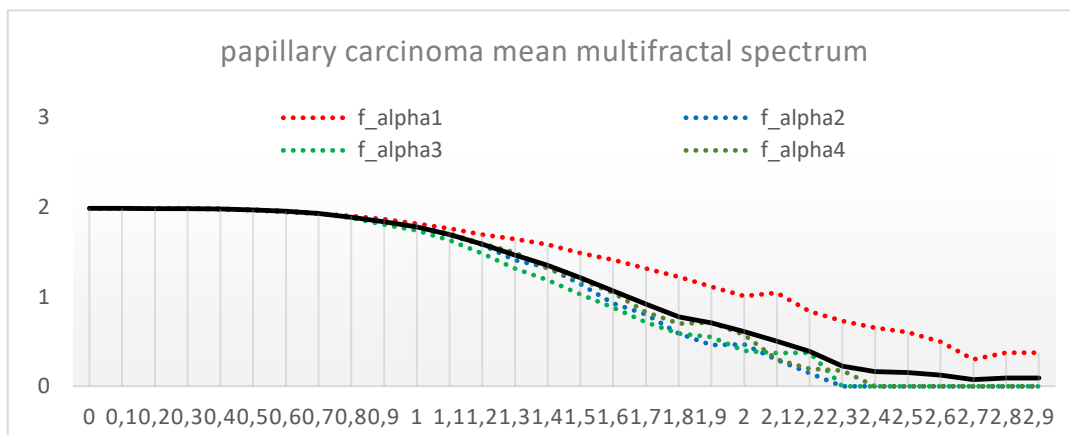


Figure III- 34: Excel diagram of the mean multifractal spectrum for the selected papillary carcinoma images.

The following diagram represent the different multifractal spectra of the four images **vesicular carcinoma class** (Figure III- 35).

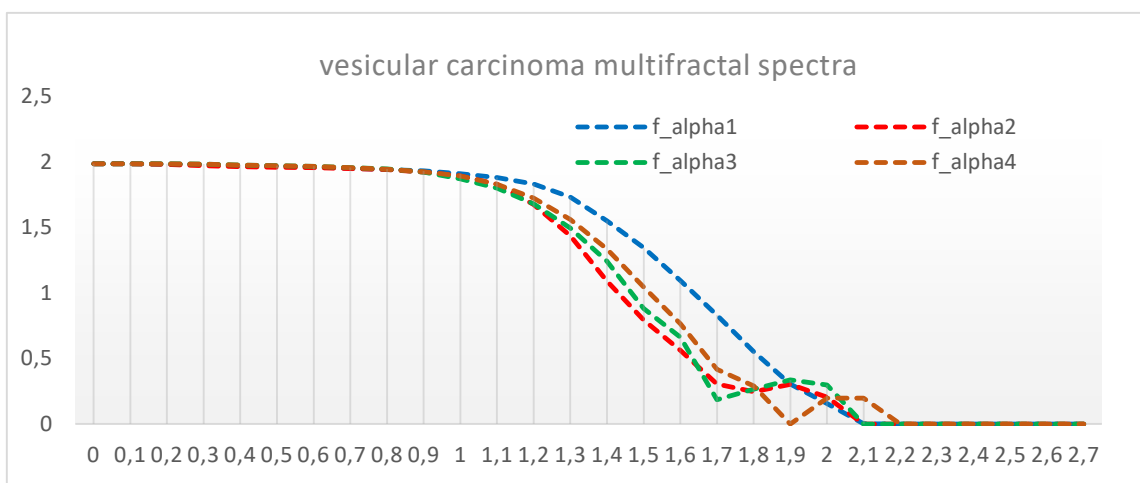


Figure III- 35: Excel diagrams of the f_{α} data as a function of α of the selected papillary carcinoma images.

Chapter III Application of the multifractal analysis method and Results

The following diagram represent the **mean multifractal spectrum** of the four images of **vesicular carcinoma** class (Figure III- 36).

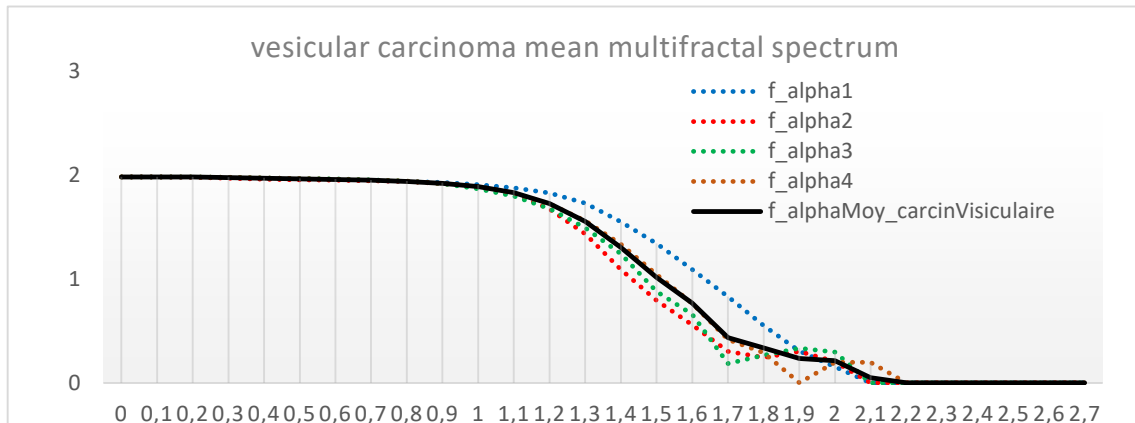


Figure III- 36: Excel diagram of the mean multifractal spectrum for the selected papillary carcinoma images.

(Figure III- 37) shows multifractal spectrum for different classes of carcinoma from second Database.

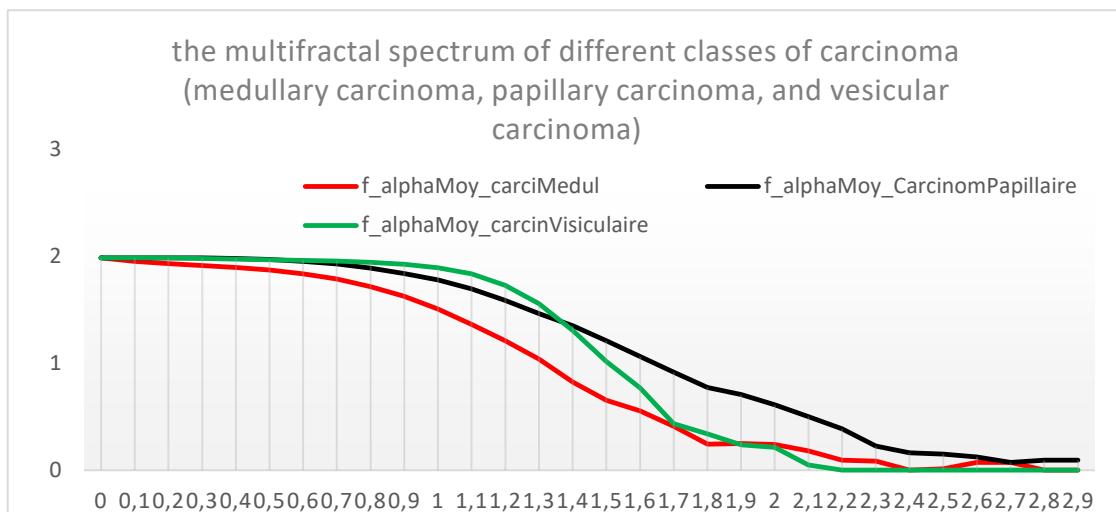


Figure III- 37: Excel diagram of the mean multifractal spectra for different classes of the second database.

III.8.2 Discussion second database result

- For the different three classes of carcinoma the same note in the previous discussion that is the maximum values of the Hölder exponent “f_alpha” have a maximum mean spectrum $f(\alpha)$ close to two (dimension of a surface).
- In the case of the medullary carcinoma images, the signal decreases rapidly and reduced until it is zero (the signal in red color).
- In the case of the vesicular carcinoma signal (the signal in black color), the signal decreases regularly compared with the other twice signals “the medullary carcinoma and papillary carcinoma”.
- In the case of the papillary carcinoma signal (the signal in red color) compared with the other signals, the signal decreases differently in three zones, the first zone α in range $[0, 0.9]$ the signal is constant and $f(\alpha)=2$ after that, with α in range $[0.9, 1.7]$ decreasing very rapidly then the twice described signals, then with α in range $[1.7, 2.8]$ the signal varying slowly.

Chapter III Application of the multifractal analysis method and Results

According to the diagram of the variation of the obtained spectra in (Figure III- 37) and its discussion, we can say that the multifractal spectrum using box counting method can be used to classify the different carcinoma classes of images and we can suggest the α in range $[0, 1.3]$ as the interested range.

III.8.3 Discussion of the pertinent parameters

Among these parameters, from the multifractal spectrum we can determine alpha min and alpha max for each class (Table III-1 and Table III-2) we can also determine the values of the peaks and the range interested in the analysis. Therefore, to improve the system for a better diagnosis tool, some of the future developments are suggested in the next section (general conclusion and perspective).

Table III- 1: Different alpha range of the classes for the first database.

Type of multifractal	<u>Follicular adenoma</u>		<u>Papillary carcinoma</u>		<u>Healthy</u>	
	α_{min}	α_{max}	α_{min}	α_{max}	α_{min}	α_{max}
Max measure	0	1.8	0	1.6	0	2.1

Table III- 2: Different alpha range of the classes for the second database.

Type of multifractal	<u>medullary carcinoma</u>		<u>papillary carcinoma</u>		<u>vesicular carcinoma</u>	
	α_{min}	α_{max}	α_{min}	α_{max}	α_{min}	α_{max}
Max measure	0	2.8	0	2.9	0	2.2

III.9 Conclusion

In this chapter, we presented our multifractal analysis approach based on box counting method as well as the different steps of our algorithm. We started with a description of the general design of our system followed by a brief description of the thyroid tissue databases. Then we moved on to the application of the different tasks in our algorithm with the discussion.

The calculation of the Hölder exponent gives good results for the differentiation between the different classes of thyroid tissue (Healthy, adenoma and carcinoma). In addition, it has been shown that a multifractal analysis of tissue images could be used for identifying different classes of cancer thyroid tissues.

The proposed multifractal methods could be combined with algorithms for extracting other features for effective classification of images of thyroid tissue.

Initial calculation of multifractal matrices requires the consumption of significant computer and time resources, especially if larger images are analyzed.

The general conclusion and perspectives are in the next section.

General Conclusion

And Perspectives

General Conclusion

Medical image analysis has significantly advanced image processing and led to the development of new diagnostic aid systems in the medical field. The latter's goal is to offer practitioners an automatic image interpretation that paves the way for the exploitation of anomalies. Due to the highly irregular shapes and complex image structures, the classification of tissue images is a difficult problem. Since it can accurately resolve local densities and represent different structures in the image, the multi-fractal analysis method has proven useful in characterizing the intensity distribution present in such images. The multifractal method uses the degree of Hölder regularity of a point measure as basic information. Instead of making and proving any assumptions, the multifractal method is simply applied to the image, and then based on the results different conclusions can be drawn about the structure and regularity of the image. In this work, we presented a method for characterizing histological images of the thyroid, which is the Multifractal analysis based on the box counting method.

First, we defined histology, its technical methods and the different technologies used in histological imaging. Then, since the images to be analyzed are thyroid images, we talked about the thyroid as well as their anatomy and histology followed by the functioning and the different pathologies and their classification. Finally, we end with a brief notion of papillary carcinoma and follicular adenoma.

In the second step, we defined the fractal geometry and the notion of fractal dimension, defining in addition, their methods of calculation. Next, regarding fractal analysis we focused specifically on multifractal analysis as an extension of fractal analysis. After having described this method and its local 'holder exponent' and global 'multifractal spectrum or singularity spectrum' characterization tools, we present the methods for estimating the multifractal spectrum.

In order to overcome the factors that limit the analysis of histological images of the thyroid, we have proposed a multifractal analysis method based on the box-counting method. The method includes four main steps: the analysis and preprocessing of the histological image, estimation of the Holder exponent and we chose the maximum intensity as a measure type, then, the estimation of the multifractal spectrum by the box-counting method, and finally, we saved the data saved previously as python data in Excel to interpret and analyze them. Excel Data can be used for extraction of pertinent parameters that are set as input layer for an automatic classifier such as SVM. Since we have not reached this stage in this research project, we are content to interpret the differences visually from the multifractal spectra. We noticed that the multifractal spectra present differences from one class of tissue to another: healthy tissue/ Adenoma / Carcinoma and a differentiation between different types of carcinoma. We notice that these differences are mainly in the final third of the spectrum (differences between the α_{\max} , peaks, and decay rate).

Therefore, we can conclude that this approach is suitable for the analysis of irregularities present in thyroid histological images. Moreover, we can finally propose some perspective to improve this work in future work.

Perspectives in future works

The results presented in this project show that multifractal analysis could be a valuable tool in the characterization of histological images for identifying irregularities and in estimating singularities. Some possible enhancements and future research directions are outlined below:

1. Use other types of intensity measures

There are many types of intensity measures in multifractal analysis that can be used: inverse-minimum measure, mean measure, summation measure, and Iso measure... etc.

2. Focus on the interval of spectrum where differences occurs and make it more precise by sub-sampling alpha vector in Holder Images.

3. Find the relevant parameters

There are many parameters that we can be used to characterize the multifractal spectrum (for instance, the alpha min and alpha max, $f_{max}(\alpha)$ and $f_{min}(\alpha)$)

4. Perform classification step using support vector machine classifier (or another automatic classifier) :

According to the results that we obtained in the previous chapter, we can use SVM classifier to separate each class automatically.

5. Introduce multi-scale techniques

- To characterize the features of interest at various resolutions, the multifractal analysis attempted in this research could be combined with multi-scale methods (for instance, wavelets).
- Explore the multi-scale advantages from data acquisition (microscope zoom tool).

References

References

- [1] I. Reljin et al., «Multifractal analysis of Gray-Scale Images,» chez *10th Mediterranean Electrotechnical Conference, MEleCon 2000*, Algeria, 2000.
- [2] M. a. Kadhim, «Using Multifractals to Remove Noise and Segmentation of Medical Images,» *Solid State Technology*, vol. 63, n° 13, pp. 4297-4306, 2020.
- [3] C. Atupelage, H. Nagahashi, M. Yamaguchi, T. A. A. Hashiguchi et M. Sakamoto, «Multifractal Feature Descriptor for Grading Hepatocellular Carcinoma,» chez *21st International Conference on Pattern Recognition (ICPR 2012)*, Tsukuba, Japan, 2012.
- [4] R. Korchiyne, A. Sbihi, S. M. Farssi, R. Touahni et M. T. Alaoui, «spectre multifractal: applications aux images médicales,» *Mediterranean Telecommunication Journal*, vol. 2, n° 12, pp. 133-137, 2012.
- [5] M. khider, *Analyse multifractale par MMT0-2D : Evaluation sur des images radar et médicales*, alger: USTHB, 2014.
- [6] C. Atupelage, H. Nagahashib et M. Y. M. Sakamoto, «Multifractal feature descriptor for histopathology,» *Analytical Cellular Pathology*, vol. 35, p. 123–126, 2012.
- [7] J. ANDJELKOVIC, N. ZIVIC, B. RELJIN, V. CELEBIC et I. SALOM, «Application of Multifractal Analysis on Medical Images,» *WSEAS TRANSACTIONS on INFORMATION SCIENCE and APPLICATIONS*, vol. 5, n° 111, pp. 1561-1572, 2008.
- [8] R. Mukundan, D. Racoceanu et T. ChiangHau, «Multifractal Analysis of Histopathological Tissue Images,» *ResearchGate*, 2014.
- [9] I. Capo, D. Miljković, B. A. Visnjic et M. Popović, «Virtual microscopy in histology and pathology education at the Faculty of,» *Medicinski Pregled*, pp. 371-376, 2017.
- [10] É. BOUCHERON, D. CHRQUI, A. GUIVARC'H et J. POIRIER, «universalis.fr,» Encyclopædia Universalis France, [En ligne]. Available: <https://www.universalis.fr/encyclopedie/histologie/>. [Accès le 9 3 2022].
- [11] A. L. Mescher, *Junqueira's Basic Histology*, Bloomington, Indiana University School of Medicine: McGraw-Hill Education., 2016.
- [12] D. C. KOHLER, *Enseignement Histologie*, Collège universitaire et hospitalier des histologistes, embryologistes, cytologistes et cytogénéticiens (CHEC) : Université Médicale Virtuelle Francophone, 2011.
- [13] B. M. Carlson, *Tissues. The Human Body*, : Academic Press, 2019, pp. 27-63.
- [14] Kurt E. Johnson, *histology and cell biology*, washington : Williams & Wilkins, Baltimore, Maryland, 1991.

- [15] T. Clark Brelje University of Minnesota, «histology guide,» Rice University, 2019. [En ligne]. Available: <https://histologyguide.com/figure-view/fig-023-tissue-types/00-figure-1.html?x=4572&y=3334&z=52.5>. [Accès le 27 janury 2022].
- [16] G. Rolls, «Leica Biosystems,» Leica Biosystems division of Leica Microsystems, 2022. [En ligne]. Available: <https://www.leicabiosystems.com/fr/knowledge-pathway/an-introduction-to-specimen-processing/>. [Accès le 08 february 2022].
- [17] D. B. McMillan et Richard J. Harris, *Atlas of Comparative Vertebrate Histology*, Western University: Elsevier Inc., 2018.
- [18] N. Parry, «Bitesize Bio,» Science Squared, 19 November 2020. [En ligne]. Available: <https://bitesizebio.com/13398/how-histology-slides-are-prepared/>. [Accès le 2022].
- [19] m. Ehtishem et r. khan, Microscope, India : researchgate, 2016.
- [20] S. S. Gajghate, «onIntroduction to Microscopy,» researchgate, 2017. [En ligne]. Available: <https://www.researchgate.net/publication/320945390>. [Accès le 2022].
- [21] U. M. Rafei, «THE MICROSCOPE,» chez *THE MICROSCOPE a practical guide*, india, world health organization, 1999, p. .
- [22] «Atlas of Plant and Animal Histology,» Dep. of Functional Biology and Health Sciences., 24 7 2019. [En ligne]. Available: <https://mmegias.webs.uvigo.es/02-english/6-tecnicas/6-optico.php>. [Accès le 2022].
- [23] Theydiffer, «Theydiffer.com,» Theydiffer, 6 7 2015. [En ligne]. Available: <https://theydiffer.com/difference-between-a-light-microscope-and-an-electron-microscope/>. [Accès le 2022].
- [24] S. Bradbury, «Britannica,» Open University (A Britannica Publishing Partner), [En ligne]. Available: <https://www.britannica.com/technology/scanning-electron-microscope>. [Accès le 2022].
- [25] R. Arrangoiz, F. Cordera, D. Caba, M. Muñoz and Eduar, "Comprehensive Review of Thyroid Embryology, Anatomy, Histology, and Physiology for Surgeons," *International Journal of Otolaryngology and Head & Neck Surgery*, vol. 7, no. , pp. 160-188, 16 7 2018.
- [26] J. SAMBAD, «SlideShare,» 20 2 2018. [En ligne]. Available: <https://www.slideshare.net/jagdishsamabd/hyperthyroidism-hypothyrodism>. [Accès le 12 02 2022].
- [27] Oliver Jones, «TeachMe,» TeachMe anatomy, 8 11 2020. [En ligne]. Available: <https://teachmeanatomy.info/neck/viscera/thyroid-gland/>. [Accès le 12 02 2022].
- [28] J.-L. Wémeau, «Les maladies de la thyroïde,» 2010. [En ligne]. Available: <https://books.google.dz/books?id=1T-4-TfwPS8C&lpq=PP1&dq=livre%20histologie%20de%20la%20thyroïde%20pdf&hl=fr&pg=PP1#v=onepage&q&f=false>. [Accès le 2022].
- [29] M. Marc, histologie des organes, paris : études vivants, collection acadimic press, 1980.

- [30] R. Arrangoiz, M. Manuel , C. Fernando et L.-d.-L. Enrique , «Comprehensive Review of Thyroid Embryology, Anatomy, Histology, and Physiology for Surgeons,» *International Journal of Otolaryngology and Head & Neck Surgery*, vol. , n° %17, pp. 160-188, July 2018.
- [31] B. Brady, "EndocrineWeb," Remedy Health Media, 26 Mar 2019. [Online]. Available: <https://www.endocrineweb.com/conditions/thyroid-nodules/thyroid-gland-controls-bodys-metabolism-how-it-works-symptoms-hyperthyroi>. [Accessed 2022].
- [32] [En ligne]. Available: http://people.eku.edu/ritchisong/308_notes_4.htm.
- [33] F. T. F. M. C. T. C. G. C. L. C. Buffet, «Cancers de la thyroïde,» *EMC - Endocrinologie-Nutrition*, vol. 13, n° %14, p. , 2016.
- [34] M. L. E. L. S. E. M. d. J.-L. W. C. Do Cao, «Nodules du corps thyroïde,» *EMC - Endocrinologie-Nutrition*, vol. 12, n° %12, p. , 2015.
- [35] N. Genere, H. Bryan, H.-S. Fady et Leonard, Wartofsky, «Endocrine Society,» Endocrine Society, 23 January 2022. [En ligne]. Available: <https://www.endocrine.org/patient-engagement/endocrine-library/thyroid-nodules>. [Accès le 2 2022].
- [36] .. [En ligne]. Available: <https://my.clevelandclinic.org/health/diseases/13121-thyroid-nodule>. [Accès le].
- [37] G. B. Salabè, «Pathogenesis of thyroid nodules: histological classification?,» *Biomedicine & Pharmacotherapy*, vol. 55, n° %11 , pp. 39-53, 2001.
- [38] M. Prelipcean, «healthline,» Healthline Media a Red Ventures Company, 15 July 2019. [En ligne]. Available: <https://www.healthline.com/health/thyroid-nodule>. [Accès le 02 2022].
- [39] E. B., «sante sur le net,» Cherry for Life Science, 4 janury 2018. [En ligne]. Available: <https://www.sante-sur-le-net.com/maladies/metabolisme/nodule-thyroidien/>. [Accès le 02 2022].
- [40] C. Daumerie, «Louvain Medical,» march 2016. [En ligne]. Available: <https://www.louvainmedical.be/fr/article/approche-clinique-dans-la-prise-en-charge-du-nodule-thyroidien>. [Accès le 2022].
- [41] M. C. Staff, Mayo Clinic Family Health Book, Rochester: Mayo Clinic , 2022.
- [42] C. B. B. R. A. R. M. B.-P. G. Russ, «Le système TIRADS en échographie thyroïdienne,» *JOURNAL DE RADIOLOGIE*, vol. 92, n° %17-8 , pp. 701-713, 2011.
- [43] A. pandey, «myUpchar,» myUpchar, 20 8 2019. [En ligne]. Available: <https://www.myupchar.com/en/test/thyroid-scan>. [Accès le 2 2022].
- [44] M. Schlumberger, «Cancer papillaire et folliculaire de la thyroïde,» 6 2007. [En ligne]. Available: www.orpha.net/data/patho/Pro/fr/CancerPapillaireFolliculaireThyroide-FRfrPro905v01.pdf. [Accès le 2022].

- [45] V. S. S, «ilovepathology,» ilovepathology , 19 5 2016. [En ligne]. Available: www.orpha.net/data/patho/Pro/fr/CancerPapillaireFolliculaireThyroide-FRfrPro905v01.pdf. [Accès le 2022].
- [46] B. A. a. K. Maroua, *AIDE AU DIAGNOSTIC DES NODULES THYROIDIENS PAR CLASSIFICATION DES COUPES HISTOLOGIQUES*, Tlemcen, Département de Génie Biomédical: , 2020.
- [47] *Thyroid Nodules Diagnosis and Management*, USA: Springer International Publishing AG, 2018 .
- [48] v. gerard, «diconombre,» diconombre, 03 02 2020. [En ligne]. Available: <http://villemin.gerard.free.fr/Wwwgvmm/Suite/Fractal.htm#histo>. [Accès le 02 2022].
- [49] «le bloguen,» FLG Design, 26 03 2013. [En ligne]. Available: <http://www.blog.francis-leguen.com/les-fractales-apollonienes/>. [Accès le 25 03 2022].
- [50] M. L. L. L. WEBER Louise, «tpe fractales montebello,» Lycée Montebello, Lille, 2013-2014. [En ligne]. Available: <https://tpefractales-montebello.weebly.com/geacuteneacuteraliteacutes-et-historique.html>.
- [51] B. Mandelbrot, *Les Objets Fractals : forme, hasard et dimension*, : Flammarion, 1975.
- [52] B. B.Mandelbrot, *The Fractal Geometry of nature*, New York : W.H. FREEMAN and company, 1977, 1982, 1983.
- [53] E. L. Jacques Lévy-Véhel, *Fractals in Engineering*, France : Springer-Verlag London Limited, 2005.
- [54] B. Mandelbrot, «How Long Is the Coast of Britain? Statistical Self-Similarity and Fractional Dimension,» *Science*, p. 636–638, 1967.
- [55] J.-P. Berroir, *Analyse Multifractale d'images*, PARIS IX : UNIVERSITE PARIS IX - DAUPHINE.
- [56] «journals plos,» [En ligne]. Available: <https://journals.plos.org/plosone/article?id=10.1371/journal.pone.0029956>.
- [57] M. , A. A. , M. S.ZEHANI, «ANALYSE FRACTALE DE TEXTURE : APPLICATION A L'IMAGE IRM ET,» *Courrier du Savoir*, vol. , n° %112, pp. 57-61, 2011.
- [58] w. E. Lorenz, *fractals and fractal architecture*, : ResearchGate, 2003.
- [59] J. LAJOIE, *COMME EXIGENCE PARTIELLE DE LA MAITRISE EN MATH'EMATIQUES ET INFORMATIQUE APPLIQU'ES*, QUEBEC: L'UNIVERSITE DU QUEBEC A TROIS-RIVIERES, 2006.
- [60] H. F. Jelinek, C. L. Jones, M. D. Warfel, C. Lucas, C. Depardieu et G. Aurel, «Understanding Fractal Analysis? The Case of Fractal Linguistics,» *Complexus*, vol. 3, pp. 66-73, 2006.
- [61] D. R. D. R. I. Z. S. B. Gabriele A. Losa, «From Fractal Geometry to Fractal Analysis,» *Applied Mathematics*, vol. 7, pp. 346-354, 2016.
- [62] L. Yong, «An Introduction to Fractal Analysis,» *Rose-Hulman Undergraduate Mathematics Journal*, vol. 22, n° %11, 2021.
- [63] L. S. Liebovitch et L. A. Shehadeh, *Introduction to Fractals*, Florida Atlantic University.

- [64] B. O. Bech, *Automatic Computation of Potential Tumor Regions in Cancer Detection using Fractal analysis techniques*, CATALUNYA, 2009.
- [65] J.-J. Gervais, *introduction aux fractals et aux systèmes dynamiques*, 2009.
- [66] A. Reha, A. E. AMRI, O. Benhammouch et A. Oulad-Said, «Fractal Antennas : A Novel Miniaturization Technique for wireless Networks,» *researchgate*, 2014.
- [67] A. Gires, *Analyses et simulations multifractales pour une gestion des eaux pluviales en milieux urbain et péri-urbain*, Paris-Est: Ecole Doctorale Science ingenierie et environnement, 2012.
- [68] J. Briggs, «nova,» nova, 10 2008. [En ligne]. Available: <https://www.pbs.org/wgbh/nova/fractals/set.html>. [Accès le . 3 2022].
- [69] I. S. RELJIN et B. D. RELJIN, «Fractal geometry and multifractals in analyzing and processing medical data and images,» *ONCONet*, vol. 10, n° 14, pp. 283-93, 2002.
- [70] H. F. Jelinek et E. Fernandez, «Neurons and fractals: how reliable and useful are calculations of fractal dimensions?,» *Journal of Neuroscien Methods* , vol. 81, pp. 9-18, 1997.
- [71] B. Yamin, *Caractésation fractale et multi-fractale du transfert de chaleur. Application aux feux*, Oran: Faculté de physique Département de physique Energétique, 2014.
- [72] N. T. Milošević, «Fractal analysis of two dimensional images: parameters of the space-filling and shape,» chez *20th International Conference on Control Systems and Science*, Belgrade, 2015.
- [73] N. e. al, *Fractal Dimension Estimation Methods for Biomedical Images*, IntechOpen, 2012.
- [74] K. Falconer, *The geometry of fractal sets*, Cambridge: Cambridge university Press , 2002.
- [75] K. Khemis, S. A. Lazzouni, M. Messadi, S. Loudjedi et A. Bessaid, «New Algorithm for Fractal Dimension Estimation based on Texture Measurements: Application on Breast Tissue Characterization,» *I.J. Image, Graphics and Signal Processing*, vol. 4, pp. 9-15, 2016.
- [76] E. Nilsson, *Multifractal-based Image Analysis with applications in Medical Imaging*, Sweden: Ume University, 2007.
- [77] D. R. D. R. I. Z. S. B. Gabriele A. Losa, «From Fractal Geometry to Fractal Analysis,» *Scientific Research*, vol. 7 , n° 14, pp. 346-354, 2016.
- [78] F. Wang et Y. Zai, «Fractal and multifractal characteristics of shale nanopores,» *Results in Physics*, vol. 25, 2021.
- [79] R. Lopes et N. Betrouni, «Fractal and multifractal analysis: A review,» *Medical Image Analysis*, vol. 13, p. 634–649, 2009.
- [80] B. Kiinkenbergh, «A Review of Methods Used to Determine the Fractal Dimension of Linear Features,» *Mathematical Geology*, vol. 26 , n° 11, pp. 23-46, 1994.
- [81] P. D. ., I. B. ., H. A.-B. ., S. M. N. B. R. Lopes, «La géométrie fractale pour l'analyse de signaux médicaux : état de l'art,» *IRBM*, vol. 31, p. 189–208, 2010.

- [82] R. Lopes, *Analyses fractale et multifractale en imagerie medicale: outils, validation et applications.*, universite Lille: universite Lille, 2009.
- [83] N. K. Serradj, S. Lazzouni et M. Messadi, «Digital mammograms analysis using fractal and multifractal methods,» *IEEE Xplore*, 2019.
- [84] A. K. Cheeseman et E. R. Vrscay, «Estimating the Fractal Dimensions of Vascular Networks and Other Branching Structures: Some Words of Caution,» *mathematics*, vol. 10, p. 839, 2022.
- [85] S. a. Zehani, «ANALYSE FRACTALE DE TEXTURE : APPLICATION A L'IMAGE IRM Et CT-SCAN DE L'OS TRABECULAIRE,» *Courrier du Savoir*, n° 112, pp. 57-61, 2011.
- [86] L. C. Ribas, D. N. Gonçalves, J. d. A. Silva, A. A. d. C. Jr, O. M. Bruno et W. N. Gonçalves, «Fractal dimension of bag-of-visual words,» *Springer-Verlag London Ltd.*, vol. 22, p. 89–98, 2018.
- [87] Y. T. Du G., «A novel Multifractal Estimation Method and Its Application to Remote Image Segmentation,» *IEEE*, vol. 40, n° 14, pp. 980-982, 2002.
- [88] W. H. K. Lee, «A robust algorithm for the fractal dimension of images and its applications to the classification of natural images and ultrasonic liver images,» *Signal Processing*, vol. 90, pp. 1894-1904, 2010.
- [89] H. L. N. Q. D. G. J. Qiu, «Fractal characterization of hyperspectral imagery,» *Photogrammetric Engineering and Remote Sensing*, vol. 65, n° 11, p. 63–71, 1999.
- [90] S. N. J. H. R. A. D. Peleg, «Multiple resolution texture analysis and classification,» *IEEE Transactions on Pattern Analysis and Machine Intelligence*, vol. 6, pp. 518-523, 1984.
- [91] P. e. a. Asvestas, «Estimation of fractal dimension of images using a fixed mass approach,» *Pattern Recognition Letters*, vol. 20, pp. 347-354, 1999.
- [92] S. A. Asma et B. Meriem, *La géométrie fractale dans l'analyse et le traitement des images médicales : Application à l'ostéoporose et à la mammographie*, Tlemcen, 2013.
- [93] A. Arneodo et S. Jaffard, «Images des maths,» 15 10 2004. [En ligne]. Available: <http://idm-old.math.cnrs.fr/L-analyse-multifractale-des.html>. [Accès le 4 2022].
- [94] L. Olsen, *Multifractal Analysis. A selected survey*, scotland: University of St Andrews.
- [95] R. Gaudio, S. D. Bartolo et G. Salvatore, «Procedures in multifractal analysis of river networks: a state-of-the-art review,» *IAHS Publ*, pp. 228-237, 2014.
- [96] C. D. V. Orozco, J. Golay et M. Kanevski, «Multifractal portrayal of the Swiss population,» *Cybergeo: European Journal of Geography [En ligne]*, 9 3 2015.
- [97] K. Mohamed, *analyse multifractale par MMTO-2D évaluation sur des images radar et médicales*, alger: L'université des sciences et de la technologie Houari-Boumediène (USTHB), 2011.
- [98] M. Ghil, R. Benzi et G. Parisi, «Turbulence and predictability in geophysical fluid dynamics and climate,» *Proceedings of the International School of Physics Enrico Fermi*, North-Holland, 1985.

- [99] H.G.E.Hentschel et ItamarProcaccia, «The infinite number of generalized dimensions of fractals and strange attractors,» *Physica D: Nonlinear Phenomena*, vol. 8, n° %13, pp. 435-444, 1983 .
- [100] S. Xie et Z. Bao, «Fractal and Multifractal Properties of Geochemical Fields,» *Mathematical Geology*, vol. 36, p. 847–864, 10 2004 .
- [101] a. Laszlo Barabasi, s. péter et tamas vicsek, «Multifractal spectra of multi-affine functions,» *Physica*, vol. A, n° %1178, pp. 17-28, 1991 .
- [102] N. Sarkar et B. Chaudhuri, «An efficient differential box-counting approach to compute fractal dimension of image,» *IEEE*, vol. 24, n° %11, pp. 115-120, 1994 .
- [103] D. G. Kelty-Stephen, K. Palatinus, E. Saltzman, E. Saltzman et J. A. Dixon, «A Tutorial on Multifractality, Cascades, and Interactivity for Empirical Time Series in Ecological Science,» *Ecological Psychology*, vol. 25, n° %1 , pp. 1-62, 2013.
- [104] A. Arneodo, G. Grasseau et M. Holschneider, «Wavelet Transform of Multifractals,» *APS Physics*, vol. 61 , n° %120, p. 2281, 1988.
- [105] X. Zhang, G. Zhang, L. Qiu, B. Zhang, Y. Sun, Z. Gui et Q. Zhang, «A Modified Multifractal Detrended Fluctuation Analysis (MFDFA) Approach for Multifractal Analysis of Precipitation in Dongting Lake Basin, China,» *mdpi Journal Water*, vol. 11 , n° %1891, pp. 2-18, 2019.
- [106] H. Wendt, P. Abry, S. G. Roux, S. Jaffard et B. Vedel, «Analyse multifractale d'images : l'apport des coefficients dominants,» , France.
- [107] A. OUAHABI, «Chapter 2 Discrete Wavelet Transform-Based Multifractal Analysis,» chez *Signal and Image Multiresolution Analysis*, ISTE Ltd, 2012, p. .
- [108] J. Barral et P. Gonçalves, «On the Estimation of the Large Deviations Spectrum,» *Journal of Statistical Physics*, vol. 144, n° %11256, p. , 2011.
- [109] C. TAY, *Algorithms for Tissue Image Analysis using Multifractal Techniques*, Singapore: University of Canterbury, 2012.
- [110] B. Lashermes, *Analyse multifractale pratique : coefficients dominants et ordres critiques. Applications à la turbulence pleinement développée. Effets de nombre de Reynolds fini*, lyon: Ecole normale supérieure de lyon - ENS LYON, 2005.
- [111] M. Ibrahim et R. Mukundan, «Multi-fractal Techniques for Emphysema Classification in Lung Tissue Images,» chez *2014 3rd International Conference on Environment, Chemistry and Biology*, Singapore, 2014.
- [112] B. O. Bech et P. B. i. Crosa, *Automatic Computation of Potential Tumor Regions in Cancer Detection using Fractal analysis techniques*, CATALUNYA: , 2009.
- [113] C. Atupelage, H. Nagahashi, M. Yamaguchi, T. Abe, A. Hashiguchi et M. Sakamoto, «Multifractal Feature Descriptor for Grading Hepatocellular Carcinoma,» chez *21st International Conference on Pattern Recognition (ICPR 2012)*, Tsukuba, Japan, 2012.

- [114] R. Korchiyne, A. Sbihi, S. M. Farssi, R. Touahni et M. T. Alaoui, «Spectre multifractal : Applications aux images médicales,» *Mediterranean Telecommunication Journal*, vol. 2, n° 12, pp. 133-137, 2012.
- [115] G. C. Sitzia-Verleure, MÉTHODES THERMODYNAMIQUES APPLIQUÉES À L'IMAGERIE MÉDICALE, Montréal: Gaël C. Sitzia-Verleure, 2003.
- [116] B. BUARD, CONTRIBUTION À LA COMPRÉHENSION DES SIGNAUX DE FLUXMÉTRIE LASER DOPPLER : TRAITEMENT DES SIGNAUX ET INTERPRÉTATIONS PHYSIOLOGIQUES, Angers: ÉCOLE DOCTORALE SCIENCES ET TECHNOLOGIES DE L'INFORMATION ET DE MATHÉMATIQUES, 2010.
- [117] E. L., Albuquerque, M. G. et Cottam, «Chapter 6 - Plasmon-Polaritons in Quasiperiodic Structures,» chez *Polaritons in Periodic and Quasiperiodic Structures*, Elsevier B.V. , 2004, pp. 125-156.
- [118] A. Biswas, H. P. Cresswell et C. S. Bing, «Application of Multifractal and Joint Multifractal Analysis in Examining Soil Spatial Variation: A Review,» chez *Fractal analysis and chaos in Geosciences*, IntechOpen, 2012.
- [119] F. J. Jiménez-Hornero, A. B. A. Villaverde et E. G. d. Ravé, «Multifractal Description of Simulated Flow Velocity in Idealised Porous Media by Using the Sandbox Method,» *World Scientific Publishing Company*, vol. 21, n° 11, p. 14, 2013.
- [120] M. H. J. L. P. K. I. P. T. C. Halsey, «Fractal measures and their singularities: The characterization of strange sets,» *Phys. Rev*, vol. 33, p. 1141–1151, 1986.
- [121] S. G. D. Bartolo, «Multifractal analysis of river networks: Sandbox approach,» *WATER RESOURCES RESEARCH*, vol. 40, 2004.
- [122] J. Vahe, Une approche multifractale pour la modélisation du micro-mélange à grand nombre de Schmidt, france: Physique [physics], 2014.
- [123] Mallat.S, Une exploration des signaux en ondelettes, france: Les éditions de l'Ecole Polytechnique, 2000.
- [124] D. L. BIHAN, «Académie nationale de médecine,» 2018. [En ligne]. Available: <https://www.academie-medecine.fr/quest-ce-quune-image-medicale-considerations-medico-economiques/>. [Accès le 2022].
- [125] tax-definition.org, «tax-definition.org,» [En ligne]. Available: <https://ar.tax-definition.org/25946-digital-image>. [Accès le 2022].
- [126] Techno-Science.net, «techno-science.net,» [En ligne]. Available: <https://www.techno-science.net/glossaire-definition/Image-numerique.html>. [Accès le 2022].
- [127] Simplilearn, «simplilearn,» 30 05 2022. [En ligne]. Available: <https://www.simplilearn.com/image-processing-article>. [Accès le 2022].
- [128] J. Guigui, L. Rotenberg, A.-E. Cabée, R. Lavayssière et G. Lenczner, «Institut du Sein Henri Hartmann,» Institut du Sein Henri Hartmann, [En ligne]. Available: <https://ishh.fr/departments/radiologie-scanner-irm/>. [Accès le 2022].

- [129] S. C. M. B.-h. K. Debashis Ganguly, *Medical Imaging*, Korea : Verlag Berlin Heidelberg, 2010.
- [130] A. Patyuchenko, «Anton Patyuchenko is an RF specialist with more than 15 years of experience in this field. He received his Master of Science in Microwave Engineering from Analog Devices,» 1995/2022. [En ligne]. Available: <https://www.analog.com/ru/technical-articles/medical-image-processing-from-formation-to-interpretation.html>.
- [131] I. Global, «igi-global,» IGI Global, [En ligne]. Available: <https://www.igi-global.com/dictionary/image-acquisition/79991>. [Accès le 2022].
- [132] N. Selmaoui, Écrivain, *Traitement et analyse d'image*. [Performance]. SlideServe, 2012.
- [133] MathWorks, «MathWorks,» MathWorks, [En ligne]. Available: <https://www.mathworks.com/help/images/image-analysis.html>. [Accès le 2022].
- [134] J. L. Awange et J. B. K. Kiema, *Environmental Geoinformatics*, London: Springer, 2013.
- [135] «Data Analytics Post,» Data Analytics Post, [En ligne]. Available: <https://dataanalyticspost.com/Lexique/svm/>. [Accès le 2022].
- [136] L. MASURE, C. DUVAL, M. O. Jean-Baptiste Le Noir de Carlan et J. BUSTILLOS, « Ensiwiki,» 2016. [En ligne]. Available: https://ensiwiki.ensimag.fr/index.php?title=Projet_Kaggle_Expedia_2016. [Accès le 2022].
- [137] R. L. D. B. M. H. O. P. D. M.F. Barnsley, *The Science of Fractal Image*, Springer Verlag, 1988.
- [138] C. BLOG, «CHM Computer History Museum,» Computer History Museum, 2018. [En ligne]. Available: <https://computerhistory.org/profile/guido-van-rossum/#:~:text=First%20released%20by%20its%20creator,Swiss%20Army%20knife%E2%80%9D%20for%20programmers..> [Accès le 2022].
- [139] S. Gérard, *apprendre à programmer avec python*, Groupe Eyrolles, 2012.
- [140] P. S. Foundation, «Python,» Python Software Foundation, 2021. [En ligne]. Available: <https://docs.python.org/3/tutorial/>. [Accès le 2022].
- [141] P.-F. Bonnefoi, *Mon'tit Python*, limoges: université de limoges, 2012.
- [142] eosgarden, «eosgarden,» eosgarden, 6 4 2013. [En ligne]. Available: <https://eosgarden.com/en/opensource/opencv-ios/overview/>. [Accès le 2022].
- [143] G. Bradiski et a. Kaehler, *learning OpenCV*, USA: Newgen publishing and data services, 2008.
- [144] N. community, *NumPy User Guide*, Numpy community, 2020.
- [145] «courspython,» courspython, 2021. [En ligne]. Available: <https://courspython.com/apprendre-numpy.html>. [Accès le 2022].
- [146] J. Hunter, D. Dale, E. Firing et M. Droettboom, *Matplotlib*, 2017.